

**LABORATORY ASSESSMENT OF MECHANICAL
PROPERTIES OF SANDSTONE UNDER SUBZERO
TEMPERATURE CONDITION**



**A Thesis Submitted in Partial Fulfillment of the Requirements for the
Doctor of Philosophy of Engineering in Civil, Transportation
and Geo-resources**

Suranaree University of Technology

Academic Year 2018

การประเมินคุณสมบัติเชิงกลศาสตร์ของหินทรายในห้องปฏิบัติการ
ภายใต้สภาวะอุณหภูมิต่ำกว่าศูนย์องศา



นางสาวเสมอแะ พรพมา

วิทยานิพนธ์นี้เป็นส่วนหนึ่งของการศึกษาตามหลักสูตรปริญญาวิศวกรรมศาสตรดุษฎีบัณฑิต
สาขาวิชาวิศวกรรมโยธา ขนส่ง และทรัพยากรธรณี
มหาวิทยาลัยเทคโนโลยีสุรนารี
ปีการศึกษา 2561

**LABORATORY ASSESSMENT OF MECHANICAL PROPERTIES
OF SANDSTONE UNDER SUBZERO TEMPERATURE CONDITION**

Suranaree University of Technology has approved this thesis submitted in partial fulfillment of the requirements for the Degree of Doctor of Philosophy

Thesis Examining Committee



(Assoc. Prof. Dr. Pornkasem Jongpradist)

Chairperson




(Asst. Prof. Dr. Decho Phueakphum)

Member (Thesis Advisor)




(Asst. Prof. Dr. Akkhapun Wannakomol)

Member



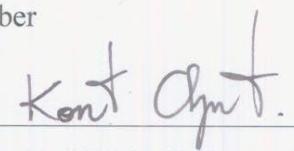
(Asst. Prof. Dr. Prachya Tepnarong)

Member



(Asst. Prof. Dr. Anisong Chitnarin)

Member



(Assoc. Prof. Ft. Lt. Dr. Kontorn Chamniprasart)



(Prof. Dr. Santi Maensiri)

Vice Rector for Academic Affairs
and Internationalization

Dean of Institute of Engineering

เสมอแชน พรอมมา : การประเมินคุณสมบัติเชิงกลศาสตร์ของหินทรายใน
ห้องปฏิบัติการภายใต้สภาวะอุณหภูมิต่ำกว่าศูนย์องศา (LABORATORY
ASSESSMENT OF MECHANICAL PROPERTIES OF SANDSTONE UNDER
SUBZERO TEMPERATURE CONDITION) อาจารย์ที่ปรึกษา : ผู้ช่วยศาสตราจารย์
ดร.เดโช เผือกภูมิ, 164 หน้า

วัตถุประสงค์ของงานวิจัยนี้เพื่อประเมินสมบัติทางกลของหินทรายภายใต้สภาวะอุณหภูมิต่ำกว่าศูนย์องศาและเพื่อประเมินประสิทธิภาพของเทคนิคการ ground freezing โดยหินทรายชุดพระวิหารจะถูกดำเนินการทดสอบกำลังรับแรงกดในแกนเดียวและสามแกนและทดสอบกำลังรับแรงดึงแบบบราซึลภายใต้อุณหภูมิต่างกัน (233, 253, 268 และ 298 เคลวิน) ภายใต้สภาวะที่แตกต่างกันในสามลักษณะ (แห้ง, อิ่มตัวด้วยน้ำและอิ่มตัวด้วยน้ำเกลือ) ผลการทดสอบคุณสมบัติเชิงกลศาสตร์แสดงให้เห็นว่ากำลังรับแรงดึงและกำลังรับแรงกดภายใต้สภาวะทั้งหมดเพิ่มขึ้นเมื่ออุณหภูมิลดลงเนื่องจากตัวอย่างภายใต้อุณหภูมิต่ำมีพลังงานความร้อนต่ำกว่าที่อุณหภูมิตั้งสูงซึ่งจะช่วยให้ตัวอย่างหินดูดซับพลังงานกลมากขึ้นและมีค่าความเค้นที่สูงขึ้นก่อนที่จะเกิดการวิบัติ อิทธิพลของอุณหภูมิต่อการเปลี่ยนแปลงรูปร่างของหินจะแสดงในรูปแบบของโมดูลัสความยืดหยุ่น (Elastic modulus) และอัตราส่วนปัวซอง (Poisson's ratio) พารามิเตอร์ความแข็งและพารามิเตอร์ยืดหยุ่นถูกพิจารณาจากผลการทดสอบคุณสมบัติเชิงกลศาสตร์ แรงยึดเหนี่ยวและมุมแรงเสียดทานภายในตามเกณฑ์ Coulomb เพิ่มขึ้นเล็กน้อยเมื่ออุณหภูมิลดลง ค่าคงที่ "m" จากเกณฑ์ Hoek และ Brown มีค่าลดลงเมื่ออุณหภูมิลดลง การจำลองเชิงตัวเลขแบบสองมิติ (2-D) โดยใช้โปรแกรม ANSYS 14.0 เพื่อคำนวณการถ่ายเทความร้อนระหว่างท่อแช่แข็ง (freezing pipe) กับหินโดยรอบ ผลการวิเคราะห์จะถูกนำมาใช้ในการประเมินการขยายตัวของพื้นที่แช่แข็ง (frozen zone) ในระหว่างกระบวนการ ground freezing โดยใช้อัตราการไหลของน้ำหล่อเย็นที่แตกต่างกันสี่แบบ (0.5, 1, 2 และ 3 กิโลกรัมต่อวินาที) และจะดำเนินการสำหรับกระบวนการแช่แข็งนาน 15 วัน จากผลการจำลองเชิงตัวเลขพบว่าระยะรัศมีของพื้นที่แช่แข็งเพิ่มขึ้นเมื่อเวลาและอัตราการไหลของน้ำหล่อเย็นเพิ่มขึ้น สมการทางคณิตศาสตร์ถูกนำเสนอในรูปของระยะรัศมีของพื้นที่แช่แข็ง (R_p), ค่าการนำความร้อน (λ), ความร้อน (c_p), อัตราการไหลของน้ำหล่อเย็น (N) และเวลาในการแช่แข็ง (T): $R_p = 134.53 (\lambda/c_p)^{1.08} N^{0.118} T^{0.465}$ สมการเชิงประจักษ์นี้สามารถนำไปพิจารณาเลือกใช้อัตราการไหลของน้ำหล่อเย็นที่เหมาะสมและเวลาในการแช่แข็งสำหรับหินแต่ละประเภทและระยะห่างของช่องแช่แข็งที่เหมาะสมได้

สาขาวิชา เทคโนโลยีธรณี
ปีการศึกษา 2561

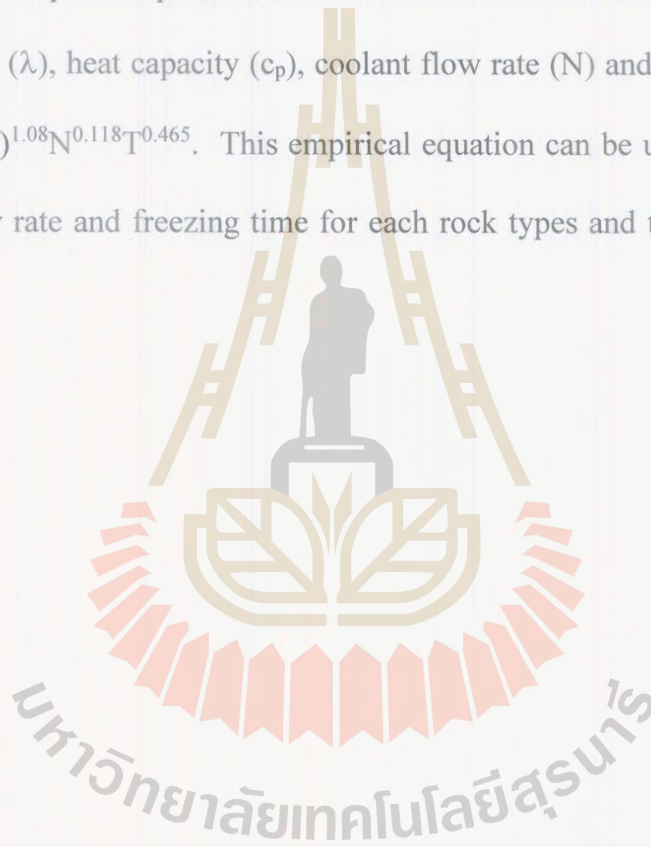
ลายมือชื่อนักศึกษา เสมอแชน พรอมมา
ลายมือชื่ออาจารย์ที่ปรึกษา ดร.เดโช เผือกภูมิ

SAMERHKEA PROMMA : LABORATORY ASSESSMENT OF
MECHANICAL PROPERTIES OF SANDSTONE UNDER SUBZERO
TEMPERATURE CONDITION. THESIS ADVISOR : ASST. PROF.
DECHO PHUEAKPHUM, Ph.D., 164 PP.

GROUND FREEZING/ STRENGTH/ FROZEN SANDSTONE/ SUBZERO
TEMPERATURE/NUMERICAL SIMULATION/FROZEN ZONE

The objectives of this study are to experimentally assess the mechanical properties of sandstone under subzero temperature condition and to assess the performance of ground freezing technique using computer simulation. The uniaxial and triaxial compression test and Brazilian tensile strength test are performed on the Phra Wihan sandstone under various temperature (233, 253, 268, and 298 Kelvin) on three different conditions (dry, saturated with water and saturated with brine). The results of the mechanical properties indicated that the tensile and compressive strengths under all of conditions increased with decreasing of temperatures. This is due to the specimens under low temperature have a lower thermal energy than those under high temperature. This allows the rock sample to absorb more mechanical energy and to develop higher stresses before the failure occur. The influencing of temperature on the rock deformability is displayed as elastic modulus and Poisson's ratio. The strength parameters and elastic parameter are determined by the results of the mechanical properties. The cohesion and internal friction angle based on Coulomb criterion, slightly increase with decreasing of temperatures. The “m” constant based on Hoek and Brown criterion decrease with decreasing temperature. Two-dimensional (2-D) axisymmetric numerical simulation using program ANSYS 14.0 is also performed to

calculate the heat transfer between freezing pipe and surrounding rock. The result obtained here can be used to assess the development of frozen zone during ground freezing operation. Four different coolant flow rates (0.5, 1, 2 and 3 kg/sec) are conducted for freezing process up to 15 days. The numerical results indicated that the frozen zone radius is increased with increasing of time and coolant flow rate. The mathematical equation presented in form of the frozen zone radius (R_p), thermal conductivity (λ), heat capacity (c_p), coolant flow rate (N) and freezing time (T): $R_p = 134.53 (\lambda/c_p)^{1.08} N^{0.118} T^{0.465}$. This empirical equation can be used to select the proper coolant flow rate and freezing time for each rock types and the proper freezing hole spacing.



School of Geotechnology

Academic Year 2018

Student's Signature เสด็จกมล น้อย

Advisor's Signature

ACKNOWLEDGMENTS

I wish to acknowledge the funding supported by Suranaree University of Technology (SUT).

I would like to express my sincere thanks to Asst. Prof. Dr. Decho Phueakphum for his valuable guidance and efficient supervision. I appreciate his strong support, encouragement, suggestions and comments during the research period. My heartiness thanks to Assoc. Prof. Dr. Pornkasem Jongpradist, Asst. Prof. Dr. Anisong Chitnarin, Asst. Prof. Dr. Prachya Tepnarong and Asst. Prof. Dr. Akkhapun Wannakomol for their constructive advice, valuable suggestions and comments on my research works as thesis committee members. Grateful thanks are given to all staffs of Geomechanics Research Unit, Institute of Engineering who supported my work.

Finally, I would like to thank beloved parents for their love, support and encouragement.

Samerhkea Promma

TABLE OF CONTENTS

	Page
ABSTRACT (THAI)	I
ABSTRACT (ENGLISH).....	II
ACKNOWLEDGEMENTS.....	IV
TABLE OF CONTENTS.....	V
LIST OF TABLES	X
LIST OF FIGURES	XIII
SYMBOLS AND ABBREVIATIONS.....	XIX
CHAPTER	
I INTRODUCTION	1
1.1 Background and rationale	1
1.2 Research objectives.....	3
1.3 Scope and limitations.....	4
1.4 Research methodology.....	5
1.4.1 Literature review.....	5
1.4.2 Sample preparation	5
1.4.3 Mechanical laboratory testing.....	7
1.4.4 Data analysis	7
1.4.4.1 Mechanical properties.....	7

TABLE OF CONTENTS (Continued)

	Page
1.4.4.2 Computer simulation.....	7
1.4.5 Discussions, conclusions and thesis writing.....	8
1.5 Thesis contents.....	8
II LITERATURE REVIEW	9
2.1 Introduction.....	9
2.2 Ground freezing method	9
2.2.1 Artificial ground freezing method	9
2.2.2 Advantages and disadvantages of ground freezing	14
2.3 Mechanical properties of material under low temperature	17
2.3.1 Mechanical properties rocks.....	17
2.3.1.1 Influence of freezing on compressive and tensile strength	17
2.3.1.2 Influence of temperature	20
2.3.1.3 Influence of water content	21
2.3.1.4 Influence of brine content	23
2.3.2.5 Influence of ice content.....	25
2.3.2 Mechanical properties soils	25
2.2.3 Mechanical properties of ice.....	30
2.4 Thermal properties	33
2.4.1 Thermal conductivity.....	33

TABLE OF CONTENTS (Continued)

	Page
2.4.1.1 Influence of porosity and fluid content.....	33
2.4.1.2 Influence of mineral content	36
2.4.1.3 Influence of temperature	36
2.4.2 Heat capacity	38
2.4.2.1 Influence of porosity and fluid content.....	38
2.4.2.2 Influence of mineral content	39
2.4.2.3 Influence of temperature	39
2.4.3 Thermal properties of rocks in Thailand	40
2.5 Heat transfer.....	41
2.5.1 Modes of heat transfer	41
2.5.2 Heat transfer for ground freezing	44
2.6 Numerical simulation for ground freezing.....	47
III SAMPLE PREPARATION.....	48
3.1 Introduction.....	48
3.2 Sample preparation	48
IV MECHANICAL LABORATORY TESTING	52
4.1 Introduction.....	52
4.2 Test method.....	52
4.2.1 Freezing method	52
4.2.2 Uniaxial and triaxial compressive strength tests	53

TABLE OF CONTENTS (Continued)

	Page
4.2.3 Brazilian tension test.....	53
4.3 Test result.....	54
4.4 Freeze-thaw cycle test.....	63
V CORRECTION BETWEEN MECHANICAL PROPERTIES AND TEMPERATURE	66
5.1 Introduction.....	66
5.2 Coulomb criterion.....	66
5.3 Hoek and Brown criterion.....	68
5.4 Modified Coulomb strength criteria.....	71
5.5 Deformation modulus	76
VI COMPUTER SIMULATION FOR GROUND FREEZING	82
6.1 Introduction.....	82
6.2 ANSYS 14.0 program.....	82
6.3 Numerical simulation.....	83
6.4 Input parameters.....	84
6.5 Computer simulation results	89
6.5.1 Influence of the ground.....	89
6.5.2 The coolant flow rate.....	90
6.6 Mathematical relationship for prediction progression of frozen zone.....	95

TABLE OF CONTENTS (Continued)

	Page
VII DISCUSSIONS AND CONCLUSIONS	100
7.1 Discussions	100
7.2 Conclusions.....	105
7.3 Recommendations for future studies	108
REFERENCES	109
APPENDICES	
APPENDIX A DIMENSIONS AND RESULTS FROM COMPRESSIVE STRENGTH TESTS	120
APPENDIX B MOHR’S CIRCLE BASED ON COULOMB CRITERIA.....	144
APPENDIX C DIMENSIONS AND RESULTS FROM BRAZILIAN TENSILE STRENGTH TESTS	151
APPENDIX D RADIUS OF PROGRESSION OF FROZEN ZONE SIMULATION FROM ANSYS14.0	155
BIOGRAPHY	164

LIST OF TABLES

Table		Page
2.1	Comparing freezing with brine and freezing with liquid nitrogen.....	16
2.2	Strength of frozen sand at various strain rates and temperatures obtained by different authors.....	28
2.3	Thermal conductivity of some common rock forming minerals.....	36
2.4	Empirical constants A and B for different rock types.....	38
2.5	Thermal properties of rocks and soil.....	41
3.1	Physical properties of Phara Wihan sandstone.....	51
3.2	Thermal properties of Phara Wihan sandstone.....	51
4.1	Compressive strengths of Phara Wihan sandstone.....	56
4.2	Tensile strength of Phara Wihan sandstone.....	58
4.3	Elastic modulus and Poisson's ratio under dry condition.....	60
4.4	Elastic modulus and Poisson's ratio under water-saturated condition.....	61
4.5	Elastic modulus and Poisson's ratio under brine-saturated condition.....	62
4.6	Test results obtained for freeze-thaw cycle testing.....	65
5.1	Cohesion and internal friction angle of Phara Wihan sandstone.....	67
5.2	Hoek-Brown's constants (σ_c , m and s) obtained for Phara Wihan sandstone under various temperature.....	69
5.3	Strength of Phara Wihan sandstone.....	74
5.4	Elastic parameters of Phara Wihan sandstone for dry condition.....	78

LIST OF TABLES (Continued)

Table		Page
5.5	Elastic parameters of Phra Wihan sandstone for water-saturated condition.....	79
5.6	Elastic parameters of Phra Wihan sandstone for brine-saturated condition.....	80
6.1	Freezing pipe geometry.....	84
6.2	Physical parameters used in the computer simulation.....	87
6.3	The radius distance progression of the frozen zone for ground.....	92
6.4	Parameters of mathematical relationship.....	96
A.1	Dry sandstone specimens prepared for compression tests.....	121
A.2	Water-saturated sandstone specimens prepared for compression tests.....	124
A.3	Brine-saturated sandstone specimens prepared for compression tests.....	127
A.4	The result of compressive strength of dry specimens under difference temperatures.....	141
A.5	The result of compressive strength of water-saturated specimens under difference temperatures.....	142
A.6	The result of compressive strength of brine-saturated specimens under difference temperatures.....	143
C.1	The result of Brazilian tensile strength of dry specimens under difference temperatures.....	152
C.2	The result of Brazilian tensile strength of water-saturated specimens under difference temperatures.....	153

LIST OF TABLES (Continued)

Table	Page
C.3 The result of Brazilian tensile strength of brine-saturated specimens under difference temperatures.....	154



LIST OF FIGURES

Figure		Page
1.1	Research methodology.....	6
2.1	Construction of Brightwater Tunnel in King County, Washington, USA uses ground freezing method.....	10
2.2	Vertical cross section of installed freezing pipes in the soil and rock.....	11
2.3	Horizontal cross section of installed freezing pipes in the soil and rock.....	12
2.4	Brine freezing system.....	13
2.5	Liquid nitrogen freezing.....	14
2.6	Strength of granite, limestone, and sandstone in uniaxial compression strength.....	18
2.7	Strength of granite, limestone, and sandstone in tensile strength.....	18
2.8	Summary of uniaxial test results for unfrozen and frozen sandstone.....	19
2.9	Uniaxial compressive strength (a) and indirect tensile strength (b) vs. degree of water saturation.....	22
2.10	Examples of stress-strain curves of Shikotsu welded tuff and Bibai sandstone.....	22
2.11	Variation of angle of friction and cohesion for frozen sand with low ice content.....	29
2.12	Tensile and compressive strength of ice as a function of temperature.....	32

LIST OF FIGURES (Continued)

Figure	Page
2.13 Tensile and compressive strength of ice as a function of strain rate	32
2.14 Tensile strength of ice as a function of grain size	33
2.15 Modes of heat transfer: conduction, convection and radiation	42
3.1 Some specimens of Phara Wihan sandstone under dry and saturated conditions in the cylindrical shape	49
3.2 Examples of sandstone specimen prepared for compressive strength test (a), Brazilian tensile strength test (b)	49
4.1 Test setup for (a) uniaxial compression test and (b) triaxial compression test using compression loading device	54
4.2 Some post-test specimens obtained from compressive strength testing under different confining pressures (σ_3) and temperatures in difference conditions	55
4.3 Principal stresses at failure as a function of confining pressure for dry (a), water-saturated (b) and brine-saturated (c) conditions	57
4.4 Some post-test specimens obtained from tensile strength testing under dry and saturated with water and brine conditions	59
4.5 Brazilian tensile strength as function of temperatures for dry and saturated with water and brine conditions	59
4.6 Examples of rock specimen prepared for freezing and thawing cyclic test	63
4.7 Porosity increment caused by freezing and thawing	65

LIST OF FIGURES (Continued)

Figure	Page
5.1 Cohesion and internal friction angle of Phara Wihan sandstone as a function of temperature from Coulomb criterion.....	68
5.2 Uniaxial compressive strength (σ_c) and parameter m as a function of temperatures.....	70
5.3 Major principal stresses at failure as a function of temperature in difference conditions.....	72
5.4 Octahedral shear strengths at failure of Phra Wihan sandstone as a function of mean stress in difference conditions.....	75
5.5 Elastic parameters of Phara Wihan sandstone as a function of temperature...	81
6.1 System model for numerical simulation.....	85
6.2 Finite element mesh for numerical model.....	86
6.3 Thermal conductivity of ground plotted as a function of their density.....	88
6.4 Heat capacity of ground plotted as a function of their density.....	88
6.5 Temperature contour obtain from numerical simulation in dry ground condition at 15 days in coolant flow rated 1 kg/s.....	91
6.6 The radius distance progression of the frozen zone as a function of time in difference flow rates.....	93
6.7 Comparison between data result (points) and proposed equation (lines) of the radius distance progression of the frozen zone.....	96

LIST OF FIGURES (Continued)

Figure	Page
6.8	Prediction of the radius distance progression of the frozen zone form the mathematical equation in this study and the closed-form equation of Sager and Sayles (1979).....
	99
A.1	Stress-strain curves obtained from dry sandstone specimens at 233 Kelvin..
	129
A.2	Stress-strain curves obtained from dry sandstone specimens at 253 Kelvin..
	130
A.3	Stress-strain curves obtained from dry sandstone specimens at 268 Kelvin..
	131
A.4	Stress-strain curves obtained from dry sandstone specimens at 298 Kelvin..
	132
A.5	Stress-strain curves obtained from water-saturated sandstone specimens at 233 Kelvin.....
	133
A.6	Stress-strain curves obtained from water-saturated sandstone specimens at 253 Kelvin.....
	134
A.7	Stress-strain curves obtained from water-saturated sandstone specimens at 268 Kelvin.....
	135
A.8	Stress-strain curves obtained from water-saturated sandstone specimens at 298 Kelvin.....
	136
A.9	Stress-strain curves obtained from brine-saturated sandstone specimens at 233 Kelvin.....
	137
A.10	Stress-strain curves obtained from brine-saturated sandstone specimens at 253 Kelvin.....
	138

LIST OF FIGURES (Continued)

Figure	Page
A.11 Stress-strain curves obtained from brine-saturated sandstone specimens at 268 Kelvin.....	139
A.12 Stress-strain curves obtained from brine-saturated sandstone specimens at 298 Kelvin.....	140
B.1 Mohr's circles form Coulomb criterion of dry sandstone under difference temperatures.....	145
B.2 Mohr's circles form Coulomb criterion of water-saturated sandstone under difference temperatures.....	147
B.3 Mohr's circles form Coulomb criterion of brine-saturated sandstone under difference temperatures.....	149
D.1 Results of the radius progression of frozen zone at 273 Kelvin for dry ground surrounding condition in difference coolant flow rates.....	156
D.2 Results of the radius progression of frozen zone at 273 Kelvin for 50% water-saturated ground surrounding condition in difference coolant flow rates.....	158
D.2 Results of the radius progression of frozen zone at 273 Kelvin for 50% water-saturated ground surrounding condition in difference coolant flow rates.....	160

LIST OF FIGURES (Continued)

Figure	Page
D.4 Results of the radius progression of frozen zone at 273 Kelvin for pure water ground surrounding condition in difference coolant flow rates.....	162



SYMBOLS AND ABBREVIATIONS

c	=	Cohesion
E	=	Elastic modulus
G	=	Shear modulus
K	=	Bulk modulus
m_s	=	Weight of dry specimen
m_w	=	Weight of moist specimen
n	=	Porosity
T	=	Temperature
w	=	Water content
η	=	Empirical constants
ω	=	Empirical constants
α	=	Empirical constant
β	=	Empirical constant
δ	=	Empirical constants
ϕ	=	Friction angle
κ	=	Empirical constants
ν	=	Poisson's ratio
ρ	=	Density
σ_1	=	Maximum principal stress
σ_2	=	Intermediate principal stress

SYMBOLS AND ABBREVIATIONS (Continued)

σ_3	=	Minimum pressures
σ_B	=	Brazilian tensile strength
σ_c	=	Uniaxial compressive strength
σ_m	=	Mean stress
σ_n	=	Normal stress
τ	=	Shear stress
τ_{oct}	=	Octahedral shear stresses
μ	=	Viscosity
ΔT	=	Gradient of temperature
A	=	Empirical constant
A_h	=	Cross sectional area in direction of heat flow
B	=	Empirical constant
C	=	Thermal capacity
C_i	=	Specific heat capacity of each component
c_p	=	Specific heat capacity
D	=	Empirical constant
h	=	Heat transfer coefficient
L	=	Latent heat of fusion of pore water
N_i	=	Mass of the rock weighted by volume fraction
Nu	=	Nusselt number
Pr	=	Prandtl number
q	=	Heat flow vector

SYMBOLS AND ABBREVIATIONS (Continued)

r	=	Radius of pipe
R	=	Radius of the frozen zone interface
Re	=	Reynolds number
t	=	Time requirement of frozen zone
T_{∞}	=	Free stream fluid temperature
T_s	=	Surface temperature
u	=	Flow velocity
σ	=	Steffan Boltzman constant
ε	=	Emissivity
λ, k	=	Thermal conductivity
λ_e	=	Mixing thermal conductivity
λ_f	=	Thermal conductivities of contained fluid
λ_s	=	Thermal conductivities of rock solids

CHAPTER I

INTRODUCTION

1.1 Background and rationale

Rock salt and potash in the Khorat and Sakon Nakhon basins in the northern Thailand have become important mineral resources for industry. The deposits in the Maha Sarakham formation consist of upper salt, middle clastic, middle salt, lower clastic and lower salt member. Potash has been found only in the lower salt member (Suwanich, 2010). For mining process of underground mine, the mining access (shaft and declined) is excavated through the deep of rock strata with the operational problems created by adverse groundwater conditions. The impact of groundwater on an underground construction project can be enormous. The groundwater is damaged the design of the structure, the construction procedures, and the overall project cost (Abdul-Rahman et al., 2006; Peaker, 2003). Generally, two major groups of groundwater controls to handling the adverse effects of the groundwater flow including dewatering and exclusion techniques (Cashman and Preene, 2001). The dewatering techniques deal with groundwater by pumping. The exclusion techniques exclude water from the excavation (such as grouting and ground freezing). The dewatering is the techniques to control the surface and subsurface hydrologic environment in such a way as to permit the structure to be constructed in the dry. The most common methods for dewatering include sumps, wells and well points. The method of dewatering for dealing with underground water flow is pumped so the underground water table is

lower groundwater levels to a short distance below the deepest excavation formation level (Sadeghpour et al., 2008). However, the deep dewatering techniques is limited to about 25 feet (7.62 m) because of the pump efficiency (Nemati, 2007). There have been some cases in very deep excavation that exclusion techniques can be used solve groundwater problem.

Grouting is one of exclusion techniques for solve the groundwater problem. The grouting process uses the grout materials (such as cement mix, silicate and chemical grouts) which injected into the ground for fill pores or cavities in soil or rock. The method decreases the permeability and support of the structure. However, the grouting method causes the residue of grout materials which remains in environment. Some areas do not permit to use of certain types of grout materials due to groundwater in this area is used consumption. To avoid this effect, ground freezing method is used to control deep underground water.

Ground freezing is a process of making soil or rock below 0 °C (273 Kelvin) in temperature and temporarily impermeable by transforming water to ice. It is normally used to provide structural support for excavation and protect ground water flow into excavated area. The method is better than another method for sinking production shafts through deep (Schmall and Maishman, 2007; Johansson, 2009). It is environmentally friendly as no barriers, diaphragm walls and chemical or other grounding materials remains in environment after application and has many comparative advantages in concerning equivalent another method (Haß and Schäfers, 2006). Therefore, the ground freezing is a suitable method to prevent the groundwater problem which encounter in Middle clastic rocks member of Maha Sarakham formation during process for sinking production shaft. Hence the mechanical properties of the Middle clastic rocks affected

from ground freezing need to study. The sampling method of the Middle clastic rocks is difficult to keep it away from disturbance. The potential for disturbance during sampling and handling often leads to changes in the fabric, void ratio, stress history, and degree of saturation of the samples. To avoid these problem, the Phra Wihan sandstone is used to represent the Middle clastic rocks due to their properties are similar.

The ground freezing method is created by installing freeze pipes and circulated a fluid coolant through a pipe in ground to be frozen. The fluid coolant flows in the pipes is the refrigerant withdraw heat from the surrounding ground for a certain period of time in order to achieve a sufficiently thick frozen wall. Therefore, it is necessary to evaluate the heat transfers between the freeze pipe and ground surrounding for design freeze pipe system in terms of size, number and spacing.

For above reason, it is necessary to investigate the mechanical properties of Phra Wihan sandstone under low temperature use to design and analysis of engineering structures. In addition, there is analyzed the thermal process of circulate fluid coolant through pipe in the ground to be frozen.

1.2 Research objectives

The objectives of this study are to examine in laboratory assess of the mechanical properties of sandstone under subzero temperature condition and to analyze the heat transfer of ground freezing technique using computer simulation. The tests are performed on dry and saturated samples under the temperatures below as 233 Kelvin (-40°C). The mechanical properties including the uniaxial compressive strength, the Brazilian tensile strength and the triaxial compressive strength were employed. The

test results are used to construct the mathematical relationship between the mechanical properties and temperature. The strength and deformability parameters underlined particular temperature can be used to assess the predictive capability of some failure criteria by which readily applied in the design and stability of excavations.

1.3 Scope and Limitations

The scope and limitations of the research include as follows.

- 1) The tested samples are Phra Wihan sandstone which obtained from the northeast of Thailand.
- 2) The samples are prepared under dry condition and saturation by water and brine.
- 3) The mechanical laboratory tests in this study include uniaxial compressive strength test, triaxial compressive strength test and Brazilian tensile strength test.
- 4) The applied confining pressures is varied from 0, 3, 7 and 12 MPa.
- 5) The nominal temperature is varied 233, 253, 268 and 298 Kelvin (-40°C, -30°C, -20°C, -5°C and 25°C) and liquid nitrogen (LN₂) is used to cool down the specimens at subzero temperatures.
- 6) Mathematical equations are used to determine the mechanical properties from laboratory testing.
- 7) Computer simulation using ANSYS 14.0 is computer program that used to calculate the parameters of ground freezing method in term of heat transfer.

1.4 Research methodology

The research methodology shown in Figure 1.1 comprises 6 steps; including 1) literature review, 2) sample preparation, 3) mechanical laboratory testing (uniaxial compressive strength test, triaxial compressive strength test and Brazilian tensile strength test), 4) analysis of the mechanical properties and the computer simulations for heat transfer for ground freezing, 5) discussions and conclusions and 6) thesis writing.

1.4.1 Literature review

The literatures related to the process of ground freezing method, the mechanical properties of soils and rock during the freezing process, the thermal properties of geological material, heat transfer related to ground freezing techniques and numerical models to determine the freezing zone around the excavations.

1.4.2 Sample preparation

The rock samples of sandstone are obtained from Phra Wihan formation locations in northeast Thailand. The sandstone specimens are drilled and cut from a rock block in a cylindrical shape. The diameter of cylindrical shape specimens is 54 mm. Preparations of these samples follow as much as practical the American Society for Testing and Materials. The specimens are carried out under dry and wet conditions. The dry specimens are prepared in air dry at ambient temperatures. The saturation specimens are prepared by submerging the samples in water and brine which keeping them in a vacuum desiccator.

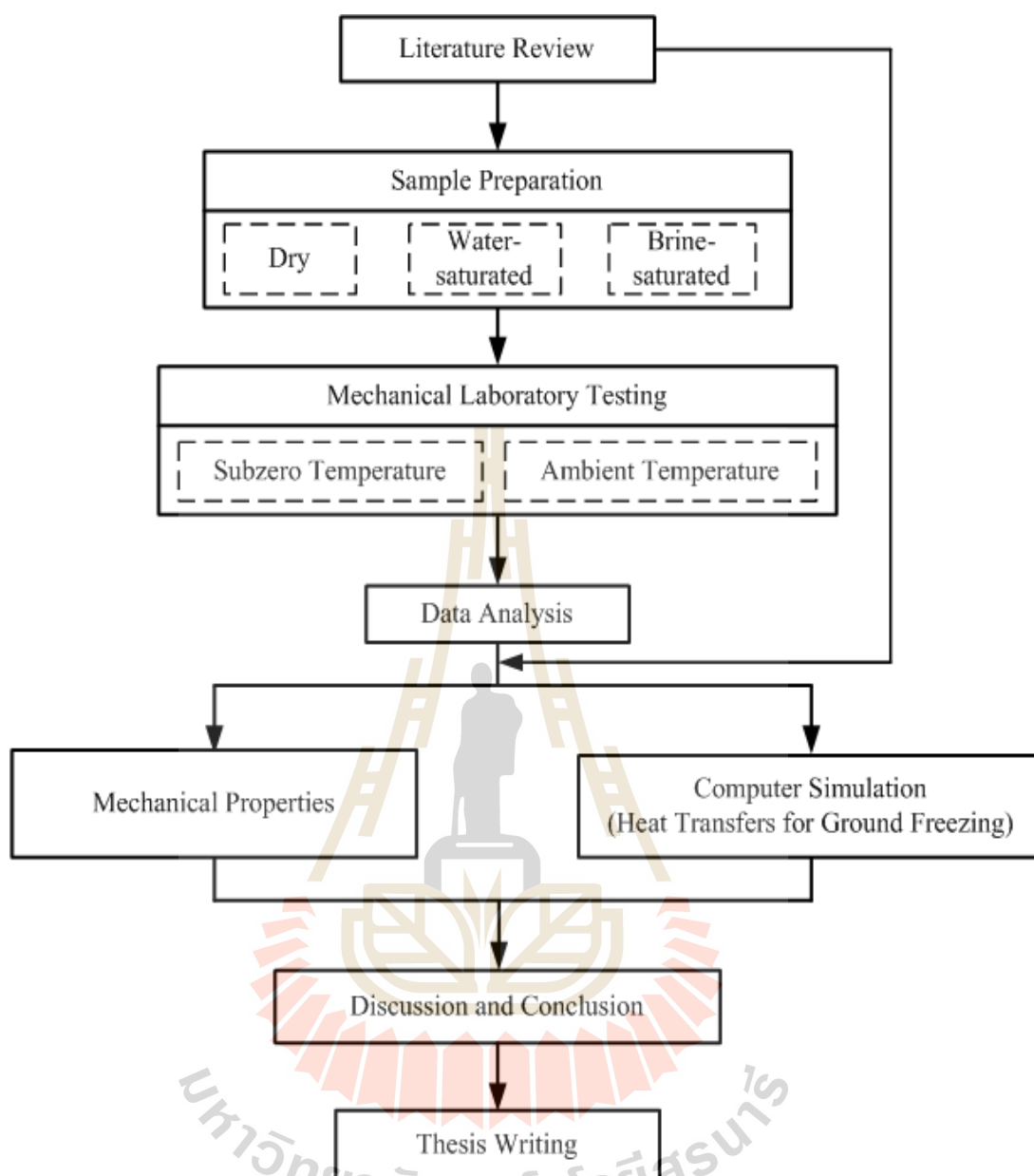


Figure 1.1 Research methodology

1.4.3 Mechanical laboratory testing

The laboratory testing is divided into three groups in include uniaxial compressive strength test, triaxial compressive strength test and Brazilian tensile strength test. The rock strengths and elasticity are determined in the laboratory under various confining pressures varying from 0, 3, 7 and 12 MPa. The specimens are tested under temperatures ranging from 233, 253, 268 and 298 (ambient temperature) Kelvin. The strength and elastic modulus are measured.

1.4.4 Data Analysis

The data analysis is analyzed to determine the mechanical properties of Phra Wihan sandstone under lower temperature in dry and saturated conditions and simulation the computer program for thermal behavior of ground freezing.

1.4.4.1 Mechanical properties

Results from laboratory testing are analyzed to determine the effects of subzero temperatures on compressive and tensile strength and elasticity of Phra Wihan sandstone. The results from data analysis are calculated in terms of the principal stresses which use to formulate mathematical relations. The mathematical equations are considered to assess the predictive capability of stability of ground during ground freezing process from some failure criteria (Coulomb criteria and Hock and Brown criteria).

1.4.4.2 Computer simulation

The computer simulation is used to study the thermal behavior of ground freezing. ANSYS 14.0 is computer program that used to simulate the location of the freezing zone for ground. The data from simulation is created the

mathematical relationship that uses to predict the temperature distribution in the ground for design the pipe system in ground freezing process.

1.4.5 Discussions, conclusions and thesis writing

All research activities, methods, and results are documented and compiled in the thesis. The discussions on validity and potential applications of the results are also mentioned in this thesis.

1.5 Thesis contents

Chapter I includes background and rationale, research objectives, scope and limitations and research methodology. Chapter II presents the results of literature review. Chapter III describes the rock samples preparation under difference conditions. Chapter IV presents mechanical laboratory testing under subzero temperature. Chapter V describes the mathematical relations used to determine the temperatures effect on the strength of rock. Chapter VI presents the computer simulation of heat transfer for ground freezing method. Chapter VII discusses and concludes the research results and provides recommendations for the future research studies.

CHAPTER II

LITERATURE REVIEW

2.1 Introduction

Literatures related to the ground freezing works are reviewed in this research. This preliminary literature review is focus on the processes of ground freezing method, change of ground properties during the freezing processes, thermal properties of geological material, heat transfer related to ground freezing techniques and numerical methods to determine the freezing zone around the excavations.

2.2 Ground freezing method

2.2.1 Artificial ground freezing method

Artificial ground freezing (Figure 2.1) is first applied to support vertical openings in South Wales, Australia in 1862 by Friedrich Poetsch (Harris, 1995). Artificial ground freezing is typically considered for excavation that is cut off groundwater by convert water into ice. In order to be able to create the required strength and required sealing some areas of the construction. Ground freezing has historically been used in shaft in soils and recently for temporary support in other areas such as mining, deep excavations.

The artificial ground freezing in the ground is created by installing freezing pipe in the ground. The process of freezing pipe is to circulate a fluid coolant through a pipe for extracting heat from the ground. The thermal material and geometric

parameters of the ground such as volumetric water content thermal conductivity, groundwater flow and freezing point of material are importance to consider the freezing pipe design (freezing pipe material, freezing pipe diameter, space of freezing pipe, heat transfer and velocity of flow). (Harris, 1995; Jumikis, 1996; Andersland and Ladanyi, 2004; Johansson, 2009).



Figure 2.1 Construction of Brightwater Tunnel in King County, Washington, USA uses ground freezing method (More Trenching Machine excavator, www, 2014)

The freeze pipes are generally made out of steel, copper or aluminum are suitable as they have better conductivity than most plastics material insulates the cold in the freeze pipe. Researchers suggest that a larger diameter of freeze pipes is more efficiently that keeping the surrounding area cool and the spacing between the freeze pipes is shorter distance (Jessberger and Vyalov, 1978; Sanger and Sayles, 1978).

The spacing of the freeze pipes should not exceed about thirteen times their diameter unless analysis indicates that a larger relative spacing will be acceptable for particular application. Shuster (1980) recommends freeze pipe diameter range between 0.05m and 0.15m. The frozen zone is created successively around the freeze pipes. The frozen zones grow up with time it will close up around each freezing pipe and form a homogenous frozen wall (Figures 2.2 and 2.3).

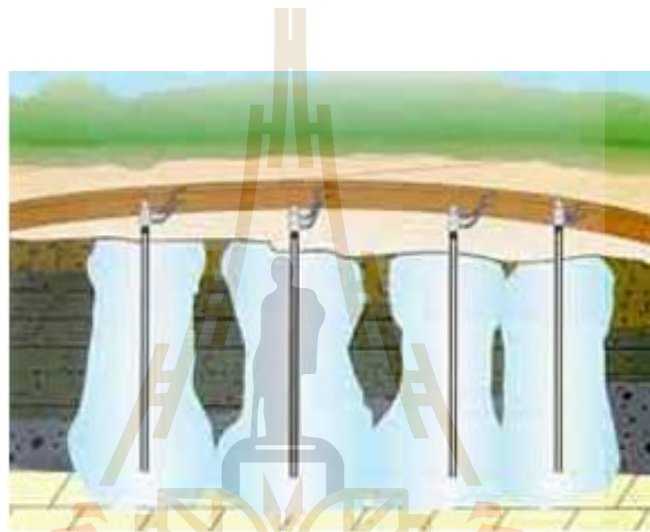


Figure 2.2 Vertical cross section of installed freezing pipes in the soil and rock (Sopko and Aluce, 2005)

The refrigeration plant is installed in order to ground freezing method depends on the type of coolant. Mostly a choice is between two main types of coolants that brine solution or liquid nitrogen. The brine freezing is also known as indirect method or closed circuit (Figure 2.4). Because the coolant is used in their method that a brine usually a calcium chloride solution (CaCl_2) and reused in a close work system. There method is used as secondary refrigerant. The primary refrigerant is a case of ammonia that used to cool down for the brine coolants. The secondary refrigerant is

brine case that pump into the freeze pipes for freeze the ground. The brine is cooled down to a temperature between $-30\text{ }^{\circ}\text{C}$ and $-40\text{ }^{\circ}\text{C}$ before it is inserted in through a downpipe (inside inner pipe) into the freeze pipe. It is through back to the annulus (space between outside of inner pipe and inside of outer pipe) and flows back into the return pipe that cool down again in the primary refrigerant.

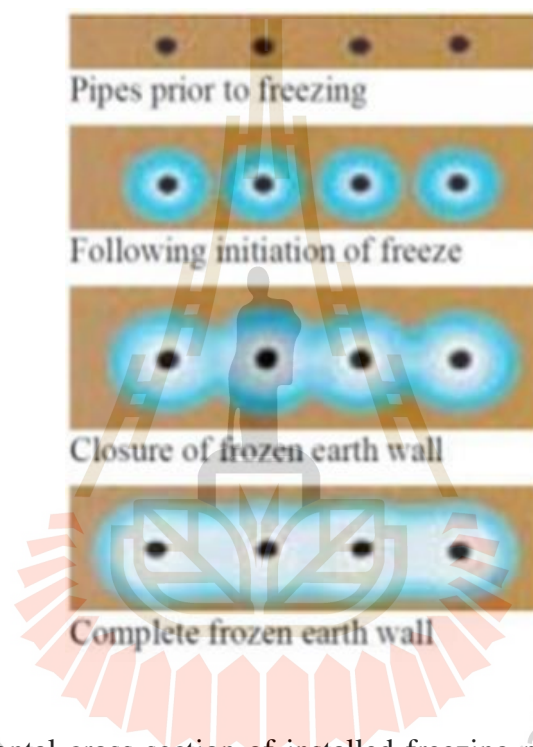


Figure 2.3 Horizontal cross section of installed freezing pipes in the soil and rock
(Sopko and Aluce, 2005)

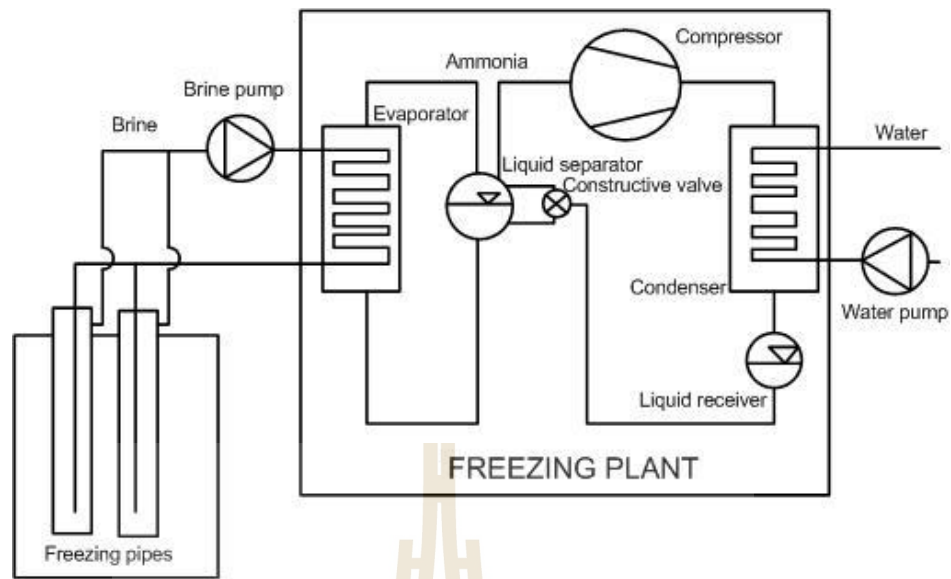


Figure 2.4 Brine freezing system (Berggren, 2000)

Liquid nitrogen freezing also called the direct method or open circuit (Figure 2.5). The coolant circulates is liquid nitrogen freezing (LN₂) that a single coolant. The liquid nitrogen has a temperature of -196 °C at a pressure of 1 bar in liquid form. The liquid nitrogen is kept in a vacuum storage tank and directly into the freeze pipes. The liquid nitrogen flows through the freezing pipe by pressure. It is not reused in the system and allow to evaporation into the atmosphere in gaseous form.

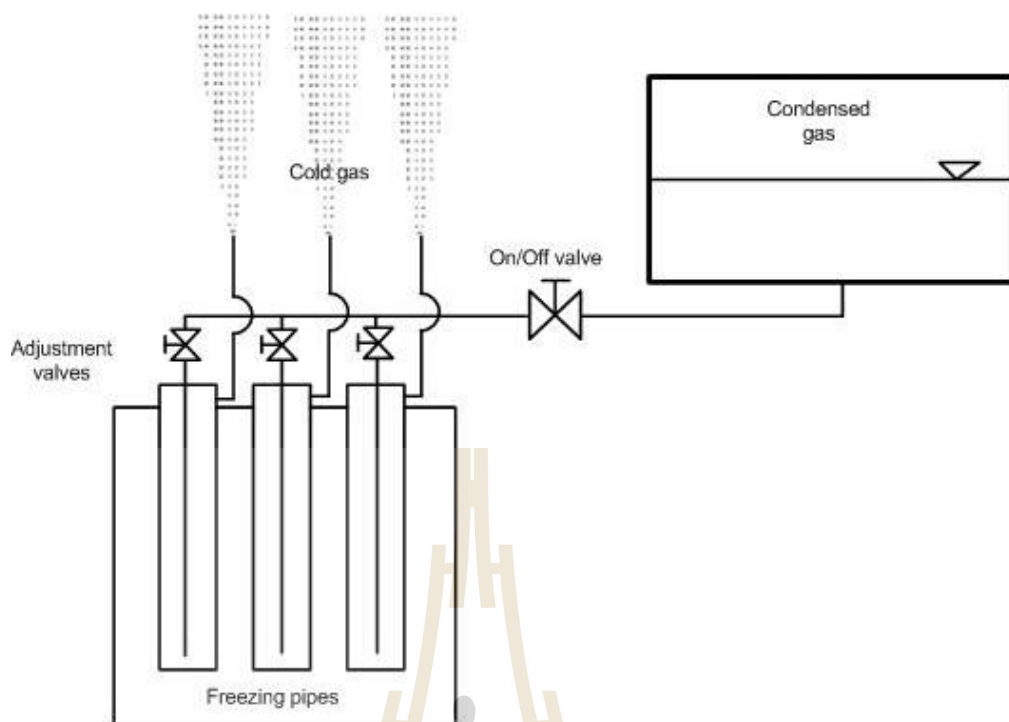


Figure 2.5 Liquid nitrogen freezing (Berggren, 2000)

2.2.2 Advantages and disadvantages of ground freezing

Two methods of the ground freezing have the advantages and the disadvantages and the application depends on the requirements of the construction works (Stoss and Valk 1979). The process of freezing with brine is need to be install a refrigerant plant at the construction site due to use a long freezing period. The freezing time until wall closure takes three weeks to three months that long than liquid nitrogen. However, brine is the most general method that used in construction because it is relatively cheap and simple method that is being used as a coolant for over 100 years. The brine coolant can be reuse in the system several times.

In the process of freezing with liquid nitrogen is short time to freeze up the frozen wall. The freezing of a closed frozen body takes in general only two to six days due to the low freezing temperatures that can be reached with liquid nitrogen. But

it is not able to reuse the coolant after one cycle. Therefore, a constant supply of new coolant is necessary which makes this method relatively expensive than brine freezing. In general, brine freezing is the most suitable when construction takes a longer period and is on a big scale. Liquid nitrogen freezing becomes more interesting when a project has a short duration and a smaller scale. In the selection of choose either one of the two methods mainly depend on economic factors or construction site as well as the time needed to freezing (Dorst, 2013).



Table 2.1 Comparing freezing with brine and freezing with liquid nitrogen (Dorst, 2013)

Site installations	Brine	Liquid nitrogen
Pumps and electric power	Required	Not Required
Water for cooling	Required	Not Required
Refrigeration plant	Required	Not Required
Vacuum storage tank	Required	Required
Pipe system for distribution coolant	Supply and return	Supply only
Low temperature material for surface pipes, valves, etc.	Not Required	Required
Low temperature material for freeze pipes	Not Required	Not Required
Execution of freezing	Brine	Liquid nitrogen
Physical condition coolant	Liquid	Liquid/Vapor
Minimal temperature achievable (theoretic)	-30°C to -60°C	-196°C
Re-use of coolant	Standard	Impractical
Control of system	Easy	Difficult
Shape of frozen body	Regular	Often irregular
Temperature profile in frozen body	Small differences	Great differences
Frost penetration	Slow	Fast
Impact on frozen body in case of damage to freeze pipe	Thawing effect	None
Noise	Little	None

2.3 Mechanical properties of material under low temperature

2.3.1 Mechanical properties rocks

2.3.1.1 Influence of freezing on compressive and tensile strength

The behavior of geological materials under subzero temperature many vary depending on many factors such as rock type, moisture content, temperature, freezing and thawing and freezing rate (Chen et al., 2004; Matsuoka, 1990; Yamabe and Neupane, 2001). Previous research studies the factors on the behavior of rock that is rock strength and deformation. Based on the research by Mellor (1971, 1973) indicate that the strength of rock increase with decreasing temperature. The three types of rocks (granite, limestone and sandstone) are used to test the uniaxial compressive and tensile strength under water saturated and dry air conditions in the temperature range 25°C to -195°C. Figure 2.6 shows the compressive strength results. It is observed that the values of strength increase with decreasing temperature is evident up to -50°C. The tensile strength results show in Figure 2.7 where the tensile strength of the dry rocks is a little change with decreasing temperature beyond -10°C. Dwivedi et al. (1998) observe that the strength increased with decrease in subzero temperature due to the temperature of the specimen is reduced while grains of rocks shrunk. This shrinkage of grains in the specimen has resulted to extension of microcracks in the rock at the time of subzero temperature.

Liu et al. (2006) study the triaxial compressive strength of sandstone at different temperatures and confining pressures. The experiment tests are only performed at three temperatures 20°C, -5°C and -10°C and each temperature corresponds four confining pressures 0, 4, 7 and 10 MPa. The triaxial compressive

strength increases with decreasing temperature. The cohesion (c) and inner frictional angle (ϕ) of rock increase with the decreasing of temperature from -20 to -10°C .

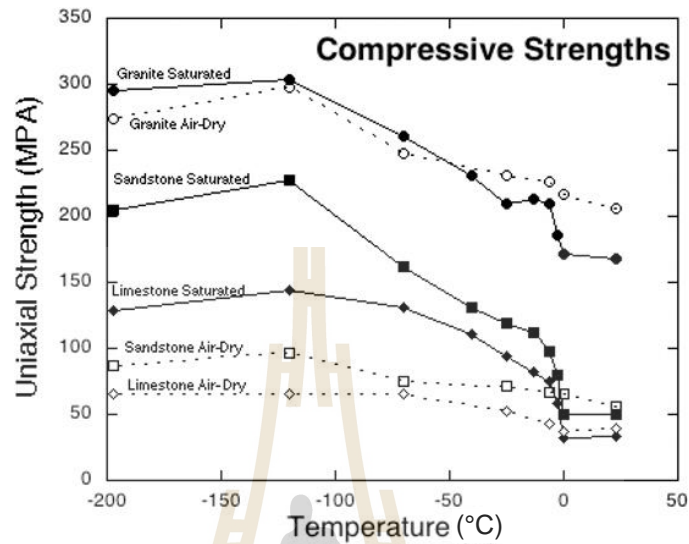


Figure 2.6 Strength of granite, limestone, and sandstone in uniaxial compression strength test (Mellor, 1971)

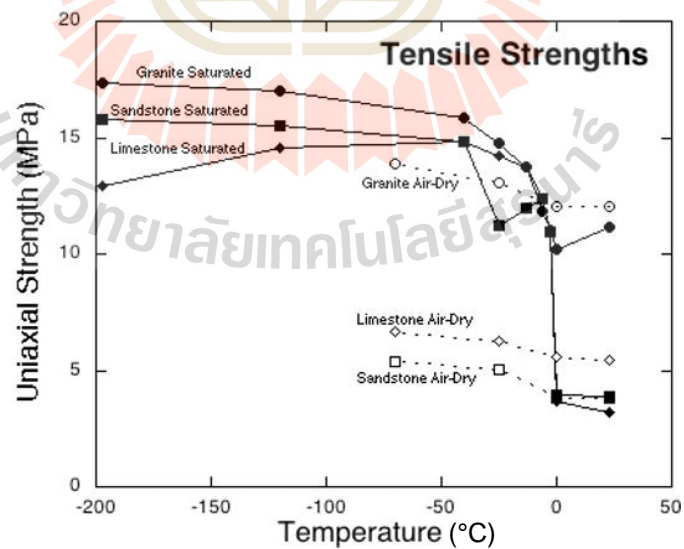


Figure 2.7 Strength of granite, limestone, and sandstone in tensile strength test (Mellor, 1971)

Yamabe and Neaupane (2001) indicate that strength increase in all of sandstone samples with subzero temperature that makes the Young's modulus of elastic increases, however at -10 to -20°C has no effects of Young's modulus of elastic (Figure 2.8). Inada and Kinoshita (2003) found that the change of Young's modulus with temperature is not seen in the dry rocks. However, saturated specimens the Young's modulus increases significantly with decreasing subzero temperatures.

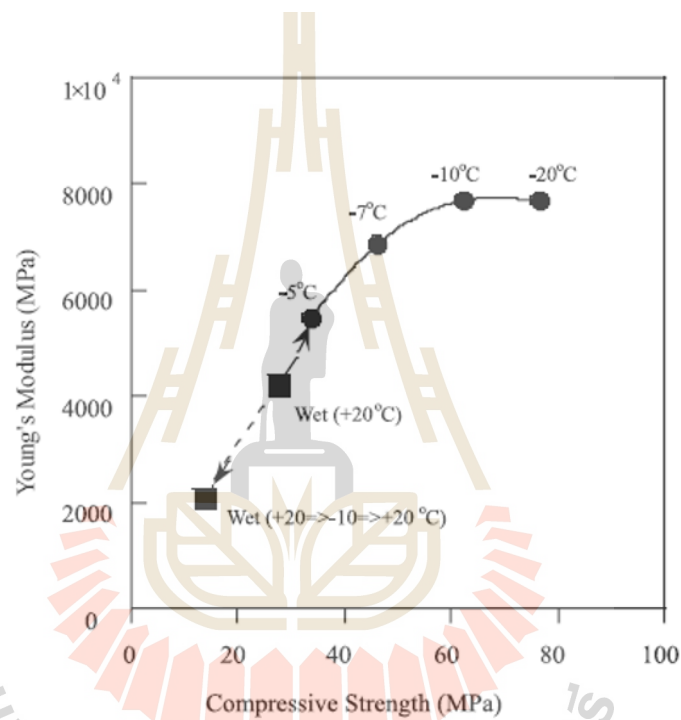


Figure 2.8 Summary of uniaxial test results for unfrozen and frozen sandstone (Yamabe and Neaupane, 2001)

2.3.1.2 Influence of temperature

The change of temperature has effects on the behaviors of the rocks. Inada et al. (1997) studies the strength and deformation characteristics of granite and tuff after undergoing thermal hysteresis of high and low temperature. The compressive and tensile strength of rocks decrease with the increasing number of thermal hysteresis. The values of Young's modulus and Poisson's ratio of after undergoing thermal hysteresis have the same tendency as those of the strength. Dwivedi et al. (2008) suggest the effect of high temperature on rocks lead to create of new microcracks or extension of pre-existing microcrack within the rocks. At the temperature drops to subzero that mineral grains shrink and the formation of ice on pore spaces contributed directly to the strength of rocks (Dwivedi et al., 1998). The strength increases with decreasing temperature that is evident temperature drop to -50°C (Mellor, 1971). Walder and Hallet (1985) predict the crack growth rates in porous granite and marble. The temperature between -4 to -15°C have most effective producing crack growth. Inada and Yokota (1984) studies the change of texture in rocks at difference temperature. At room temperature, the microcrack in the wet specimens are greater than dry specimens. At low temperature, the microcrack is grown because of the difference in shrinkage and expansive factors of the mineral particles. Nevertheless, the result of the strength test of rocks at low temperature increase about some 10-50% that relation to the strength at room temperature. It is concluded that these extending cracks do not cause complete specimen failure in the strength test.

2.3.1.3 Influence of water content

The effect of water on the rock strength have been studied by many researchers that increase in water content and the associated physic-mechanical change consequently lead to significant drop of about 80-90% in the strength of rock (Ergular and Ulusay, 2009). When water is combined with rock at subzero temperature it is likely that the behaviors of rock might be similarly affected depending on the degree of water saturation. Kodoma et al. (2013) investigate the uniaxial compressive and indirect tensile strength of two rock types under three different levels of water content at -20°C . It is found that the rock strength tended to increases with water content at the subzero temperature (Figure 2.9).

The test data of Mellor (1971, 1973) indicates that the saturated sample show the saturated samples show a stronger increase in strength than the dry samples at subzero temperature. Inada et al. (1997) and Inada and Kinoshita (2003) observe that at 15°C the strength for saturated rock samples is lower than that of the strength for dry samples. However, at -160°C the strength for saturated samples is greater than the dry strength due to the conversion of the water in the pores to ice. Hara et al. (2014) state the effect of water content on the deformation depend on rock type. They study the difference porosity of rock (welded tuff and sandstone) indicate that the higher porosity is sensitive with the water content than lower porosity. The deformation of welded tuff is more than that the deformation of sandstone (Figure 2.10).

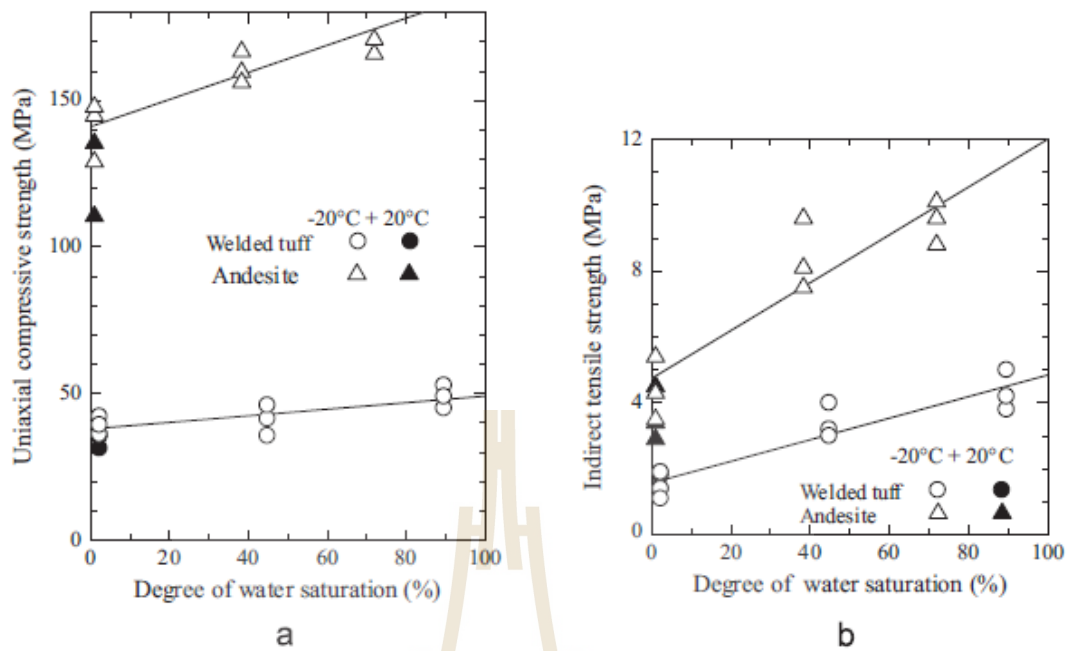


Figure 2.9 Uniaxial compressive strength (a) and indirect tensile strength (b) vs. degree of water saturation (Kodoma et al., 2013)

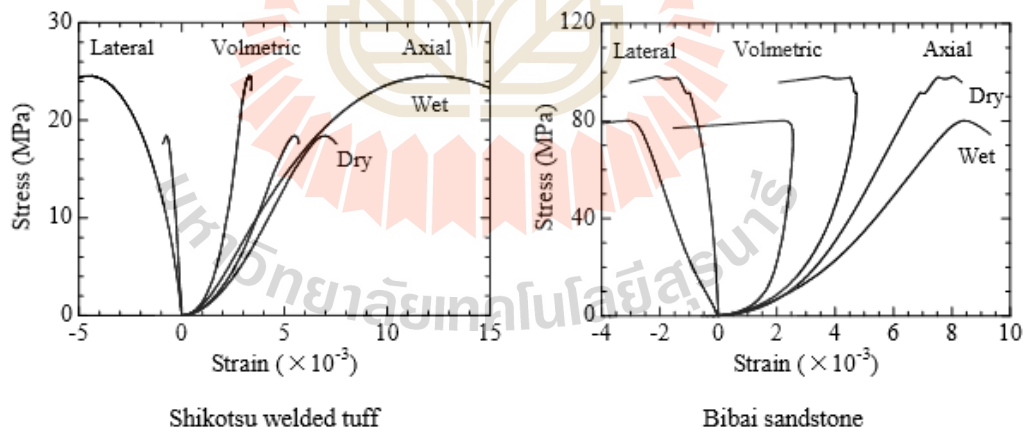


Figure 2.10 Examples of stress-strain curves of Shikotsu welded tuff and Bibai sandstone (Hara et al., 2014)

The pore water pressure is the impotent factor which affected on the strength and deformation of rock. Dasir et al. (2013) determine the effects of pore water pressure on the compressive strength and elastic properties of sandstones in Thailand. They found that the pore water pressure can significantly reduce the strength and elastic modulus up to 1-27% in the ambient temperature. Khamrat et al. (2016) observe the strength and deformability of low porosity rocks are more sensitive to the confining pressure than to the pore water pressure. When temperature drop to below 0°C water begins to freeze in rock. If the pore is filled with water during freezing will generate pressure. This pressure exceeds the microcrack occurs in the rock (Chan et al., 2004). However, the temperature drops to subzero about -20°C that stress concentration around cracks is reduced leads to strengths are increased in frozen rock because of the increase in the fracture initiation stress due to are duction in the stress concentration in the pores or interstitial spaces with in the rock (Kodama et al., 2013).

2.3.1.4 Influence of brine content

The effects of salinity brine on rock properties is still not completely understand. However, some researchers have investigated the physical and mechanical properties of the rocks from brine saturation. Shukla et al. (2013) investigate the mechanical behavior of two types of sandstone that are different in their lithology, mineralogy and texture. They define specimens for two types: specimen first type is the “S-type” sandstone, identified as feldspathic greywacke, composed of almost equal amount of matrix and quartz clasts with K-feldspar and tourmaline grains present in minor amount. The second type is of the “M-type”, identified as lithic greywacke. It is basically composed of quartz with minor amount of K-feldspar, plagioclase and tourmaline, while sericite, chlorite and muscovite make up the matrix.

The two types of sandstone in the NaCl brine. The uniaxial compressive strength values of saturated sandstone have been found to be far below 35 and 120 MPa compared to the dry strength of around 80 and 170 MPa for S-type and M-type sandstones. It is observed that the soft sandstone (S-type) is highly sensitive to moisture content and the mechanical properties change drastically with the change in NaCl concentration in the pore fluid. But the effect is lower in the stronger sandstone (M-type) whereas the stress-strain behavior seems unaltered. Saturation seems to play a significant role in reducing the strength of soft rock materials and the strength reduction could be up to about 80%. The change in strength of NaCl saturated sandstone can be because of the mineralogical interaction of the rock minerals and the salts present in the brine.

The detrimental effects of NaCl concentration on sandstone properties has been studied by Rathnaweera et al. (2014) found the sandstone saturated with higher percentages of NaCl solution (more 20% of NaCl) show an increase in the uniaxial compressive strength which compared to the water saturation. SEM analysis is used to identify the physical phenomenon in the sandstone saturated with NaCl solution. The data analysis observed that the pore fluid has a higher degree of salinity, there is a considerable number of NaCl crystals in the pore structure of rocks. The NaCl crystals probably improve the rock strength by reducing the number of voids. In contrast, the lower percentages of NaCl solution (10% of NaCl) do not exhibit any noticeable number of NaCl crystals in the pore structure. In addition to these, there has been studied the effect of brine in the soluble rock such as gypsum by Liang et al. (2012) indicates that the strength of gypsum soaked in 50% brine greater than 100% brine because chemical reaction happens between brine (NaCl solution) and gypsum (CaSO_4)

with product of Na_2SO_4 and CaCl_2 . This phenomenon is that pores or fissures in gypsum become opening from the chemical reaction.

2.3.1.5 Influence of ice content

The frozen rock has multiple structure that compound of rock mineral grains, ice, unfrozen water and gaseous components. The proportion relation of unfrozen water and ice in pore of rock are controlled by thermal of frozen rock. The change of unfrozen water and ice content are affect to physical and mechanical properties of rock that result in complex microscopic mechanical response. Liu et al. (2015) studies water and ice content of rock during freezing process. They use the CT scanning test divided frozen rock into three regions (unfrozen water, ice and rock mineral grains). The result is observed that the temperature drops to -5°C there is appear little unfrozen water that create fracture and pore are expand. After temperature decrease to -10°C , there is no unfrozen water and appear two phase mediums (ice and rock mineral grains) that the ice fill full in the pore media. The unfrozen water and ice content is a necessary indicator for thermal performance of frozen rock.

2.3.2 Mechanical properties soils

The mechanical behavior of frozen soil is affected by physical properties such as specimen homogeneity, grain size, moisture content and density. In the different location that the structure of soil is different compositions and structure. The mechanical properties of the frozen soils are as follows: compression strength and tensile strength, shear strength, creep strength and long-term strength, compressibility. The strength of frozen soil is dependent of temperature and time and is governed by cohesion of soil and internal friction of soil ice matrix system (Harris, 1995; Andersland

and Ladanyi, 2004). Several researches investigated the behavior of frozen soil to evaluate strength and deformation of natural and artificially frozen soils.

Parameswaran (1980) studies of deformation behavior and compressive strength of frozen sand as a function of strain rate and temperature. The experimental of samples is artificially frozen sand of uniform grain size and compositions. The cylindrical samples of frozen sand are prepared in a split Plexiglas mould by a method describe by Baker (1976). The specimens are frozen in the mould inside an insulated box with inside a cold room at -60°C . The test is carried out at a strain rate varying between 10^{-7} to 10^{-2} s^{-1} and temperature range -2 and -15°C . The following results indicate that strength and tangent modulus increases with increasing strain rates and decreasing temperatures. In this study suggest that deformation of frozen sand occurs by deformation of ice in soil between grains. In this study have a compare the results with some previous work on similar materials under similar condition that present in Table 2.2.

The three mechanisms control the strength of frozen soils; ice strength, soil strength, and interaction between the ice matrix and soil skeleton. The soil skeleton and ice matrix yield at different strengths when sheared in compression under low confining pressures (Ting, 1983). Andersland and Ladanyi (2004) consider the frozen soil stress-strain behavior is strongly affected by strain rate. For lower strain rates a sample exhibits plastic flow followed by small elastic deformation and as the strain rate increases the strength increases and failure mode changes from ductile to brittle. The soil strength dominates at larger strain rates influencing the long term frozen soil strength. The strain rate at which transition to brittle behavior occurs is higher for clays than gravels presumed due to the greater unfrozen water contents cohesive strength of

frozen soils increases with strain rate. The ice matrix under normal pressure and temperature is more rigid than the soil skeleton where it reaches peak strain under much lower strains.

Nater et al. (2008) determine strength of soils in terms of internal friction (ϕ) and cohesion (c) utilizing Mohr-Coulomb failure criterion. The laboratory tests are carried out on undisturbed samples of soils. In this study proposes that the correct parameterization with temperature dependent parameters such as the volumetric ice content. Because the strength of frozen soils depends on the temperature. This study observed that the angle of internal friction decreases with the volumetric ice content, however the cohesion increases with increasing ice content (Figure 2.11). The temperature has less influence on the friction angle of a frozen sample, than on the cohesion. The friction angle is decrease with subzero temperatures and the cohesion is increase significantly, especially in non-cohesive soils and very weak rock masses where the ice is bonding together the particles (Johansson, 2009).

Table 2.2 Strength of frozen sand at various strain rates and temperatures obtained by different authors (Parameswaran, 1979)

Authors	Temperature (°C)	Strain rate (s ⁻¹)	Maximum stress (MPa)	Soil type and test method
Sayles (1966)	-40	5.5×10^{-4}	38.9	Saturated Ottawa find sand (avg. grain dia. = 0.2-0.6 mm) (Stress independent of temp. below -50 °C)
	-50 to -186		35.9	
Sayles and Epanch (1966)	-3	3.33×10^{-4}	10.35 - 15.86	Saturated Ottawa find sand (avg. grain dia. = 0.2-0.6 mm)
	-6.5		13.79 - 20.69	
	-10		17.93 - 27.58	
	-30		28.96 - 48.27	
Sayles (1968)	-10	5.5×10^{-4}	17.44	Saturated Ottawa find sand (avg. grain dia. = 0.2-0.6 mm)
	-4.2		10.10	
	-1.7		9.0	
	-0.56		5.14	
Sayles (1974)	-3.85	1.67×10^{-5}	8 - 17	Saturated Ottawa find sand (avg. grain dia. = 0.2-0.6 mm)
		1.67×10^{-2}		
Goughnour and Andersland (1968)	-3.85	4.43×10^{-6}	5.38	Saturated Ottawa find sand (avg. grain dia. = 0.2-0.6 mm)
	-12	2.22×10^{-6}	8.27	
	-12	4.43×10^{-6}	9.38	
	-7.5	4.43×10^{-6}	7.59	
Alkire and Andersland (1973)	-12	4.43×10^{-6}	7	Saturated silica sand (avg. particle dia. = 0.6-0.84 mm) Constant load creep test
		$10^{-7} - 10^{-6}$	0.5 - 0.6	
Chamberlain et al. (1972)	-10	9.67×10^{-4}	24.55	Saturated Ottawa banding (dia. = 0.1-0.2 mm) under confining pressure of 3.5 MPa

Table 2.2 Strength of frozen sand at various strain rates and temperatures obtained by different authors (Parameswaran, 1979) (cont.)

Authors	Temperature (°C)	Strain rate (s ⁻¹)	Maximum stress (MPa)	Soil type and test method
Eckardt (1978)	-15	2.10 × 10 ⁻⁷ 9.72 × 10 ⁻⁷ 4.07 × 10 ⁻⁶ 1.53 × 10 ⁻⁵	4 6 7 8	Frozen medium sand (water content = 12%)
Parameswaran and Jones (1979)	-12	10 ⁻⁵ - 10 ⁻²	16 - 28	Saturated Ottawa find sand under confining pressure of 5 MPa
Parameswaran (results)	-2 -6 -10 -15	10 ⁻⁷ - 10 ⁻²	6 - 12.5 10 - 20 11.5 - 25 12 - 29	Saturated Ottawa find sand

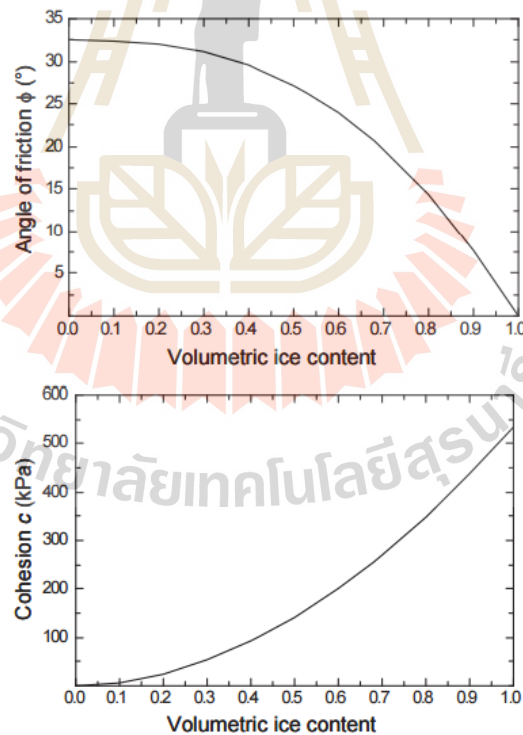


Figure 2.11 Variation of angle of friction and cohesion for frozen sand with low ice content (Nater et al., 2008)

Ma et al. (2016) investigate the effect of confining pressure on frozen soil. They found that the strength and strain energy gradually increase with the increase in the confining pressure. The variability of frozen sand is influenced significantly by confining pressure. The variability strength of frozen soil under confining pressure due to pressure melting of pore ice, particle crushing and microcrack growth. The strength of a frozen soil increases to a maximum value with increasing confining pressure but decreases beyond confining pressures of approximately 15-45 MPa (Wang et al., 2005). At confining pressures greater than 50 MPa, dilation is completely suppressed indicating crushing of individual soil particles. The pressure melting is suggested to become critical at these confining stresses given the suppression of dilation (Chamberlain, 1973).

2.3.3 Mechanical properties of ice

Ice has a crystalline structure. Ice crystals are cubic and belong to hexagonal. The crystals strength is different that is obtained by freezing of water at the different amorphous state under low temperature (Schulson, 1999). The behavior of mechanic properties of ice have three consecutive striges: elastic stage, plastic stage and brittle stage (Weinberg, 1938). The elastic stage of deformation is not depending on the time. The next stage is plastic stage that the deformation increases with the course of time. The stage three is brittle stage that the body of ice is break under action of external forces. The characteristics of three stages that related to the acting stress and the temporary deformation. Gold (1988) measured the elastic modulus and Poisson's ratio of the ice at a temperature of -10°C . The elastic modulus was range 9.7-11.2 GPa and Poisson's ratio was 0.29-0.32. The strength of ice has investigated by many researcher (Hooke et al., 1980; Jones, 1982; Schulson, 1999) in the temperature range

-10 to -20°C. The compressive strength of ice was range 5-25 MPa. The tensile strength was wide range from 0.7-3.1 MPa.

Many researchers have studied the mechanical properties of ice at functions of temperature, strain rate and grain size. These factors are importance of the elastic modulus and the strength of ice. The effects of temperature on strength on the compressive was more than the tensile strength (Hooke et al., 1980). This the strength increases with decreasing temperature was shown in Figure 2.12. The compressive strength was sensitive of the strain rate but, the tensile strength is not that represent in Figure 2.13. This suggest that the stress-strain curves of compressive is ductile behavior at low strain rate. At high strain rate, the behavior of compressive stress-strain curves is brittle (Schulson, 1999). The effect of grain size of ice on the mechanical properties that can observe remarkable in the tensile strength of ice. The tensile strength of ice decreases with increasing ice grain size diameter as shown in Figure 2.14. The reason of process is the propagation of micro-cracks that are nucleated by dislocation pile-ups against grain boundaries (Currier and Schulson, 1982). The mechanical behavior of ice exhibits a similarity to the mechanical behavior of brittle ceramics. However, ice strength and elastic properties are all significantly lower than ceramic materials (Petrovic, 2003).

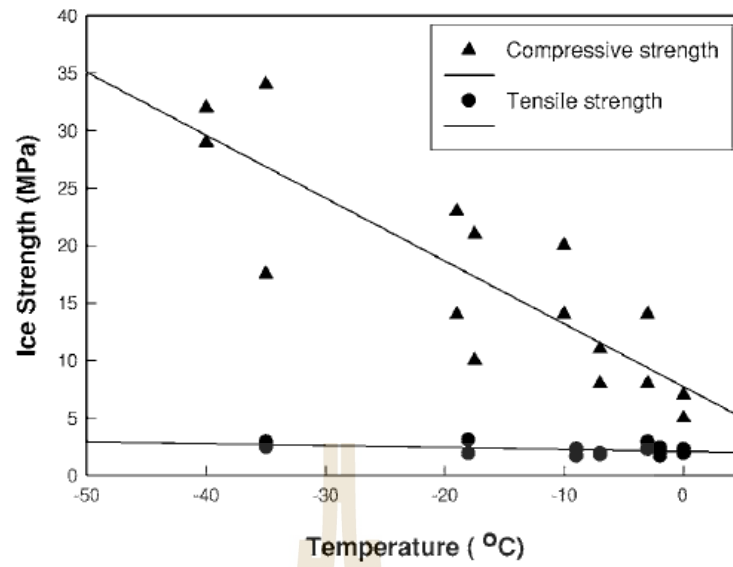


Figure 2.12 Tensile and compressive strength of ice as a function of temperature (Hooke et al., 1980)

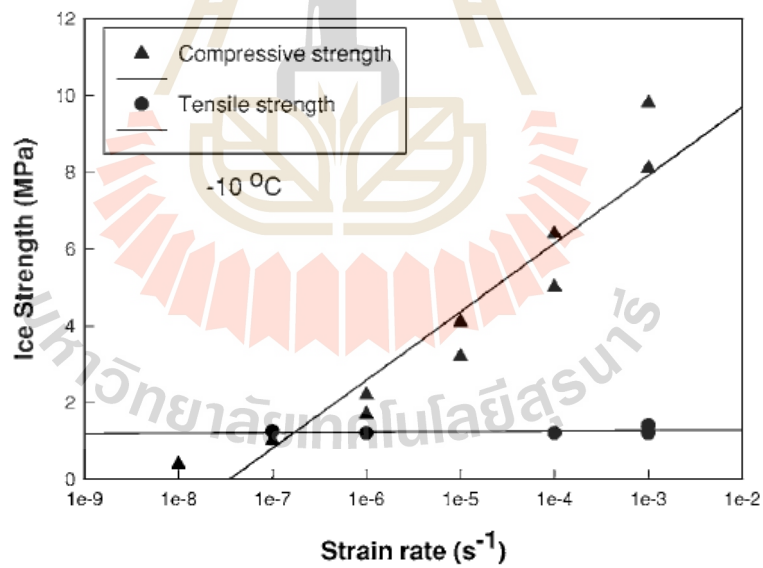


Figure 2.13 Tensile and compressive strength of ice as a function of strain rate (Schulson, 1999).

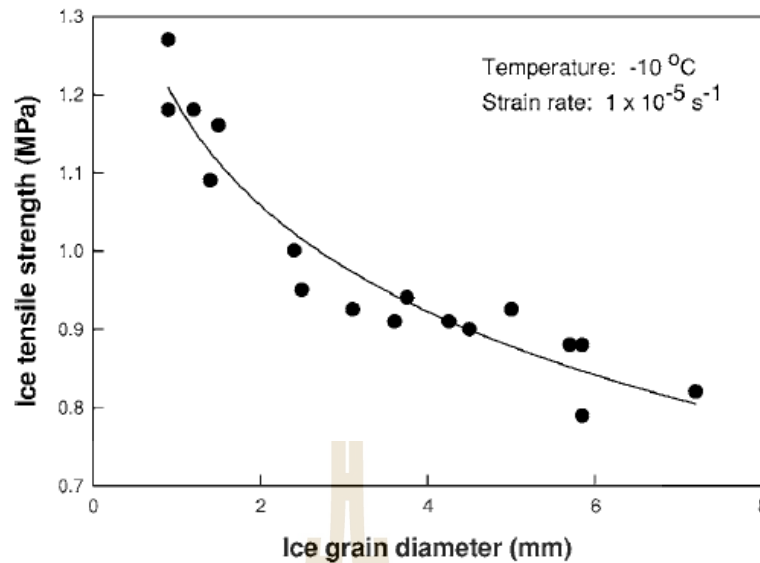


Figure 2.14 Tensile strength of ice as a function of grain size (Currier and Schulson, 1982)

2.4 Thermal properties

The thermal properties are important for thermal analysis. The basic thermal properties of materials are thermal conductivity, heat capacity and diffusivity. Thermal conductivity is defined as the rate of heat transfer. The ratio of the thermal conductivity over heat capacity is defined as thermal diffusivity. There one of thermal properties is defined as the quantity of the heat energy necessary to change the temperature of a unit mass. This is called specific heat capacity. The volumetric heat capacity is expressed on a unit volume mass. These properties can vary with compositions of materials. Some of the effective factors on thermal properties are temperature, materials type, water content, degree of saturation, dry density, organic contents (Jumikis, 1977).

2.4.1 Thermal conductivity

2.4.1.1 Influence of porosity and fluid content

The porosity and fluid content can affect the thermal conductivity of rock especially sedimentary rock (Cermak and Rybach, 1982). Several researchers have created the models for prediction of the effect of porosity and fluid content on the thermal conductivity. The mixing law models is the one equation that can be estimation of thermal conductivity of multicomponent systems (rock/fluid system). The mixing law models are combine by values of the thermal conductivities of the rock solids (λ_s) with the conductivity of the contained fluid (λ_f) on the basis of fractional porosity (ϕ) (Somerton, 1992).

Zimmerman (1989) suggested the mixing law model for predict the thermal conductivity of fluid saturated rock. The thermal conductivity is occurred in porosity and rock solid, there is equal probability of their occurring in series or in parallel.

The mixing thermal conductivity (λ_e) in series is given by

$$\lambda_e = \left[\frac{\phi}{\lambda_f} + \frac{1+\phi}{\lambda_s} \right]^{-1} \quad (2.1)$$

The mixing thermal conductivity (λ_e) in parallel is given by

$$\lambda_e = \phi\lambda_f + (1+\phi)\lambda_s \quad (2.2)$$

These two models were shown by Wiener (Zimmerman, 1989).

The models have the problem that they are physically unrealistic, since a body consisting of alternating slabs of solid and fluid material would possess no structural rigidity. However, there is also model of Hashin and Shtrikman (1962) that are tighter

than the series or in parallel. The model can be prediction of thermal conductivity of two phase system follow as:

$$\lambda_e = \lambda_s + \frac{3\lambda_s(\lambda_f - \lambda_s)\phi}{3\lambda_s + (\lambda_f - \lambda_s)(1 - \phi)} \quad (2.3)$$

and

$$\lambda_e = \lambda_s + \frac{3\lambda_f(\lambda_s - \lambda_f)(1 - \phi)}{3\lambda_f + (\lambda_s - \lambda_f)\phi} \quad (2.4)$$

Woodside and Messmer (1961) propose the mixing law models that is the weighted geometric mean model given by:

$$\lambda_e = \lambda_s \left(\frac{\lambda_f}{\lambda_s} \right)^\phi \quad (2.5)$$

Best example of mixing-law models is the dispersive or extended Maxwell model which is the direct analogue of electrical case and having firm physical basis (Beck, 1976). It is expressed as:

$$\lambda_e = \lambda_s \left[\frac{\left(\frac{2\lambda_s}{\lambda_f} - 1 \right) - 2\phi \left(\frac{\lambda_s}{\lambda_f} - 1 \right)}{\left(\frac{2\lambda_s}{\lambda_f} + 1 \right) - \phi \left(\frac{\lambda_s}{\lambda_f} - 1 \right)} \right] \quad (2.6)$$

This model is based on the physically real situation where spheres of thermal conductivity of fluid are dispersed in a medium of thermal conductivity of solid.

2.4.1.2 Influence of mineral content

Sundberg (1998) suggests that different mineral distributions can result in totally different thermal conductivities of both rock and soil. However, minerals have a much higher effect on the thermal conductivity of a rock than on the conductivity of soil. The thermal conductivity of some common rock forming minerals is shown in Table 2.4. The thermal conductivity of crystalline rock can be calculated from the mineral content with rather high accuracy. Sedimentary rocks are depended on the porosity of the rock. The values of the thermal properties of sedimentary rocks calculated on assumed porosity and mineral content that is showed in Table 2.3.

Table 2.3 Thermal conductivity of some common rock forming minerals (Sundberg, 1998)

Mineral	Thermal Conductivity (W/(m K))
Quartz	7.7
Microcline	2.5
Plagioclase (dependent on the fraction of anorthite)	1.9 (mean value)
Biotite	2.0
Muscovite	2.3

2.4.1.3 Influence of temperature

Clauser and Huenger (1995) reviewed the empirical relationship for the thermal conductivity at elevated temperature from previous work. Zoth and Hänel (1998) suggest a relationship follow:

$$\lambda(T) = A + \frac{B}{350 + T} \quad (2.7)$$

where λ is the thermal conductivity (W/mK), T is temperature (°C) and A and B are empirical constants from a least-squares fit to measured data for different rock types can be represent in Table 2.4.

Buntebarth (1991) determine the linear relationship between λ and temperature from measurements on 113 samples of metamorphic rock at temperature range 50-200 °C follow as:

$$\frac{1}{\lambda(T)} = D + E \cdot T \quad (2.8)$$

where D and E determined for gneiss are $D = 0.16 + 0.03 \text{ mKW}^{-1}$ and $E = 0.37 + (0.14 \times 10^{-3}) \text{ mW}^{-1}$. and $D = 0.33 + 0.03 \text{ mKW}^{-1}$ and $E = 0.22 + (0.14 \times 10^{-3}) \text{ mW}^{-1}$ for metabasite.

Sass et al. (1992) propose the empirical relationship at temperature range 0-250°C for crystalline rock.

$$\lambda(T) = \frac{\lambda(0)}{1.007 + \left(0.0036 + \frac{0.0072}{\lambda(0)}\right)} \quad (2.9)$$

where $\lambda(0) = \lambda(25) \cdot 1.007 + 25 \left(0.0036 - \frac{0.0074}{\lambda(0)}\right)$,

$\lambda(25)$ is the measured room temperature thermal conductivity

For the sedimentary rocks, Kutas and Gordienko (1970) propose the empirical formulation for estimating the thermal conductivity at temperature 300°C.

$$\lambda(T) = \lambda(20) - [\lambda(20) - 3.3] \cdot \left[\exp\left(0.725 \cdot \frac{T - 20}{T - 130}\right) - 1 \right] \quad (2.10)$$

where $\lambda(20)$ is the thermal conductivity coefficient at 20°C

2.4.2 Heat capacity

2.4.2.1 Influence of porosity and fluid content

The thermal capacity of rock is calculated as a Kopp's Law that the weighted average of the thermal capacities of the various solids and liquids (Somerton, 1992 and Hurst and Harrison, 1992). The correlation follows the general format:

$$C = \sum_{i=1}^N (N_i C_i) \quad (2.11)$$

where C_i is specific heat capacity of each component, N_i is mass of the rock weighted by the volume fraction of the N individual phases relative to the total rock volume.

Table 2.4 Empirical constants A and B for different rock types (after Zoth and Hänel, 1998)

Rock type	T (°C)	A	B
(1) Rock salt	-20-40	-2.11	2960
(2) Limestone	0-500	0.13	1073
(3) Metamorphic rock	0-1200	0.75	705
(4) Acid rock	0-1400	0.64	807
(5) Basic rock	50-1400	1.18	474
(6) Ultra-basic rock	20-1400	0.73	1293
(7) Rock type (2) through (5)	0-800	0.70	770

Waples and Waples (2004) give a relation for the thermal capacity of a mixture of solids and liquids as the weighted average of the thermal capacities of the component solids and liquids:

$$c_{p,rock} = \frac{\rho_{solid} c_{p,solid} (1 + \phi) + \rho_{water} c_{p,water} \phi}{\rho_{rock}} \quad (2.12)$$

where ϕ is the fractional porosity, ρ_{solid} is the average solid density, ρ_{water} is the density of water, ρ_{rock} is the density of the rock, and $c_{p,solid}$ and $c_{p,water}$ are the mean specific heat capacity of the solid and the specific heat capacity of the water respectively.

2.4.2.2 Influence of mineral content

The mineral composition also tends to control the heat capacity of rocks. The heat capacities of sedimentary rocks are typically lower than the heat capacities of crystallized rocks. Due to the sedimentary rocks are contained heavy metals (sulfides, silver halides, tungstates, some oxides and carbonates). Waples and Waples (2004) compiled an extensive database of heat capacities for the minerals. For low and medium density minerals ($\rho \leq 4.0 \text{ g/cm}^3$) they derived a predictive relationship between mineral density and thermal capacity at 20 °C:

$$c_{p,mineral} = 1.0263 \exp(0.2697 \rho_{mineral}) \quad (2.13)$$

where $\rho_{mineral}$ is mineral density (g/cm^3)

2.4.2.3 Influence of temperature

Heat capacity refers to the energy required to increase the temperature of a mass unit of one degree. When the temperature of material increases, this heat is stored in the material's molecules in the form of higher translational, rotational, and vibrational energies the researchers have measured values of heat

capacity and their temperature dependencies should be expressed mathematically. A polynomial equation is used to describe the temperature dependency of the heat capacity of minerals and rocks (Waples and Waples, 2004):

$$c_p = A + BT + CT^2 \quad (2.14)$$

For sandstones, the constants A, B, and C are 2.05, 0.00381, and 3.55, respectively and T is temperature (K).

2.4.3 Thermal properties of rocks in Thailand

Phueakphum (2008) determine the specific heat and thermal conductivities of rock and soil that are found in Thailand. The rock samples were categorized into six group include four sandstones, three granites, two rock salt, marble, limestone and basalt. The four sandstones had Phu Kradung Sandstone, Phu Phan Sandstone, Phra Wihan Sandstone and Sao Khua Sandstone. The result of this study shows in Table 2.5. They found that basalt is highest specific heat value and rock salt is highest thermal conductivities. In this study suggested that the thermal conductivity and heat capacity of rock tend to be independent of their density because rocks contain various mineral compositions that is each mineral show difference in thermal properties.

Table 2.5 Thermal properties of rocks and soil (after Phueakphum, 2008)

Rock type	Density (g/cm ³)	Thermal Conductivity (W/(m K))	Heat Capacity (J/(m ³ K))
Compacted Soil	-	1.19 ± 0.00	2.43 ± 0.01
Saraburi Marble	2.58	3.01 ± 0.00	2.91 ± 0.05
Burirum Basalt	2.81	1.70 ± 0.05	3.30 ± 0.71
Lopburi Limestone	2.64	2.93 ± 0.00	2.54 ± 0.01
Phu Kradung Sandstone	2.54	4.02 ± 0.01	1.80 ± 0.03
Phu Phan Sandstone	2.26	2.69 ± 0.01	2.00 ± 0.04
Phra Wihan Sandstone	2.33	3.75 ± 0.00	1.77 ± 0.02
Sao Khua Sandstone	2.33	2.06 ± 0.01	1.79 ± 0.02
Chinese Granite	2.64	3.16 ± 0.00	1.69 ± 0.01
Tak Granite	2.62	2.84 ± 0.00	2.21 ± 0.01
Vietnamese Granite	2.62	3.26 ± 0.00	2.04 ± 0.03
Middle Salt	2.16	5.80 ± 0.01	1.83 ± 0.01
Lower Salt	2.19	5.51 ± 0.01	2.54 ± 0.01

2.5 Heat transfer

2.5.1 Modes of heat transfer

Heat transfer is an energy in transition due to temperature differences that heat flow from high temperature to low one. In the study of heat transfer extends is the fundamental process of the thermodynamic (Long and Sayma, 2009). The modes of heat transfer though the development of relations used to calculate heat rate. The different types of the heat transfer are usually referred to as the modes of heat transfer. There are three of these: conduction, convection and radiation (Figure 2.15).

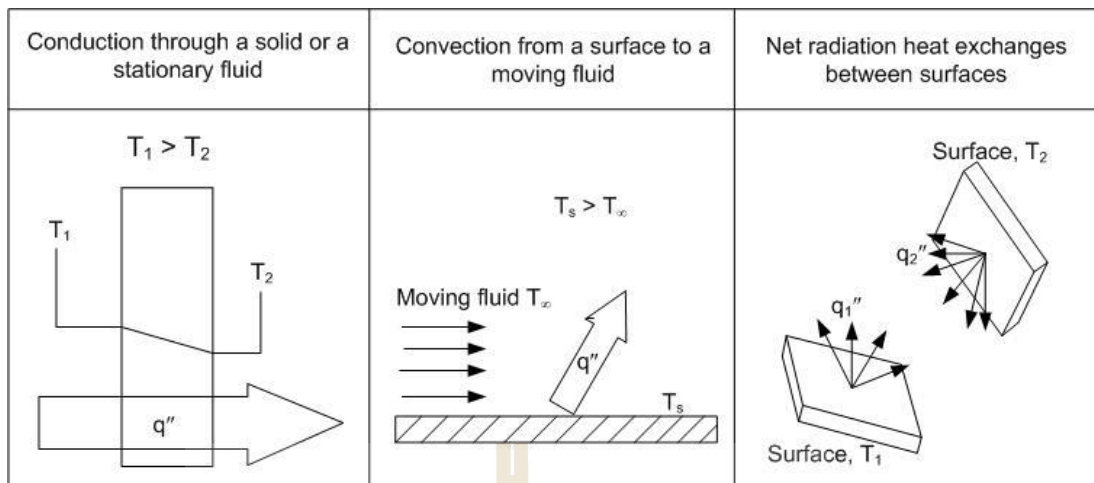


Figure 2.15 Modes of heat transfer: conduction, convection and radiation (after Long and Sayma, 2009)

Conduction is the energy transfer across a system boundary due to temperature difference by transfer of vibrational energy from one molecule to another which can be solid or fluid. The quantify heat transfer processes is the terms of appropriate rate equations. These equations may be used to calculate the amount of energy being transferred per unit time. For heat conduction, the rate equation is known as Fourier's law. The general rate equation is based on much experimental evidence.

$$q = -kA_h\Delta T \quad (2.15)$$

where q is heat flow vector, (W), k is thermal conductivity (W/m K) (a thermodynamic property of the material), A_h is cross sectional area in direction of heat flow. (m^2) and ΔT is gradient of temperature (K/m) in direction.

Convection is energy transfer by convection arises from the mixing of elements of fluid. The mixing of fluid occurs as a result of density differences when the liquid is heated from below that process is known as natural convection. The mixing

of fluid results from eddy movement in the fluid which fluid flows through a pipe heated on the outside that called forced convection. The heat transfer by convection is described by the Newton's law of cooling.

$$q = hA_h(T_s - T_\infty) \quad (2.16)$$

where q is heat transfer rate (W), h is a heat transfer coefficient ($\text{W}/\text{m}^2 \text{K}$), T_s is surface temperature (K) and T_∞ is free stream fluid temperature (K).

Radiation heat transfer involves the transfer of heat by electromagnetic radiation that arises due to the temperature of the surface. The radiation falls on surface it may be absorbed, pass through or reflect off of the surface. The equation for emissivity is derived from Stefan Boltzmann law which describes for the net transfer from an idealized body (Black body). A black body is an ideal object that does not reflect radiation or let energy pass through. It absorbs all incident radiation and re-emits thermal energy at a rate dependent on the black body that not the incident radiation that heats it.

$$q = \sigma \varepsilon T_s^4 \quad (2.17)$$

where ε is emissivity which is a surface property ($\varepsilon = 1$ is black body), σ is Steffan Boltzman constant = $5.67 \times 10^{-8} \text{ (W}/\text{m}^2 \text{ K}^4)$ and T_s is absolute temperature of the surface (K).

2.5.2 Heat transfer for ground freezing

The heat transfer for ground freezing is studied between pipe components and between the pipe and surrounding ground. In the freeze pipe is separated two components that the downpipe and annulus. Vitel et al. (2015) propose that the modes of heat transfer during ground freezing method. The pipe that filled with coolant fluid is had the heat conduction and convection. However, in pipe encountered flow rate of fluid with this reason the conduction within the fluid is negligible compared to convection. The heat transfer at the ground surrounding pipe is had the heat conduction from ground into the pipe. Therefore, consider of the modes of heat transfer during ground freezing is the convection modes in the freeze pipes and the conduction between surrounding ground and pipes.

In the freeze pipe of ground freezing that consider the heat convection in the cylindrical shape. The fluid is flow in freeze pipe that is the forced convection. Because circulating currents are produced by an external agency as a result of turbulent flow in a pipe. In general, the magnitude of the circulation in forced convection is greater and higher rates of heat transfer are obtained than in natural convection (Sinnott, 1993). The heat convection can be calculated by Newton's law of cooling. The many factors influence the value of heat transfer coefficient (h) that is almost impossible to determine their individual effects by direct experimental methods. It is found that the heat transfer rate per unit area (q) is dependent on those physical properties which affect flow pattern that viscosity (μ) and density (ρ), the thermal properties of the fluid that the specific heat capacity (c_p) and the thermal conductivity (k), linear dimension of the surface (L), the velocity of flow (u) of the fluid over the surface, the temperature difference (ΔT) There can be relate in equation

$$\frac{qL}{k\Delta T} = \frac{hL}{k} = f \left[\left(\frac{Lu\rho}{\mu} \right) \left(\frac{C_p\mu}{k} \right) \right] \quad (2.18)$$

and

$$Nu = f [Re, Pr] \quad (2.19)$$

This equation takes the form of simple power law.

$$Nu = C Re_L^m Pr^n \quad (2.20)$$

where Re is Reynolds number $\left(Re = \frac{Lu\rho}{\mu} \right)$,

Pr is Prandtl number $\left(Pr = \frac{\mu C_p}{k} \right)$ and C, m and n are constant.

$$Nu = \frac{hL}{k} \quad (2.21)$$

where Nu is Nusselt number, L is characteristic length and k is thermal conductivity of object in fluid.

Notes: - Reynolds number is the ratio of inertia and viscous forces.

- Prandtl number is the ratio of moment diffusivity to thermal diffusivity.

- Nusselt number is the ratio of conductive to convective thermal resistance.

The modes of heat transfer between the surrounding ground and freeze pipe is had the heat conduction. The conduction equation is to derive analytical solutions in the cylindrical shape that solution by Fourier's law equation. The heat

transfer of convection is considered in detail for the flow of heat through a wall pipe that have thickness. In the condition for ground freezing is consider under the temperatures on the inside and outside are constant. The heat flow is proportional to the radius and hence the temperature gradient is inversely proportional to the radius.

$$q = -k2\pi rL \frac{dT}{dr} \quad (2.22)$$

where q is heat flow, L is the length of tube, T is temperature and r is a radius of pipe.

Integrating between the limits r_1 and r_2 :

$$q \int_{r_1}^{r_2} \frac{dr}{r} = -k2\pi L \int_{T_1}^{T_2} dT \quad (2.23)$$

or

$$q = \frac{k2\pi L(T_1 - T_2)}{\ln(r_2/r_1)} \quad (2.24)$$

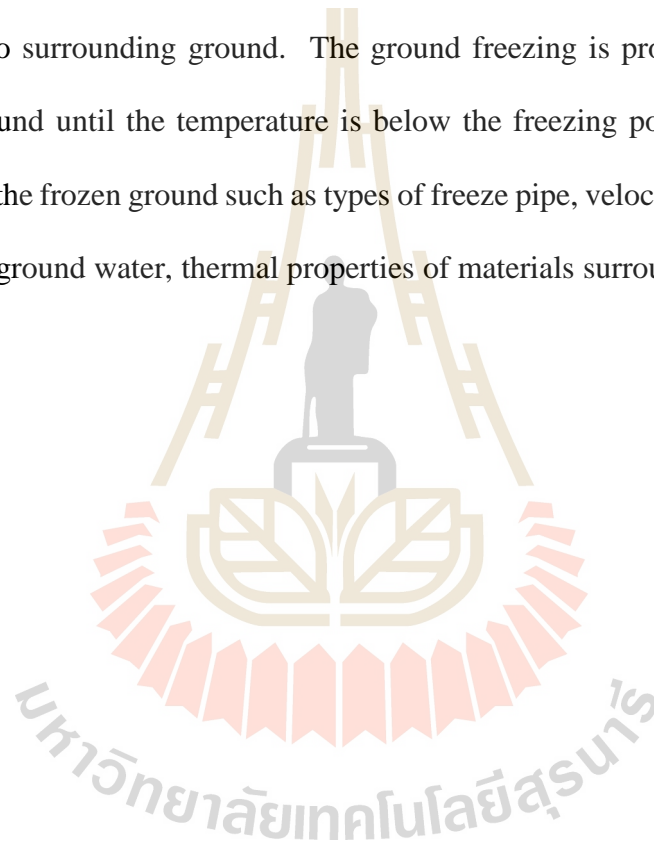
On addition

$$q = \frac{k(2\pi r_m L)(T_1 - T_2)}{r_2 - r_1} \quad (2.25)$$

where $r_m = (r_2 - r_1) / \ln(r_2 / r_1)$ is known as the logarithmic mean radius.

2.6 Numerical simulation for ground freezing

The numerical simulation of the heat transfer during ground freezing is based on equation from modes of heat transfer. Many researches have been selected the finite difference (FDM) and finite element method (FEM) to solution of heat transfer process in the ground freezing (Ou et al., 2009, Kim et al., 2012 and Zhou and Meschke, 2014). The numerical simulation is the simple method to predict the heat transfer problem from freeze pipe to surrounding ground. The ground freezing is process for remove heat from the ground until the temperature is below the freezing point. Many factors are influence on the frozen ground such as types of freeze pipe, velocity of coolant, seepage velocities of ground water, thermal properties of materials surrounding etc.



CHAPTER III

SAMPLE PREPARATION

3.1 Introduction

The rock samples selected for testing are the sandstone, which are obtained from Phara Wihan formation in northeast Thailand (hereafter designated as Phara Wihan sandstone). This rock is commonly found in the northeast of Thailand. Phueakphum (2008) gives the detailed descriptions of the sandstone. It can be classified as fine-grained sandstone with well sorted. These sandstones are highly uniform texture and density. The color is brownish white with scattered black. The sandstone is composed mostly of quartz and feldspar with minor micas. These brittle sandstones are medium strong.

3.2 Sample preparation

Sample preparations are carried out in the laboratory at the Suranaree University of Technology (SUT). The sandstone specimens are drilled and cut from a rock block in a cylindrical shape (Figure 3.1). The sandstone samples sizes are different for each purpose. For compressive strength test, the cylinder specimens are prepared with 54 mm in diameter and 108 mm in length ($L/D = 2.0$). Brazilian tensile strength is determined on the cylindrical shape samples with 54 mm in diameter and 27 mm in length ($L/D = 0.5$). Preparations of these samples follow the American Society for Testing and Materials (ASTM D7012, D2664 and D3967) as closely as possible (Figure3.2). The specimens are prepared to test under dry and saturated conditions with water and brine.

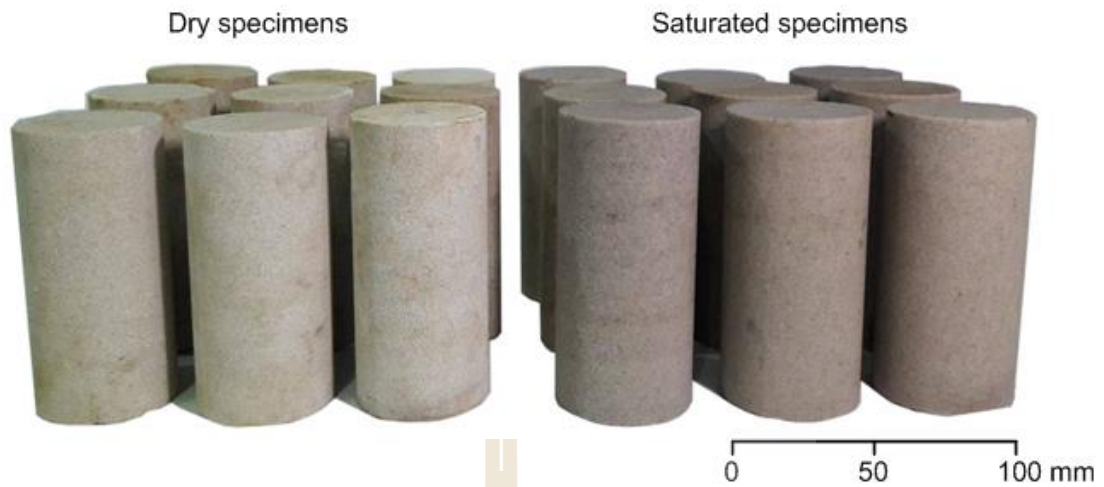


Figure 3.1 Some specimens of Phara Wihan sandstone under dry and saturated conditions in the cylindrical shape

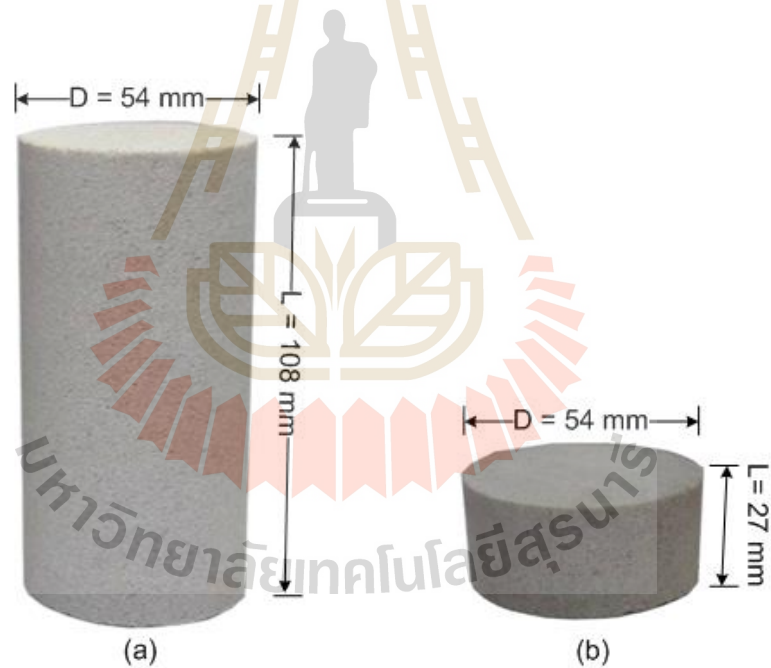


Figure 3.2 Examples of sandstone specimen prepared for compressive strength test
(a), Brazilian tensile strength test (b)

Under dry condition, the specimens are left to air dry at ambient temperature for a minimum of two weeks. Under saturated conditions, the sandstone specimens are fully submerged in water and brine. To do this, the specimens are submerged in water and brine using a pressure vacuum chamber for more than two weeks. The average physical properties of the sandstone samples are shown in Table 3.1.

The saturated contents (water and brine contents) are determined by using the ASTM (D2216) and calculated from the following equation:

$$w = \left[\frac{(m_w - m_s)}{m_s} \right] \times 100 \quad (3.1)$$

where w is the water content; m_w is the weight of the moist specimen, and m_s is the weight of the dry specimen.

The effective porosity is determined by using the ASTM (C830) and calculated from the following equation:

$$n = \left[\frac{(W - D)}{V} \right] \times 100 \quad (3.2)$$

where n is porosity, W is the saturated water weight, D is the dry weight, and V is the total bulk volume of the specimen.

The thermal properties of Phara Wihan sandstone are measured by Phueakphum (2008). The thermal constants analyzer (hot disk) is used to determine the thermal properties. The results for thermal properties are summarized in Table 3.2. The thermal properties of sandstone are the data base of calculation the thermal properties mixing

rock and fluid and will be input into computer simulation program for predict heat transfer.

Table 3.1 Physical properties of Phara Wihan sandstone

Physical Properties	Average
Dry density, ρ_d (g/cm ³)	2.26 ± 0.08
Saturated water density, ρ_w (g/cm ³)	2.38 ± 0.04
Saturated brine density, ρ_b (g/cm ³)	2.41 ± 0.03
Saturated water content, w_w (%)	4.97 ± 0.38
Saturated brine content, w_b (%)	6.13 ± 0.45
Effective porosity, n (%)	11.01 ± 1.01

Table 3.2 Thermal properties of Phara Wihan sandstone (after Phueakphum, 2008)

Properties	Average
Density, ρ (g/cm ³)	2.33 ± 0.00
Thermal diffusivity (mm ² /s)	2.11 ± 0.18
Thermal conductivity (W/mK)	3.75 ± 0.00
Specific heat (MJ/m ³ K)	1.77 ± 0.28

CHAPTER IV

MECHANICAL LABORATORY TESTING

4.1 Introduction

The laboratory testing is divided into three groups including the uniaxial compressive strength test, the triaxial compressive strength test and the Brazilian tensile strength test. The rock strengths and elasticity are determined in the laboratory under various confining pressures varying from 0, 3, 7 and 12 MPa and temperature of 233, 253, 268 and 298 Kelvin. The specimens are conducted test under dry condition and saturated conditions by water and brine. The temperatures effect on strength results is analyzed to evaluate the surrounding of ground freezing method. The freeze-thaw cycle is also conducted to examine microstructure changes in rock specimens by measuring the inducing of the porosity.

4.2 Test method

4.2.1 Freezing method

The sandstone specimens of all conditions (dry, water-saturated and brine-saturated) are tested under lower temperature. The specimens of all conditions are wrapped in low-density polyethylene to prevent any moisture loss. The low temperature specimens are kept in refrigeration for 24 hours to cool down, then are exposed to coolant (liquid nitrogen, LN₂) for protecting the specimens from thermal shock. The temperature is measured using a thermocouple. The changes of specimen

temperatures between before and after testing are less than 5 Kelvin. As a result, the specimen temperatures are assumed uniform and constant with time during the mechanical testing.

4.2.2 Uniaxial and triaxial compressive strength tests

The uniaxial and triaxial compression tests are performed to determine the compressive strength and deformation of dry, water-saturated and brine-saturated sandstone specimens under various confining pressure and lower temperature. A compression load frame is used to apply axial stress and conventional triaxial (Hoek) cell is used to apply confining pressure on the specimens (Figure 4.1). For this study, the conventional triaxial cell is frozen in the refrigerator before testing in order to keep temperature during installation of the samples and testing. The confining pressure ranges from 0, 3, 7 to 12 MPa, and the constant axial stress rate of 0.1 MPa/s is applied until failure occurs. Testing of the sandstone is done on specimens with temperatures ranging from 233, 253, 268 and 298 Kelvin. The specimen installation, equipment setup, and loading are completed within 5 min. The test is started by increasing the axial stress at the constant rate using the hydraulic pump. Both the axial strain and lateral strain are recorded by a dial gage during the test.

4.2.3 Brazilian tension test

The Brazilian tensile strength test is conducted to determine the indirect tensile strength of the specimens. Ten specimens of dry and saturated sandstone are tested under temperatures ranging from 233, 253, 268 and 298 Kelvin. The compression load frame is used. The diametrical load is applied to the specimen. The cylindrical surfaces are free from obvious tool marks and any irregularities across the thickness of

the specimen. The constant stress rate is maintained about 0.1 MPa/s. The load is applied until failure which normally occurs under 2 minutes.

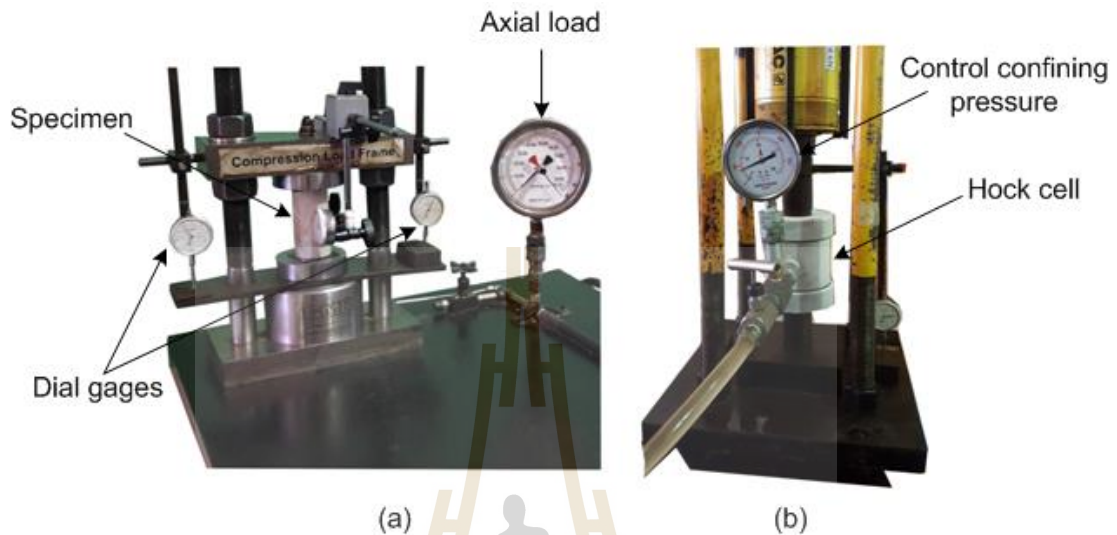


Figure 4.1 Test setup for (a) uniaxial compression test and (b) triaxial compression test using compression loading device

4.3 Test result

The compressive strengths of dry, water-saturated and brine-saturated sandstones are determined under the temperatures of 233, 253, 268 and 298 Kelvin and confining stresses of 0, 3, 7 to 12 MPa. Some post-test specimens of dry and saturated conditions show shear failure mode in the confining pressure and the specimens without confining pressure display the longitudinal failure mode (Figure 4.2). Table 4.1 shows the average of compressive strength results. The effects of the confining pressure on the compressive strength of the specimens can be observed from the σ_1 - σ_3 diagrams, as shown in Figure 4.3. The compressive strength tends to increase with the confining pressure in all temperatures. The specimens with lower temperature show higher strengths than those with higher temperatures in both the dry and saturated conditions.

At high temperature, the strength of dry condition is higher than the strength of saturated with water and brine condition. The brine saturated conditions are the highest strength at the low temperature. It is observed that the effect of temperature on strength in saturated with water and brine conditions are greater than dry condition at the subzero temperature.

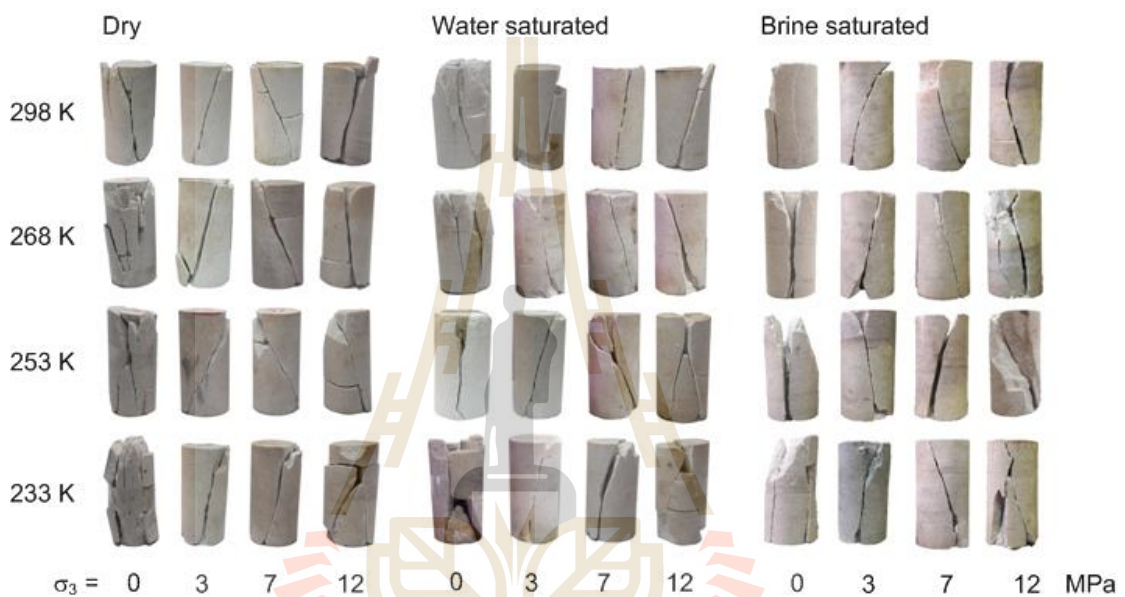


Figure 4.2 Some post-test specimens obtained from compressive strength testing under different confining pressures (σ_3) and temperatures in difference conditions

Table 4.1 Compressive strengths of Phara Wihan sandstone

Temperature (Kelvin)	σ_3 (MPa)	Dry		Water-saturated		Brine-saturated	
		σ_1 (MPa)	SD	σ_1 (MPa)	SD	σ_1 (MPa)	SD
233 (-40°C)	0	90.53	2.48	115.20	2.67	126.42	1.40
	3	113.58	2.68	143.40	3.31	148.89	1.64
	7	143.62	1.95	167.08	4.50	175.13	2.57
	12	175.96	5.89	189.77	3.85	206.21	3.86
253 (-20°C)	0	77.71	2.59	96.59	3.13	101.44	1.29
	3	104.91	3.82	114.36	3.51	118.96	1.12
	7	134.24	3.47	142.85	4.31	148.99	3.60
	12	163.82	2.42	173.99	6.35	183.90	2.13
268 (-5°C)	0	72.02	1.89	69.49	1.97	72.31	1.79
	3	92.04	2.43	88.22	3.06	92.52	2.03
	7	121.73	3.56	116.92	3.40	123.47	1.80
	12	154.58	4.83	148.60	3.74	156.60	3.35
298 (25°C)	0	68.75	1.54	60.93	2.34	65.28	1.04
	3	86.28	1.60	77.48	2.02	82.27	1.26
	7	116.82	4.66	108.68	2.34	111.73	2.35
	12	152.13	1.35	136.39	3.77	143.84	2.98



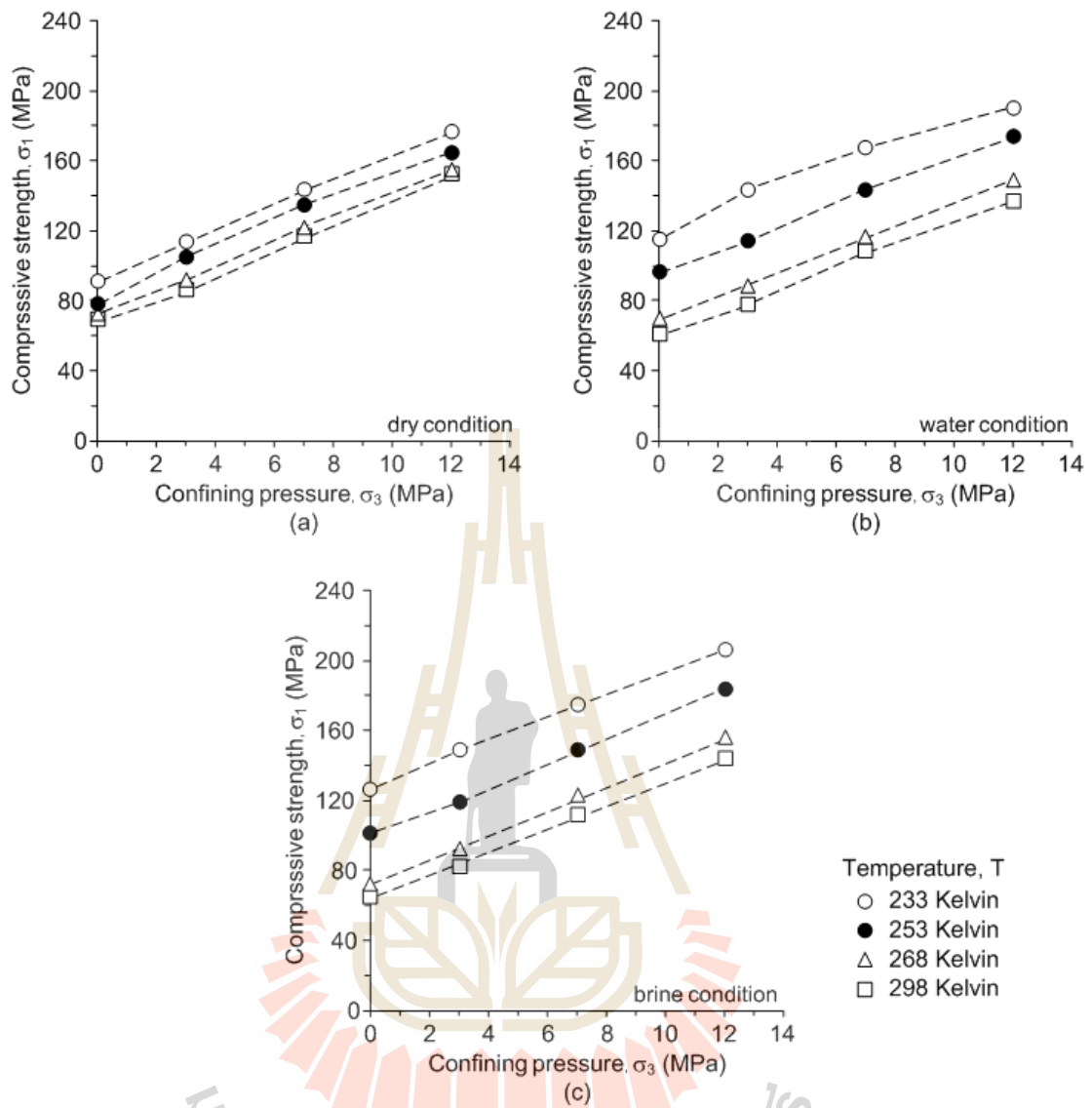


Figure 4.3 Principal stresses at failure as a function of confining pressure for dry (a), water-saturated (b) and brine-saturated (c) conditions

The Brazilian tensile strength of the sandstone has been determined from disk specimens with temperatures ranging from 298 Kelvin freeze down to 233 Kelvin under difference conditions. The results of average tensile strength are shown in Table 4.2 and the results of all specimens can be seen in Appendix C. The tensile strengths increase with decreasing temperatures of all conditions (Figure 4.5). The initially tensile strength of the saturated specimens (saturated with brine and water) are lower than dry specimens due to the inducing pore fluid pressure. More discussion are drawn in Chapter VII. When temperature are lower than 253 Kelvin, the tensile strength of saturated specimens are greater than that of dry specimens. The increase in strength of saturated samples under this temperature conditions (less than 253 Kelvin) because of the pore-water change to ice and its strength increases as temperature decrease. The tensile strength of brine saturated condition is higher than water saturated condition but not much. It seems that brine is not affect to the tensile strength of sandstone specimen.

Table 4.2 Tensile strength of Phara Wihan sandstone

Temperature (Kelvin)	Dry		Water saturated		Brine saturated	
	σ_B (MPa)	SD	σ_B (MPa)	SD	σ_B (MPa)	SD
233	7.80	0.81	9.00	1.29	9.58	0.57
253	6.94	0.74	7.08	0.54	7.56	0.55
268	6.55	0.77	5.44	0.25	6.05	0.40
298	6.48	0.52	5.32	0.55	5.71	0.68

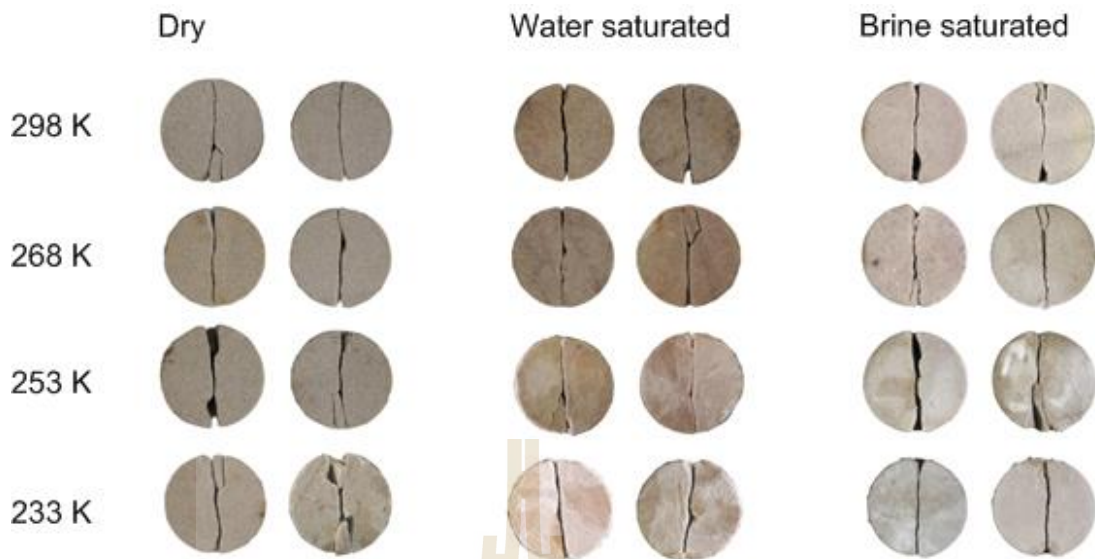


Figure 4.4 Some post-test specimens obtained from tensile strength testing under dry and saturated with water and brine conditions

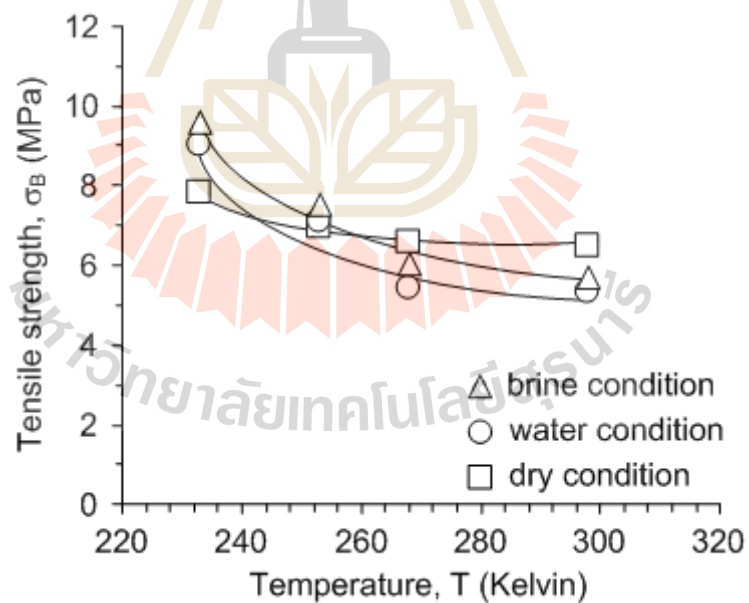


Figure 4.5 Brazilian tensile strength as function of temperatures for dry and saturated with water and brine conditions

The elastic modulus (E) and Poisson's ratio (ν) have been calculated from measured stress-strain curves obtained from compressive strength test. The stress-strain curves of all specimens are present in Appendix A. The results of elastic modulus and Poisson's ratio under dry and saturated conditions are shown Table 4.3 to 4.5.

Table 4.3 Elastic modulus and Poisson's ratio under dry condition

Temperature (Kelvin)	σ_3 (MPa)	E (GPa)	SD	ν	SD
233	0	10.33	1.71	0.28	0.025
	3	10.30	1.50	0.30	0.034
	7	10.89	0.50	0.29	0.017
	12	11.94	0.65	0.29	0.016
253	0	10.51	0.67	0.28	0.011
	3	11.03	0.74	0.30	0.023
	7	10.48	1.59	0.29	0.011
	12	10.89	0.85	0.30	0.015
268	0	10.77	1.91	0.28	0.006
	3	10.13	0.31	0.30	0.014
	7	10.86	1.10	0.28	0.014
	12	11.10	0.94	0.29	0.004
298	0	10.38	0.24	0.28	0.003
	3	10.69	1.40	0.28	0.008
	7	10.41	0.36	0.29	0.013
	12	10.70	1.56	0.29	0.016

Table 4.4 Elastic modulus and Poisson's ratio under water-saturated condition

Temperature (Kelvin)	σ_3 (MPa)	E (GPa)	SD	ν	SD
233	0	11.29	0.46	0.30	0.023
	3	11.28	0.76	0.27	0.005
	7	11.88	0.58	0.28	0.007
	12	11.84	0.81	0.28	0.009
253	0	10.01	0.39	0.29	0.011
	3	11.59	0.92	0.29	0.020
	7	11.14	0.84	0.28	0.009
	12	11.25	0.78	0.29	0.013
268	0	9.59	1.35	0.27	0.011
	3	11.53	1.93	0.29	0.016
	7	10.42	0.88	0.29	0.028
	12	10.66	1.28	0.29	0.020
298	0	9.48	0.67	0.29	0.006
	3	9.38	0.87	0.28	0.015
	7	10.17	0.87	0.29	0.019
	12	11.12	0.43	0.30	0.023



Table 4.5 Elastic modulus and Poisson's ratio under brine-saturated condition

Temperature (Kelvin)	σ_3 (MPa)	E (GPa)	SD	ν	SD
233	0	11.53	0.42	0.28	0.003
	3	11.43	0.32	0.28	0.015
	7	11.74	0.21	0.29	0.019
	12	11.79	0.07	0.29	0.008
253	0	11.06	0.78	0.28	0.009
	3	10.96	0.58	0.28	0.011
	7	11.17	0.24	0.27	0.008
	12	11.23	0.57	0.28	0.012
268	0	10.22	0.05	0.28	0.010
	3	10.73	0.21	0.27	0.003
	7	10.48	0.39	0.27	0.007
	12	11.24	0.46	0.27	0.019
298	0	10.16	0.02	0.28	0.011
	3	10.37	0.77	0.28	0.003
	7	10.65	0.59	0.27	0.005
	12	10.53	0.37	0.28	0.005



4.4 Freeze-thaw cycle test

The freeze-thaw cycle on the cubical rock specimens (with nominal size of $26 \times 26 \times 26 \text{ mm}^3$ as shown in Figure 4.6) are conducted to examine microstructure increment in rock specimens by measure the inducing of the porosity. Three test cycles are conducted here. For each cycle the saturated specimens were frozen under subzero temperatures (253 Kelvin) in a thermostatic chamber for a week. Then they were thawed under ambient temperatures and dry in oven at $373 \pm 5 \text{ Kelvin}$ ($100 \pm 5^\circ\text{C}$) for two days. The specimens under dry and saturated surface dry were weighted for each cycle used to determine the changing of their apparent porosity (Hoek and Brown, 2004). The porosity increments were plotted as a function of freeze-thaw cycle.

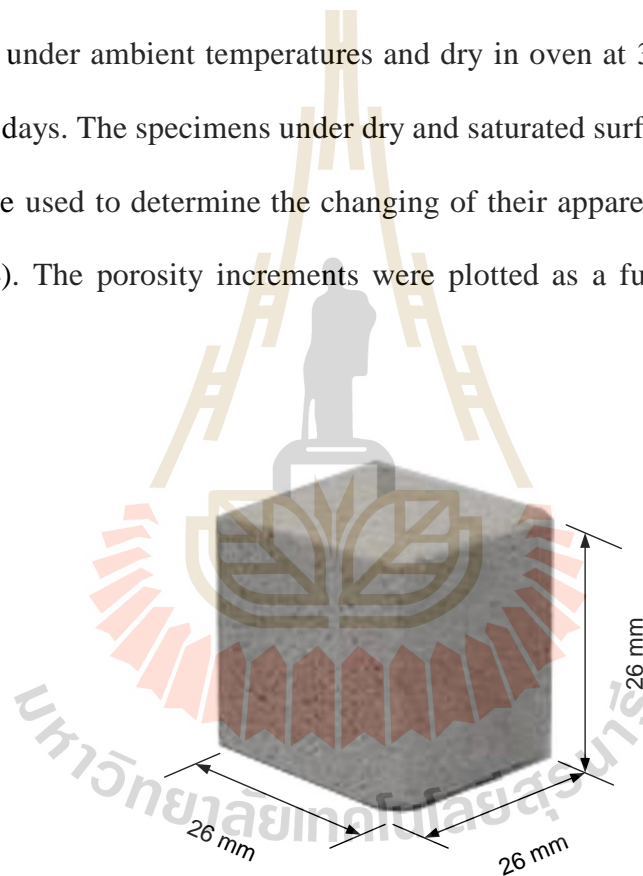


Figure 4.6 Examples of rock specimen prepared for freezing and thawing cyclic test

The freeze-thaw cycle was conducted to examine microstructure changes in term of porosity increment in rock specimens by measuring the inducing of the porosity. The porosity increment (ASTM C830, 2011) can be calculated as:

$$[(n_i - n_o) / n_o] \times 100\% \quad (4.1)$$

where n_o is the porosity of rock before subjecting by low temperature and n_i is the porosity of rock after subjecting by low temperature at cycle 1, 2 or 3, respectively. Table 4.5 summary the test results obtained for freeze-thaw cycle testing.

The change of the effective porosity after each set of cycles of freezing and thawing are represented in Figure 4.7. The water content of the specimen gives some influence to the porosity change. The reason of the increase in porosity may be mineral grains occurred shrinkage lead to expansion of pore water. This shrinkage of rock matrix accompanied by dilation of pore spaces results in micro crack formation and the material is not return to original state after thermal unloading (Yamabe and Neupane, 2001).

Table 4.6 Test results obtained for freeze-thaw cycle testing

Samples No.	Effective Porosity (%)			
	Cycle 0	Cycle 1	Cycle 2	Cycle 3
1	11.29	11.61	11.72	11.88
2	11.30	11.46	11.64	11.90
3	10.59	11.32	11.81	12.50
4	11.89	12.42	12.96	13.51
5	11.24	12.56	N/A	N/A
6	12.19	12.24	12.70	12.88
7	11.39	12.51	12.90	13.03
8	11.86	12.17	12.72	13.29
9	11.33	11.98	12.59	13.20
10	11.09	12.34	12.51	13.06

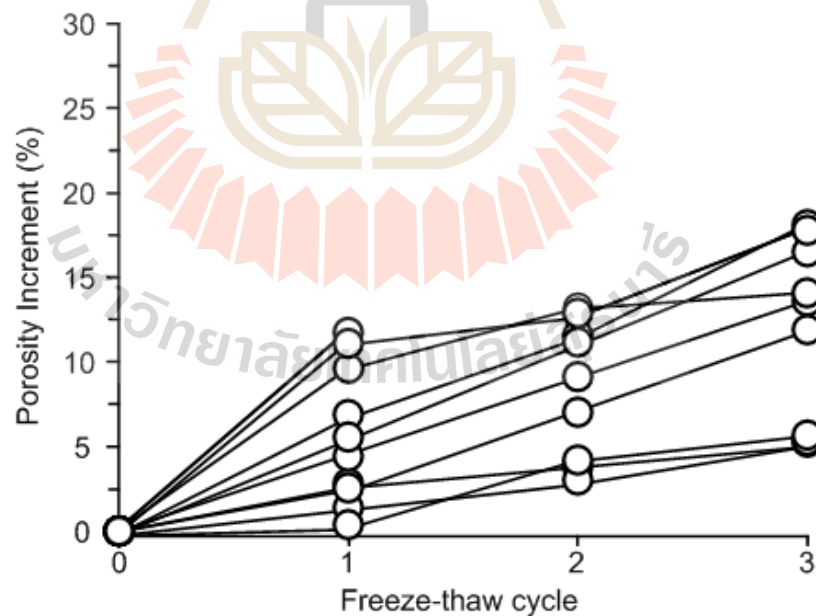


Figure 4.7 Porosity increment caused by freezing and thawing

CHAPTER V

CORRECTION BETWEEN MECHANICAL PROPERTIES AND TEMPERATURE

5.1 Introduction

The objective of this chapter is to correlate the mechanical properties (strength and deformation modulus) with temperature for Phra Wihan sandstone under both dry and saturated conditions. The test results presented in Chapter IV are used in this analysis. Two failure criteria (Coulomb criterion and Hoek and Brown criterion) are adopted here as it allows incorporating the rock strength parameters. The mathematical equations are considered to assess the predictive capability of stability of ground during ground freezing process.

5.2 Coulomb criterion

Based on the Coulomb criterion the cohesion (c) and internal friction angle (ϕ) can be determined from the strength results for each temperature using the following relations:

$$\sigma_1 = 2c \tan (45+\phi/2) + \sigma_3 \tan^2 (45+\phi/2) \quad (5.1)$$

where σ_1 and σ_3 are major and minor principal stresses at failure obtained for dry and saturated samples. Table 5.1 summarized the values of cohesion and internal friction angle of Phara Wihan sandstone. The graphs that used to determine these values are present in Appendix B.

Table 5.1 Cohesion and internal friction angle of Phara Wihan sandstone

Temperature (Kelvin)	Cohesion, c (MPa)			Friction angle, ϕ (°)		
	Dry	Water	Brine	Dry	Water	Brine
233	17.18	24.44	24.24	48.93	45.83	47.49
253	15.18	18.82	18.97	48.91	47.22	48.47
268	13.77	13.43	13.56	48.87	47.61	48.83
298	12.73	11.93	12.47	48.93	46.95	47.58

Figure 5.1 plotted the cohesion and internal friction angle as a function of temperature. The average friction angle of this rock types is about 48 degrees. The temperatures have no apparent influence the internal friction angle under both dry and saturated condition. The results suggest that the cohesions for both dry and saturated conditions increase with decreasing temperature. At subzero temperature, the ice filled in pore space of rock can be cement matrix of rock under saturated condition. Hence the cohesive force between rock grains and ice can strengthen the rock strength. This agrees reasonably well with the increased strength as the temperature decreases. More discussions are given in the Chapter VII.

The power equation is used to fit the test results. These correlations try to explain how the temperature has influenced on the bonding between rock grains and ice in pore space. The regression are as follows:

$$c_d = (1.37 \times 10^4) T^{1.23} \quad (\text{MPa}) \quad (5.2)$$

$$c_w = (3.0 \times 10^8) T^{3.03} \quad (\text{MPa}) \quad (5.3)$$

$$c_b = (1.0 \times 10^8) T^{2.82} \quad (\text{MPa}) \quad (5.4)$$

where T is temperature (in Kelvin), c_d , c_w and c_b are the cohesion (in MPa) obtained for dry, saturated with water and brine, respectively. The regression coefficient obtained for dry, saturated with water and brine are 0.965, 0.921 and 0.900, respectively. Good correlation is obtained for all conditions.

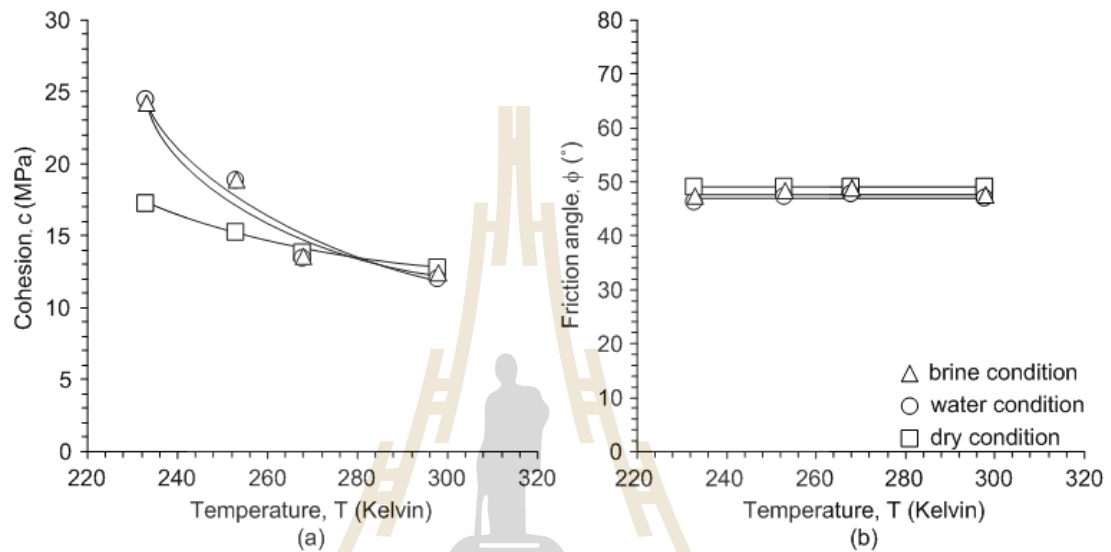


Figure 5.1 Cohesion and internal friction angle of Phara Wihan sandstone as a function of temperature from Coulomb criterion

5.3 Hoek and Brown criterion

The Hoek-Brown criterion defines the relationship between the principal stresses associated with the failure of rock as:

$$\sigma_1 = \sigma_3 + (m\sigma_c\sigma_3 + s\sigma_c^2)^{1/2} \quad (5.5)$$

where “ m ” and “ s ” are material constants (for intact rock, $s = 1$) and “ σ_c ” is the uniaxial compressive strength of the intact rock. Table 5.2 summarized Hoek-Brown’s constants (σ_c , m and s) obtained for Phara Wihan sandstone under various temperature. Figure 5.2

plotted the uniaxial compressive strength and “m” constant as a function of temperature. It is found that “m” constants decrease with decreasing temperatures. The uniaxial compressive strength (σ_c) increase with decreasing of temperatures for all conditions. Hence the rock strength decreased with increasing of temperature. More discussions are given in Chapter VII.

Table 5.2 Hoek-Brown’s constants (σ_c , m and s) obtained for Phara Wihan sandstone under various temperature

Temperature (Kelvin)	Test Conditions	Hoek-Brown’s Constants			R ²
		σ_c (MPa)	m	s	
233	Dry	88.68	17.69	1.00	0.998
	Water-saturated	119.58	12.55	1.00	0.984
	Brine-saturated	125.97	14.35	1.00	0.999
253	Dry	78.18	18.15	1.00	0.999
	Water-saturated	93.46	15.31	1.00	0.994
	Brine-saturated	96.91	16.83	1.00	0.990
268	Dry	67.98	18.80	1.00	0.993
	Water-saturated	65.41	17.87	1.00	0.992
	Brine-saturated	68.06	18.49	1.00	0.993
298	Dry	62.35	20.27	1.00	0.984
	Water-saturated	56.69	17.82	1.00	0.991
	Brine-saturated	59.95	18.59	1.00	0.988

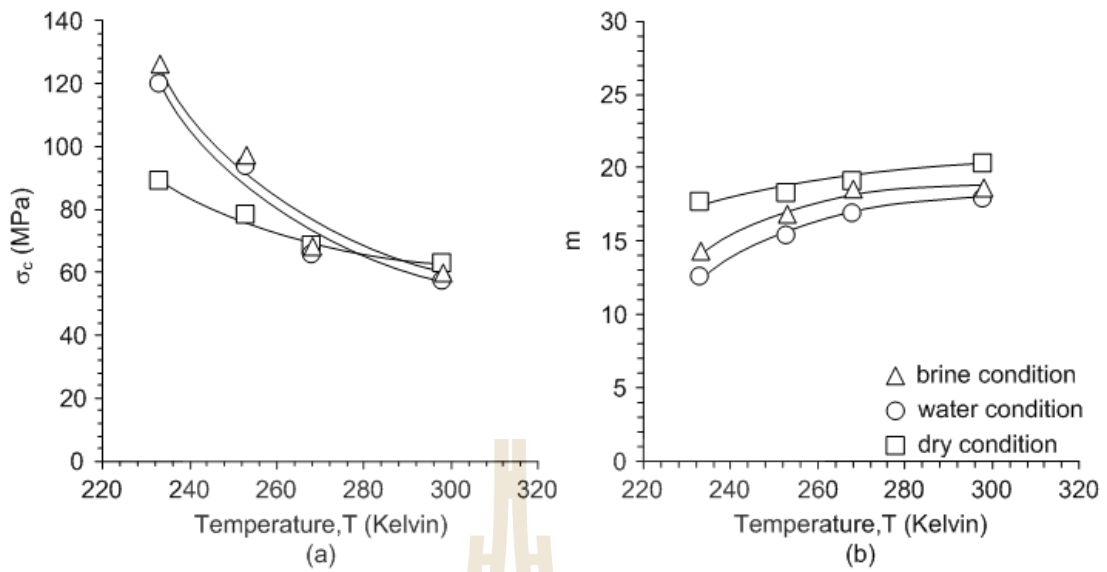


Figure 5.2 Uniaxial compressive strength (σ_c) and parameter m as a function of temperatures

The exponential function is used to fit with Hoek-Brown's constants. The regression are as follows:

$$\sigma_{c_d} = (2.63 \times 10^5) T^{-1.47} \quad (\text{MPa}) \quad (5.6)$$

$$\sigma_{c_w} = (4.00 \times 10^9) T^{-3.16} \quad (\text{MPa}) \quad (5.7)$$

$$\sigma_{c_b} = (3.00 \times 10^9) T^{-3.14} \quad (\text{MPa}) \quad (5.8)$$

where T is temperature (in Kelvin), σ_{c_d} , σ_{c_w} and σ_{c_b} are the uniaxial compressive strength (in MPa) obtained for dry, water-saturated and brine-saturated conditions, respectively. The regression coefficient obtained for dry, water-saturated and brine-saturated conditions are 0.959, 0.931 and 0.923, respectively. Good correlation is obtained for all conditions.

5.4 Modified Coulomb strength criteria

The compressive strength results are determined in terms of the maximum principal stresses (σ_1) and confining stresses (σ_3) at failure for dry and saturated conditions (water and brine). The results indicate that the maximum principal stresses tend to increase with decreasing temperature. The relationship between maximum principal stresses and lower temperatures (Figure 5.3) can be represented by an empirical equation:

$$\sigma_1 = \kappa \exp(-\beta T) + \alpha \sigma_3 \quad (5.9)$$

where “ $\kappa \exp(-\beta T)$ ” represent the unconfined compressive strength ($\sigma_c = 2c \tan(45 + \phi/2)$) and “ α ” represent the internal friction angle ($\tan^2(45 + \phi/2)$) based on Coulomb criteria. σ_1 is maximum principal stresses, κ , β , and α are empirical constants, T is temperature, and σ_3 is confining stresses. A good coefficient of correlation between the proposed equation ($R^2 = 0.984$ for dry condition, $R^2 = 0.972$ for water condition and $R^2 = 0.971$ for brine condition).

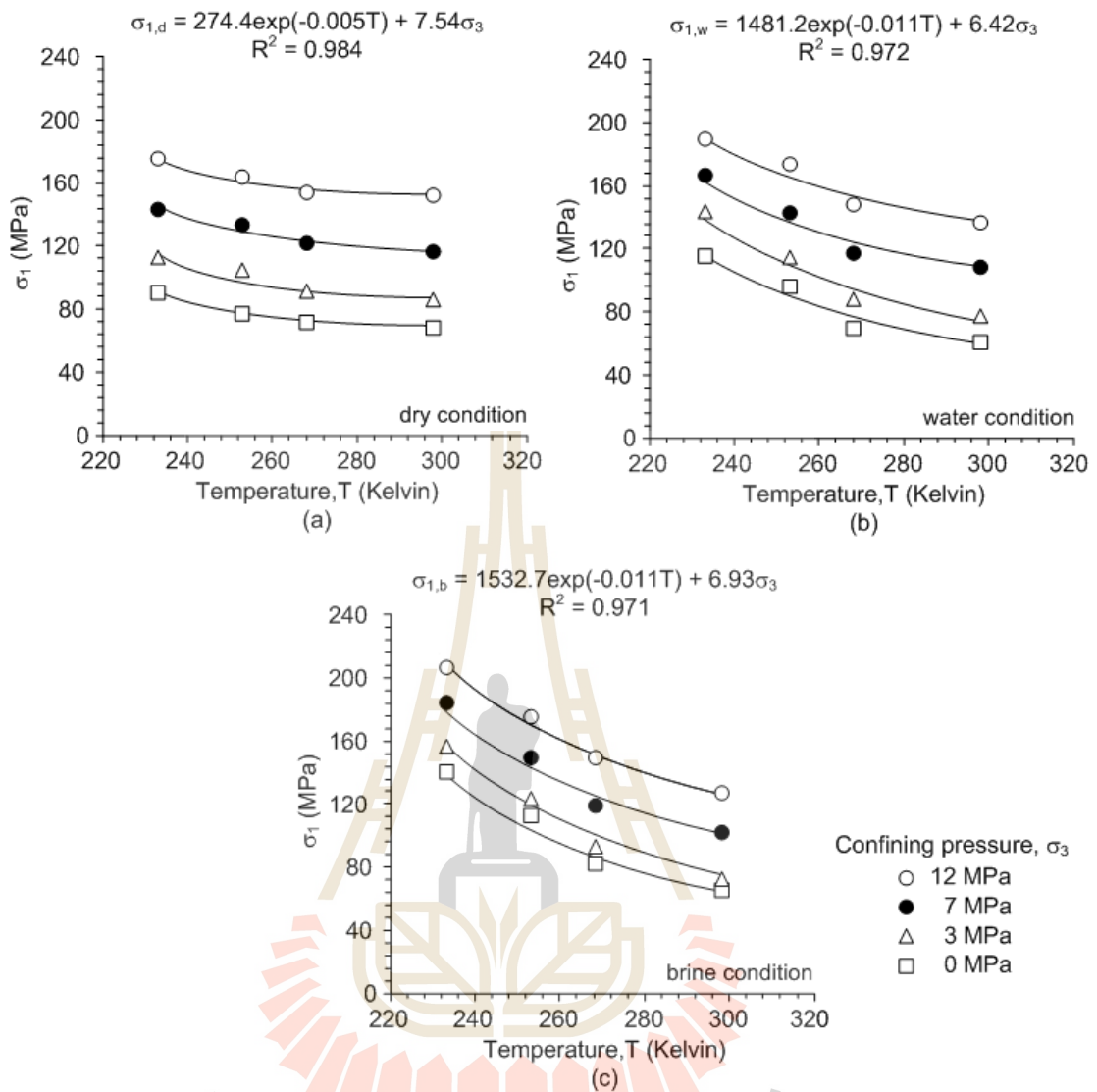


Figure 5.3 Major principal stresses at failure as a function of temperature in difference conditions

The test results can be presented in terms of octahedral shear stress at failure as a function of mean stress which is determined using the relations given by Jaeger et al., (2007) as shown in Table 5.3.

$$\tau_{\text{oct}} = \left\{ \frac{1}{3} (\sigma_1 - \sigma_2)^2 + (\sigma_2 - \sigma_1)^2 + (\sigma_3 - \sigma_1)^2 \right\}^{1/2} \quad (5.10)$$

$$\sigma_m = \frac{1}{3} (\sigma_1 + \sigma_2 + \sigma_3) \quad (5.11)$$

where τ_{oct} is octahedral shear stress and σ_m is mean stress. The octahedral shear stresses and mean stress at failure can be calculated from the principal stresses and the confining stresses. The octahedral shear stresses are plotted as a function of mean stress in Figure 5.4. The octahedral shear strength for saturated sandstones is more sensitive to the temperature than the dry sandstone. The empirical equation is proposed to predict the octahedral shear stress and mean stress under lower temperatures as follows:

$$\tau_{\text{oct}} = \delta \exp(-\eta T) + \omega \sigma_m \quad (5.12)$$

where δ , η and ω are empirical constants. A good correlation is obtained ($R^2 = 0.997$ for dry condition, $R^2 = 0.986$ for water condition and $R^2 = 0.986$ for brine condition).

Table 5.3 Strength of Phara Wihan sandstone

Temperature (Kelvin)	σ_3 (MPa)	σ_1 (MPa)			σ_m (MPa)			τ_{oct} (MPa)		
		Dry	Water	Brine	Dry	Water	Brine	Dry	Water	Brine
233	0	90.53	115.20	126.42	30.18	38.40	42.14	73.92	94.06	103.22
	3	113.58	143.40	148.89	39.86	49.80	51.63	90.29	114.64	119.11
	7	143.62	167.08	175.13	52.54	60.36	63.04	111.55	130.71	137.28
	12	175.96	189.77	206.21	66.65	71.26	76.74	133.87	145.15	158.57
253	0	77.71	96.59	101.44	25.90	32.20	33.81	63.45	78.87	82.83
	3	104.91	114.36	118.96	36.97	40.12	41.65	83.21	90.93	94.68
	7	134.24	142.85	148.99	49.41	52.28	54.33	103.89	110.92	115.94
	12	163.82	173.99	183.90	62.61	66.00	69.30	123.96	132.27	140.36
268	0	72.02	69.49	72.31	24.01	23.16	24.10	58.80	56.74	59.04
	3	92.04	88.22	92.52	32.68	31.41	32.84	72.70	69.58	73.09
	7	121.73	116.92	123.47	45.24	43.64	45.82	93.68	89.75	95.10
	12	154.58	148.60	156.60	59.53	57.53	60.20	116.41	111.53	118.06
298	0	68.75	60.93	65.28	22.92	20.31	21.76	56.13	49.75	53.30
	3	86.28	77.48	82.27	30.76	27.83	29.42	68.00	60.81	64.72
	7	116.82	108.68	111.73	43.61	40.89	41.91	89.66	83.02	85.51
	12	152.13	136.39	143.84	58.71	53.46	55.95	114.41	101.57	107.65

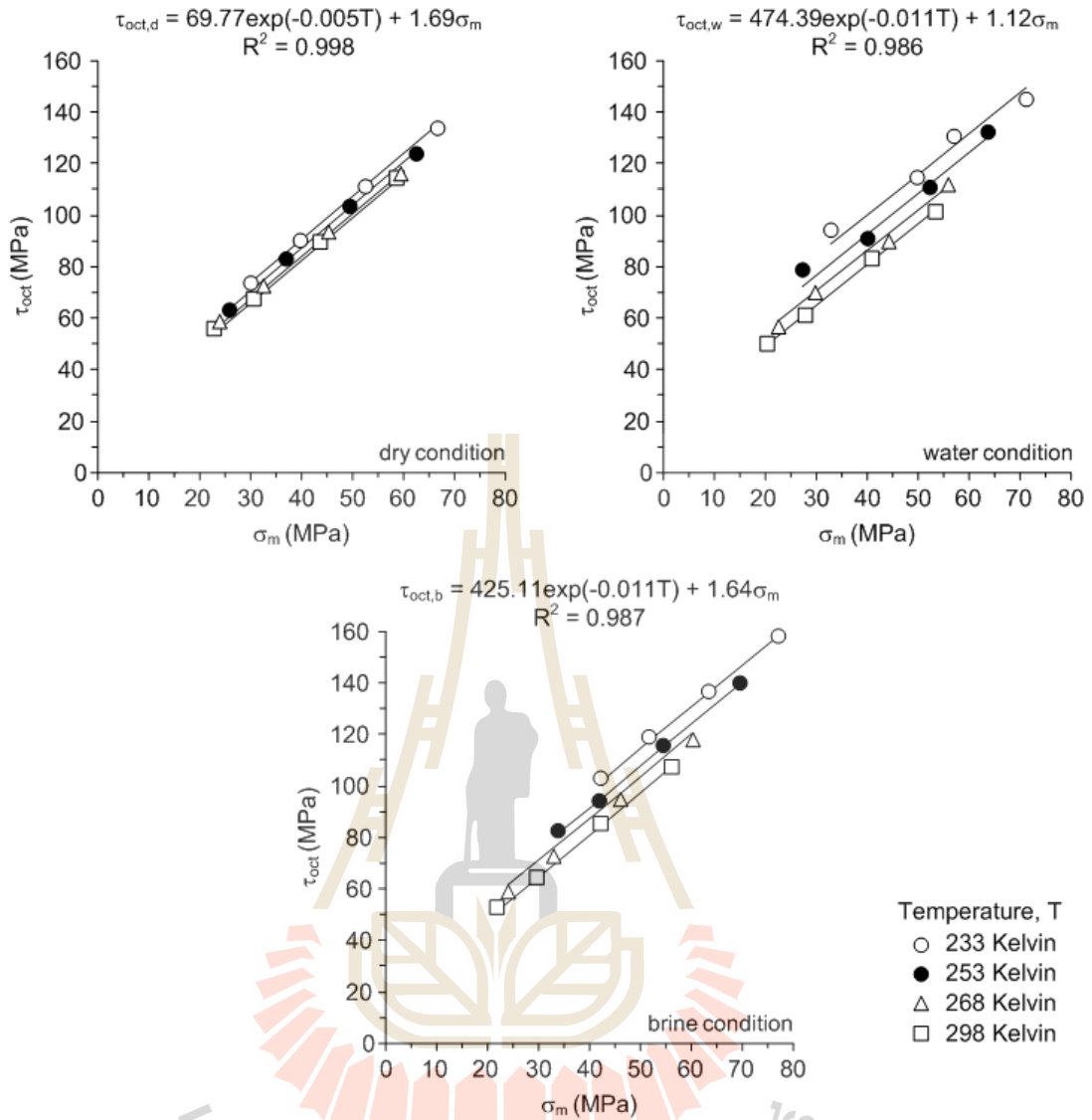


Figure 5.4 Octahedral shear strengths at failure of Phra Wihan sandstone as a function of mean stress in difference conditions

5.5 Deformation modulus

The elastic modulus and Poisson's ratio have been calculated from measured stress-strain curves obtained from the tangent of the stress-strain curves at 50% failure stress. The shear modulus (G) and bulk modulus (K) can be determined from relations equation from Jaeger et al. (2007). Tables 5.4 to 5.6 summarizes the measurement results for each specimen in terms of the elastic modulus, shear modulus, bulk modulus, and Poisson's ratio. The change of elastic parameter with temperature for the dry and saturated conditions of sandstone are shown in Figure 5.5. The linear variations of the four parameters with respect to lower temperatures can be represented by the following equations under each condition.

- 1) For dry condition as follow:

$$E_d = (-4.7 \times 10^{-3})T + 11.94 \quad (\text{GPa}) \quad (5.13)$$

$$G_d = (-1.7 \times 10^{-3})T + 4.60 \quad (\text{GPa}) \quad (5.14)$$

$$K_d = (-5.3 \times 10^{-3})T + 9.83 \quad (\text{GPa}) \quad (5.15)$$

$$\nu_d = (-4.0 \times 10^{-5})T + 0.29 \quad (5.16)$$

- 2) For saturated water condition as follow:

$$E_w = (-2.4 \times 10^{-2})T + 16.41 \quad (\text{GPa}) \quad (5.17)$$

$$G_w = (-9.6 \times 10^{-3})T + 6.70 \quad (\text{GPa}) \quad (5.18)$$

$$K_w = (-1.4 \times 10^{-2})T + 12.14 \quad (\text{GPa}) \quad (5.19)$$

$$\nu_w = (1.0 \times 10^{-4})T + 0.26 \quad (5.20)$$

3) For saturated brine condition as follow:

$$E_b = (-1.8 \times 10^{-2})T + 15.80 \quad (\text{GPa}) \quad (5.21)$$

$$G_b = (-6.9 \times 10^{-3})T + 6.09 \quad (\text{GPa}) \quad (5.22)$$

$$K_b = (-1.8 \times 10^{-2})T + 12.91 \quad (\text{GPa}) \quad (5.23)$$

$$\nu_b = (-1.0 \times 10^{-4})T + 0.30 \quad (5.24)$$

The results indicated that the elastic, shear and bulk modulus increase in a linear manner with decreasing temperature. Poisson's ratio tends to be slightly sensitive of the temperature. The modulus parameters G and K can be defined as a function of the testing temperature which correlate to the strength of sandstone from different temperatures under dry and saturated conditions. Discussion the results are given in Chapter VII.

Table 5.4 Elastic parameters of Phra Wihan sandstone for dry condition

Temperature (Kelvin)	σ_3 (MPa)	E (GPa)	ν	G (GPa)	K (GPa)
233	0	10.33	0.28	4.05	7.69
	3	10.30	0.30	3.96	8.57
	7	10.89	0.29	4.23	8.53
	12	11.94	0.29	4.62	9.55
	Mean \pm SD	10.86 \pm 0.77	0.29 \pm 0.01	4.21 \pm 0.29	8.58 \pm 0.76
253	0	10.51	0.28	4.12	7.80
	3	11.03	0.30	4.25	9.07
	7	10.48	0.29	4.07	8.23
	12	10.89	0.30	4.19	8.99
	Mean \pm SD	10.73 \pm 0.27	0.29 \pm 0.01	4.16 \pm 0.08	8.52 \pm 0.61
268	0	10.77	0.28	4.20	8.24
	3	10.13	0.30	3.91	8.28
	7	10.86	0.28	4.25	8.17
	12	11.10	0.29	4.31	8.73
	Mean \pm SD	10.72 \pm 0.42	0.29 \pm 0.01	4.17 \pm 0.18	8.35 \pm 0.26
298	0	10.38	0.28	4.04	8.02
	3	10.69	0.28	4.18	8.04
	7	10.41	0.29	4.03	8.34
	12	10.70	0.29	4.14	8.62
	Mean \pm SD	10.55 \pm 0.17	0.29 \pm 0.01	4.10 \pm 0.07	8.26 \pm 0.28

Table 5.5 Elastic parameters of Phra Wihan sandstone for water-saturated condition

Temperature (Kelvin)	σ_3 (MPa)	E (GPa)	ν	G (GPa)	K (GPa)
233	0	11.29	0.30	4.34	9.43
	3	11.28	0.27	4.43	8.32
	7	11.88	0.28	4.63	9.14
	12	11.84	0.28	4.62	9.08
	Mean \pm SD	11.57 \pm 0.33	0.29 \pm 0.01	4.5 \pm 0.14	8.9 \pm 0.47
253	0	10.01	0.29	3.89	7.82
	3	11.59	0.29	4.50	9.05
	7	11.14	0.28	4.35	8.50
	12	11.25	0.29	4.37	8.83
	Mean \pm SD	11.00 \pm 0.68	0.29 \pm 0.00	4.28 \pm 0.27	8.55 \pm 0.53
268	0	9.59	0.27	3.77	7.02
	3	11.53	0.29	4.48	9.05
	7	10.42	0.29	4.03	8.34
	12	10.66	0.29	4.12	8.58
	Mean \pm SD	10.55 \pm 0.80	0.29 \pm 0.01	4.10 \pm 0.29	8.25 \pm 0.87
298	0	9.48	0.29	3.67	7.62
	3	9.38	0.28	3.65	7.25
	7	10.17	0.29	3.93	8.20
	12	11.12	0.30	4.28	9.22
	Mean \pm SD	10.04 \pm 0.80	0.29 \pm 0.01	3.88 \pm 0.30	8.07 \pm 0.86

Table 5.6 Elastic parameters of Phra Wihan sandstone for brine-saturated condition

Temperature (Kelvin)	σ_3 (MPa)	E (GPa)	ν	G (GPa)	K (GPa)
233	0	11.53	0.28	4.52	8.61
	3	11.43	0.28	4.48	8.49
	7	11.74	0.29	4.57	9.11
	12	11.79	0.29	4.56	9.47
	Mean \pm SD	11.62 \pm 0.17	0.28 \pm 0.01	4.53 \pm 0.04	8.91 \pm 0.45
253	0	11.06	0.28	4.32	8.40
	3	10.96	0.28	4.29	8.26
	7	11.17	0.27	4.39	8.13
	12	11.23	0.28	4.40	8.39
	Mean \pm SD	11.10 \pm 0.12	0.28 \pm 0.01	4.34 \pm 0.15	8.29 \pm 0.28
268	0	10.22	0.28	3.98	7.91
	3	10.73	0.27	4.21	7.88
	7	10.48	0.27	4.11	7.74
	12	11.24	0.27	4.42	8.16
	Mean \pm SD	10.67 \pm 0.43	0.27 \pm 0.01	4.18 \pm 0.19	7.92 \pm 0.17
298	0	10.16	0.28	3.98	7.59
	3	10.37	0.28	4.06	7.70
	7	10.65	0.27	4.19	7.75
	12	10.53	0.28	4.12	7.91
	Mean \pm SD	10.43 \pm 0.21	0.28 \pm 0.01	4.09 \pm 0.09	7.74 \pm 0.13

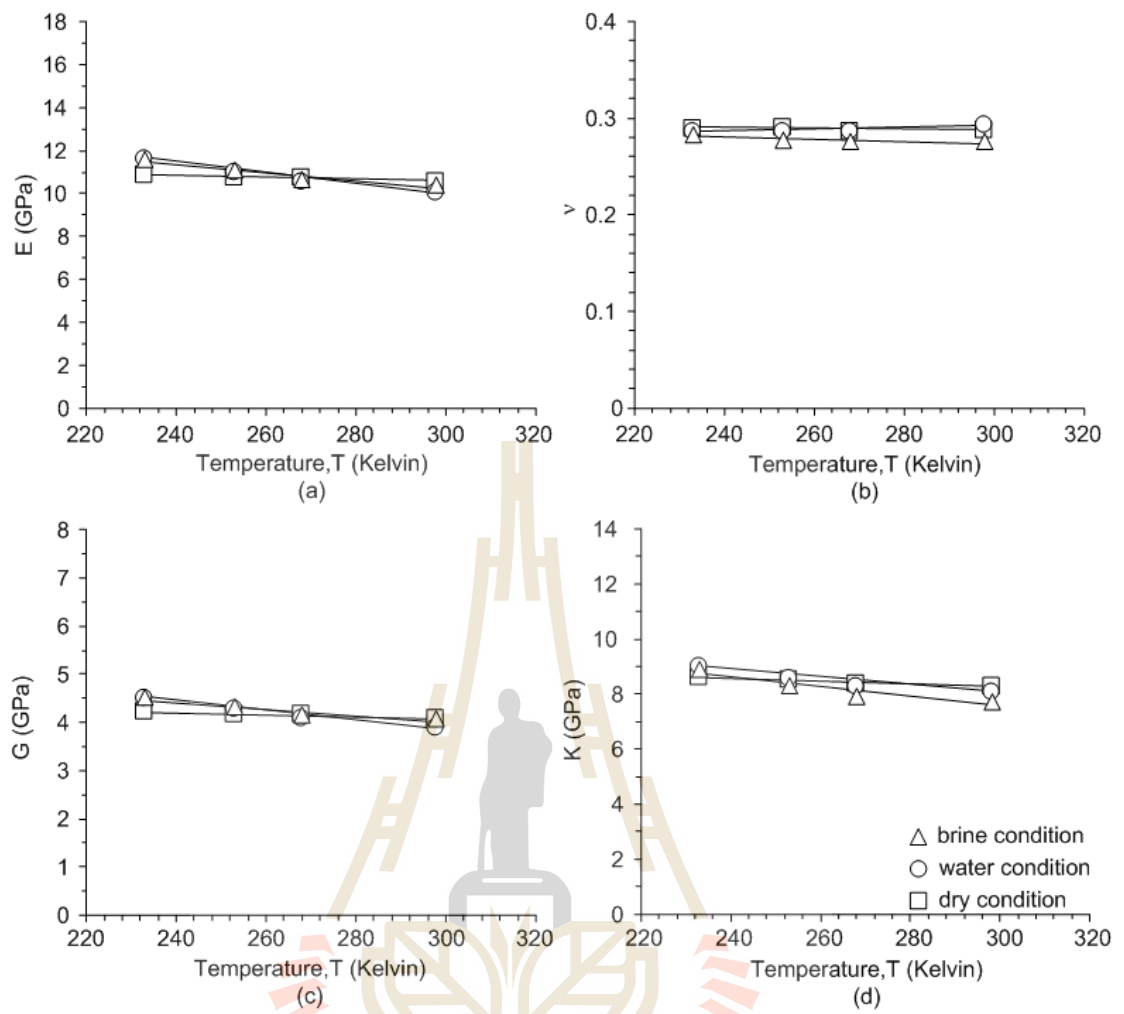


Figure 5.5 Elastic parameters of Phara Wihan sandstone as a function of temperature

CHAPTER VI

COMPUTER SIMULATION

6.1 Introduction

This chapter present the analysis for heat transfer between the freezing pipe and surrounding rock using finite element analysis (ANSYS 14.0 program). The results from computer simulation demonstrate the frozen zone boundary in rock formation around the freezing pipe. This zone represents the temperature at 273K (0°C). The results are used to correlate the mathematical relationship for predict the distribution of frozen zone around freezing pipe as a function of flow rate.

6.2 ANSYS 14.0 program

ANSYS is a software program used to simulate various engineering problem by the finite element method (FEM). The software can analyze engineering aspects of solid mechanics, fluid mechanic, thermodynamics and electromagnetics. Most ANSYS simulations are performed using the ANSYS Workbench software. The ANSYS Workbench software consists of multi-purpose analysis tool that can be used in a wide range of engineering. However, this study uses ANSYS FLUENT to simulate the problem. The ANSYS FLUENT is an application for set up and solve two or three-dimensional of fluid flow and heat transfer problem. There are three main steps in ANSYS FLUENT analysis: model generation, solution and review results (Madenci and Guven, 2006). Each of these steps corresponds to specific processors with in the

Processor level. The model generation is done in Preprocessor which involves creation of a model, material definition and finally generate finite element model (mesh). Solution processor performs specify boundary condition, define analysis type and analysis options. The important task within this processor is obtained the solution for the finite element model that is generated within the preprocessor. Finally, the results are viewed in the postprocessor. This included the plotting of contours, vector displays, deformed shapes and listings of the results in tabular format.

6.3 Numerical simulation

The numerical model is created in two-dimensional finite element mesh which has cross-section covering the freezing pipe and the ground surrounding in ANSYS FLUENT. In this study use the parameters of pipe from Viter et al. (2015) that show in Table 6.1. The material of freezing pipe is steel that is the common material using in the ground freezing method. It has a depth of 50 m from the ground surface. The freezing pipe is considered fill with a single-phase flow of LN₂ which is not considered of gas-liquid mixture flow. The LN₂ is usually inject in an inside of inner pipe and flows back though the space between an external of inner pipe and an inside outer pipe. The finite element mesh is analysis in axis symmetry that set up at the middle inner pipe. Figure 6.1 shows the systems models for numerical simulation. The mesh size created to be small at the freezing pipe and the ground surrounding because the thermal gradients are high on this zone. Hence, at the area far away from the pipe where the thermal gradients are lower, the size of elements are bigger. The finite element mech consist of 260088 elements and 536736 nodes (Figure 6.2). The number of step time

for numerical simulation begins at 86400 seconds (1 day) and calculates the time step size at 60 seconds.

Table 6.1 Freezing pipe geometry

Property	Value	Reference
Inside of inner pipe, r_{in} (mm)	13.46	Viter et al. (2015)
External of inner pipe, r_{en} (mm)	15.88	
Inside of outer pipe, r_{io} (mm)	50.80	
External of outer pipe, r_{eo} (mm)	57.15	

6.4 Input parameters

The input parameters for simulation related to the characteristics of the coolant (LN_2), the freezing pipe (inner and outer pipe) and the ground (rock surrounding). The parameters used here include the initial temperature, the flow rate and the thermal properties. The initial temperature of the coolant is set at 77.15 Kelvin ($-196^\circ C$). the freezing pipe and the ground temperature are set at 303.13 Kelvin ($30^\circ C$). The flow rates of the coolant are determined 0.5, 1, 2 and 3 kg/s for a period of 1 to 15 days. The parameters of physical properties show in Table 6.2. The ground surrounding is considered in four conditions include dry, 50% water saturated, 100% water saturated and pure water. This simulation is based on the thermal properties of the ground from Phueakphum (2008). The mixing values of the thermal properties between solid and liquid use equation of Max Well Model for the thermal conductivity and the equation of Kopp's Law for the heat capacity that present in Chapter II (Somerton, 1992). Figures 6.3 and 6.4 show the comparison of the thermal conductivity and the heat capacity of the ground for simulation.

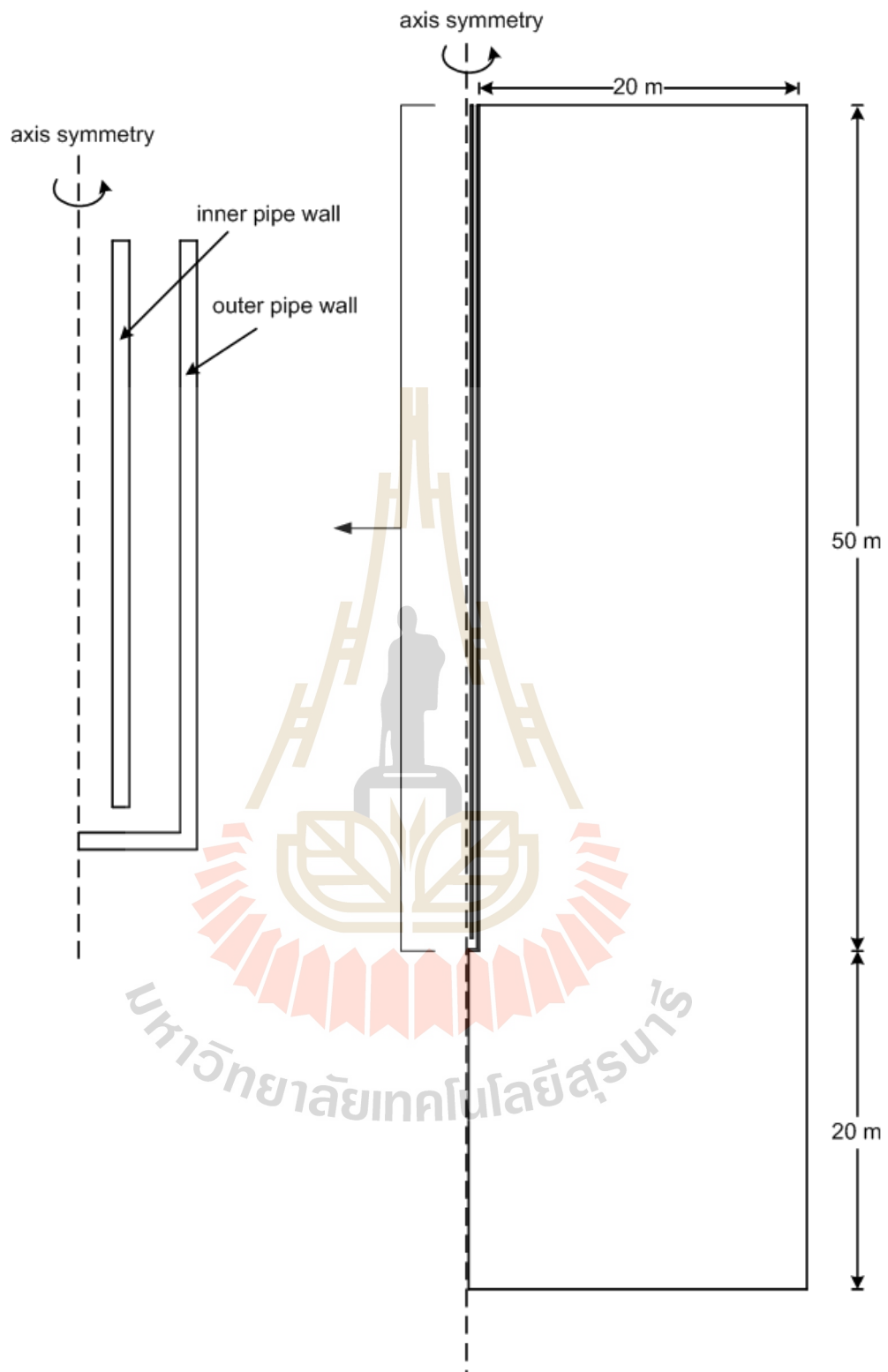


Figure 6.1 System model for numerical simulation

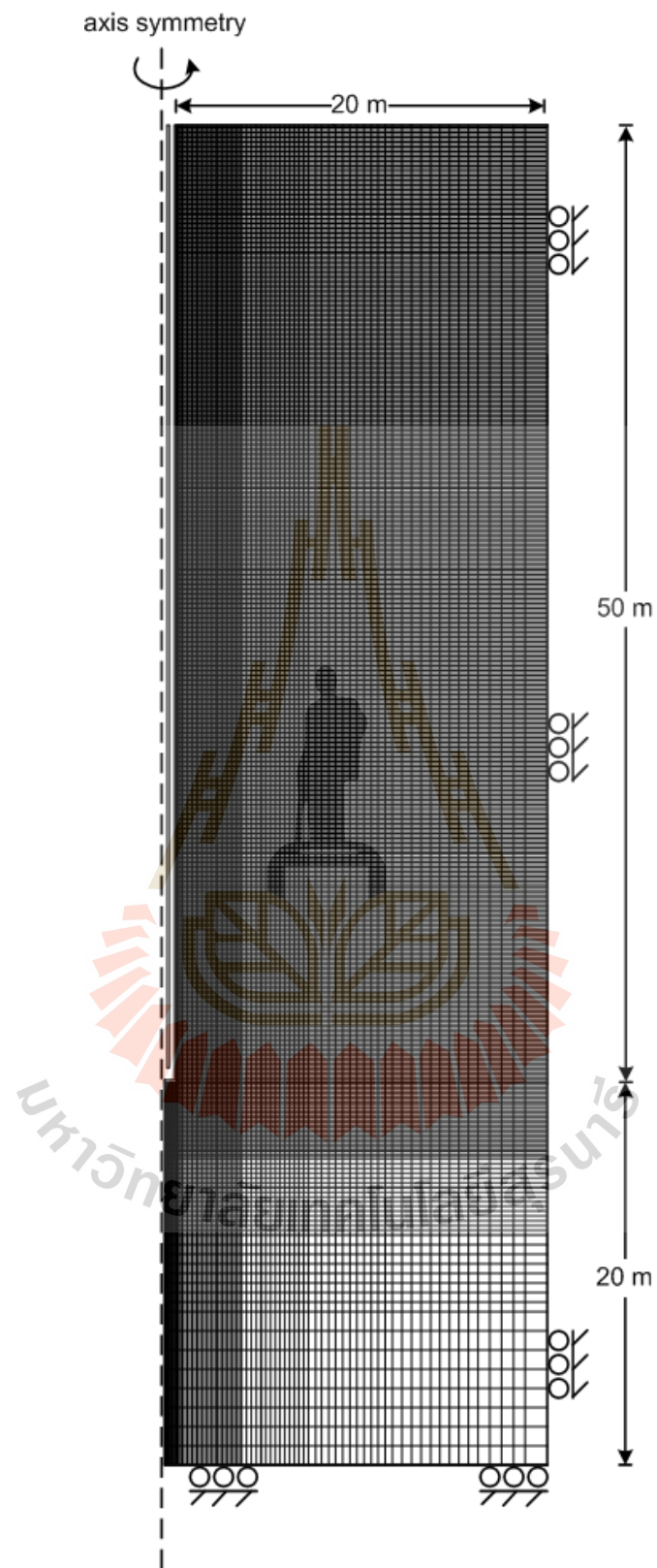


Figure 6.2 Finite element mesh for numerical model

Table 6.2 Physical parameters used in the computer simulation

Parameters	Unit	Value	Reference
1) Coolant (LN ₂) - Thermal conductivity, λ - Heat capacity, c_p - Viscosity, μ - Density, ρ	W/m-K J/kg-K kg/m-s kg/m ³	0.146 2041.5 0.00016065 806.08	Bergeron and Pasquier (2013)
2) Water - Thermal conductivity, λ - Heat capacity, c_p - Viscosity, μ - Density, ρ	W/m-K J/kg-K kg/m-s kg/m ³	0.6 4182 0.001003 998.2	ANSYS 14.0
3) Freezing pipe (steel) - Thermal conductivity, λ - Heat capacity, c_p - Density, ρ	W/m-K J/kg-K kg/m ³	16.27 502.48 8030	ANSYS 14.0
4) Dry sandstone - Thermal conductivity, λ - Heat capacity, c_p - Density, ρ	W/m-K J/kg-K kg/m ³	3.75 759.65 2260	Phueakphum (2008)
5) 50% water saturated of sandstone - Thermal conductivity, λ - Heat capacity, c_p - Density, ρ	W/m-K J/kg-K kg/m ³	3.47 855.69 2310	Somerton (1992) and Phueakphum (2008)
6) 100% water saturated of sandstone - Thermal conductivity, λ - Heat capacity, c_p - Density, ρ	W/m-K J/kg-K kg/m ³	3.21 946.48 2380	Somerton (1992) and Phueakphum (2008)

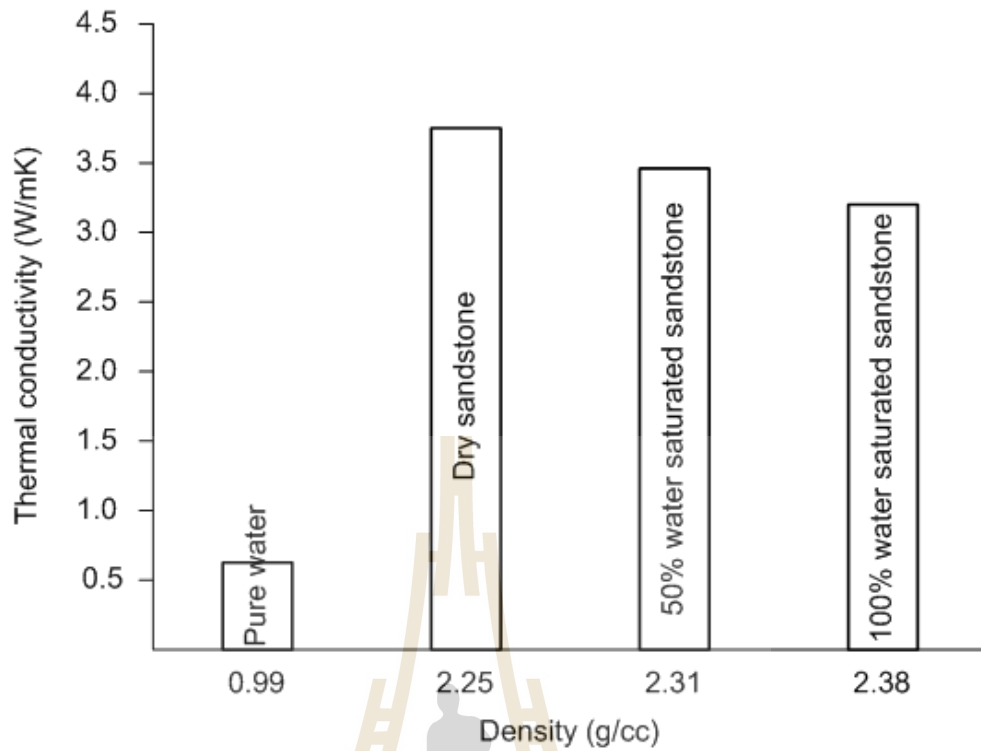


Figure 6.3 Thermal conductivity of ground plotted as a function of their density.

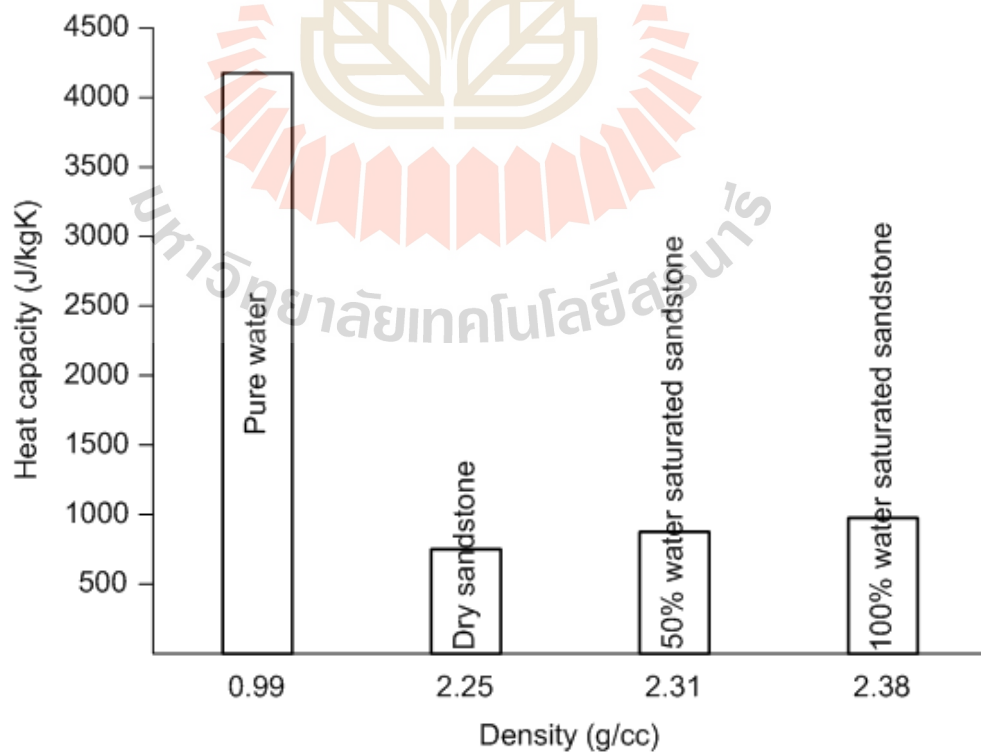


Figure 6.4 Heat capacity of ground plotted as a function of their density.

6.5 Computer simulation results

Results of the computer modeling are shown in Appendix D. The radius progression of frozen zone at 273 Kelvin (0 °C) for difference time (1 to 15 days) in each ground condition. Figure 6.5 demonstrate the temperature contour obtain from the numerical simulation of some cases which are analyzed in this study.

6.5.1 Influence of the ground

The heat transfer in the ground is modeled and a thermal boundary conditions applied at the pipe wall. The four cases are studied in this research. The first one is dry sandstone that set is a solid condition. The second one is 50% water saturated sandstone that set is porous zone condition. The third case is similar to the second condition but the ground is 100% water saturated sandstone. Finally, is the pure water that set is liquid condition. Each case of ground is simulated in homogenous without the fracture effects and hydraulic conductivity. The parameters properties (λ , c_p , ρ , μ) of the ground have been carried out because it has been representative of the energy that is used in the heat transfer between the ground and the pipe. Table 6.3 compares the radius distance progression of the frozen zone for each case at different flow rates. The progression of dry sandstone is bigger than the other cases. Because the dry sandstone is characterized by low heat capacity value and high thermal conductivity value which compared to other cases. As for pure water, it is much less distance progression of the frozen zone than all the other cases. This disparity can be explained its low heat capacity lead to low energy to remove the heat from the ground and high thermal conductivity indicates the transmission of heat energy by heat conduction is better.

6.5.2 Coolant flow rate

The coolant in this study is liquid nitrogen (LN_2) which the flow rates are range from 0.5 to 3 kg/s. The model developed in this study is consider the injection temperature of coolant constant over time which is injected into inner pipe. The results of the comparison between flow rates in each ground condition are illustrated in Figure 6.6. This figure shows the radius distance progression of the frozen zone from pipe at 273 Kelvin as a function of time after 1 to 15 days of cooling. The progression of the frozen zone depends on the heat transfer at the pipe wall, itself depending on the temperature difference between the coolant in the outer pipe and outer pipe wall. As can be seen, the high flow rates lead to the expansion of frozen zone faster than low flow rates. Due to the high flow rates do more the temperature of outer pipe wall is similar to that in the outer pipe. It is cumulative cool where the frozen zone grows larger and the progression at 273 Kelvin is further up. Similarly, the colder it is, the higher energy it removes heat from the ground because the ground cools more. For pure water, the progression of frozen zone in each flow rates do not difference value because the initial temperature of the coolant is almost equal to the temperature that flow through the space between the external of inner pipe and the inside of outer pipe. In such a way this the coolant has less time to heat up in contact with ground, it can be used low flow rate to simulated the pure water ground.

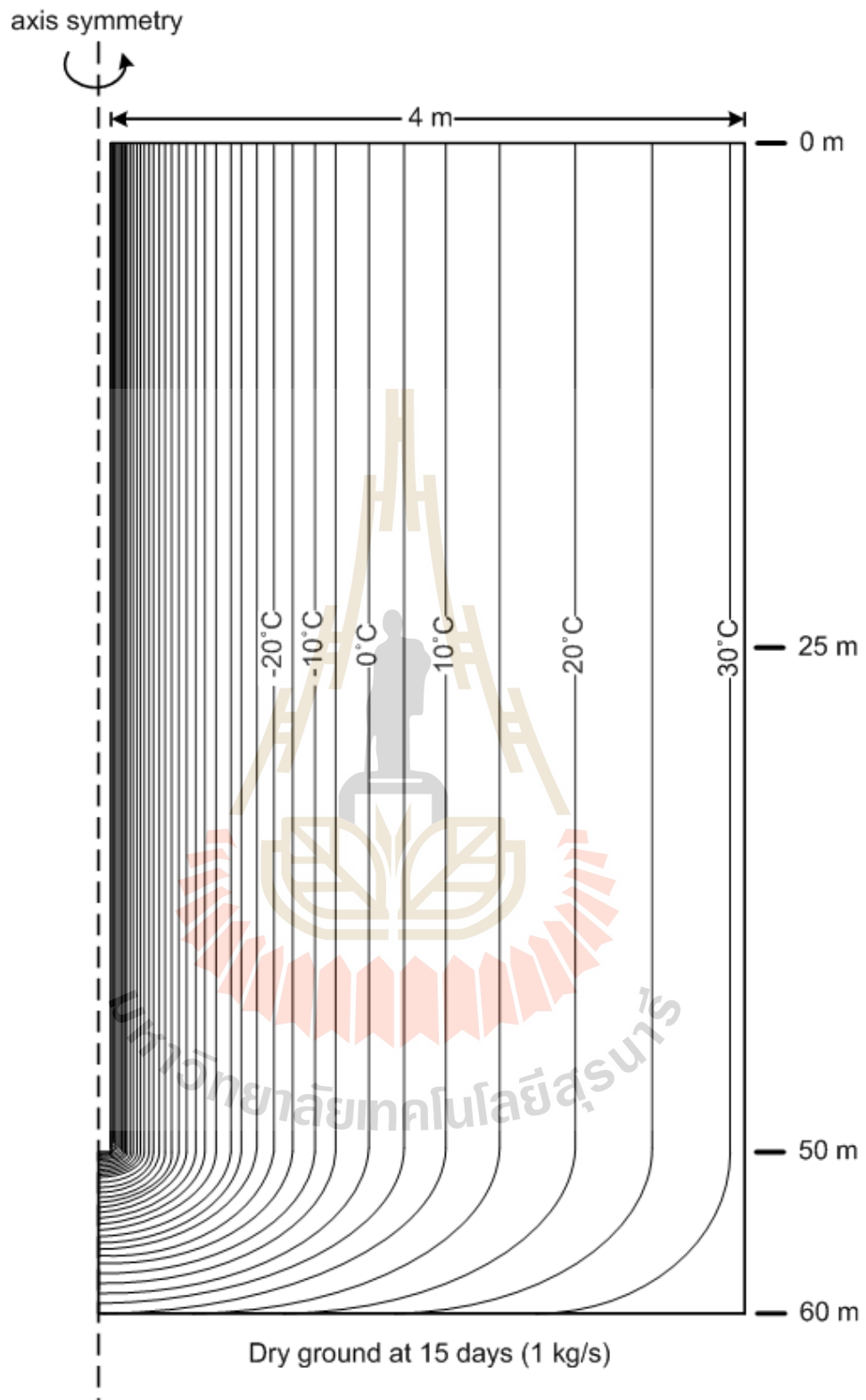


Figure 6.5 Temperature contour obtain from numerical simulation in dry ground condition at 15 days in coolant flow rated 1 kg/s

Table 6.3 The radius distance progression of the frozen zone for ground

Rate (kg/s)	Time (day)	Progression of frozen zone (m)			
		Dry	50% water saturated	100% water saturated	Pure water
0.5	1	0.324	0.312	0.236	0.147
	2	0.537	0.424	0.342	0.206
	3	0.672	0.500	0.419	0.254
	4	0.784	0.565	0.484	0.289
	5	0.873	0.624	0.543	0.318
	6	0.955	0.677	0.590	0.348
	7	1.026	0.719	0.637	0.371
	10	1.209	0.842	0.755	0.436
	15	1.445	1.037	0.926	0.519
1	1	0.401	0.371	0.289	0.159
	2	0.613	0.506	0.419	0.218
	3	0.755	0.601	0.513	0.265
	4	0.873	0.677	0.584	0.307
	5	0.967	0.742	0.649	0.336
	6	1.050	0.807	0.708	0.366
	7	1.126	0.860	0.761	0.389
	10	1.321	1.008	0.902	0.454
	15	1.592	1.238	1.114	0.543
2	1	0.454	0.396	0.318	0.165
	2	0.666	0.532	0.454	0.224
	3	0.808	0.632	0.548	0.271
	4	0.926	0.715	0.631	0.313
	5	1.020	0.785	0.696	0.342
	6	1.109	0.850	0.761	0.371
	7	1.185	0.903	0.814	0.395
	10	1.386	1.062	0.961	0.466
	15	1.651	1.316	1.185	0.554
3	1	0.472	0.412	0.360	0.171
	2	0.684	0.548	0.490	0.230
	3	0.826	0.654	0.584	0.277
	4	0.943	0.736	0.673	0.318
	5	1.044	0.801	0.738	0.348
	6	1.126	0.872	0.797	0.377
	7	1.209	0.925	0.850	0.401
	10	1.409	1.078	0.991	0.478
	15	1.681	1.332	1.203	0.566

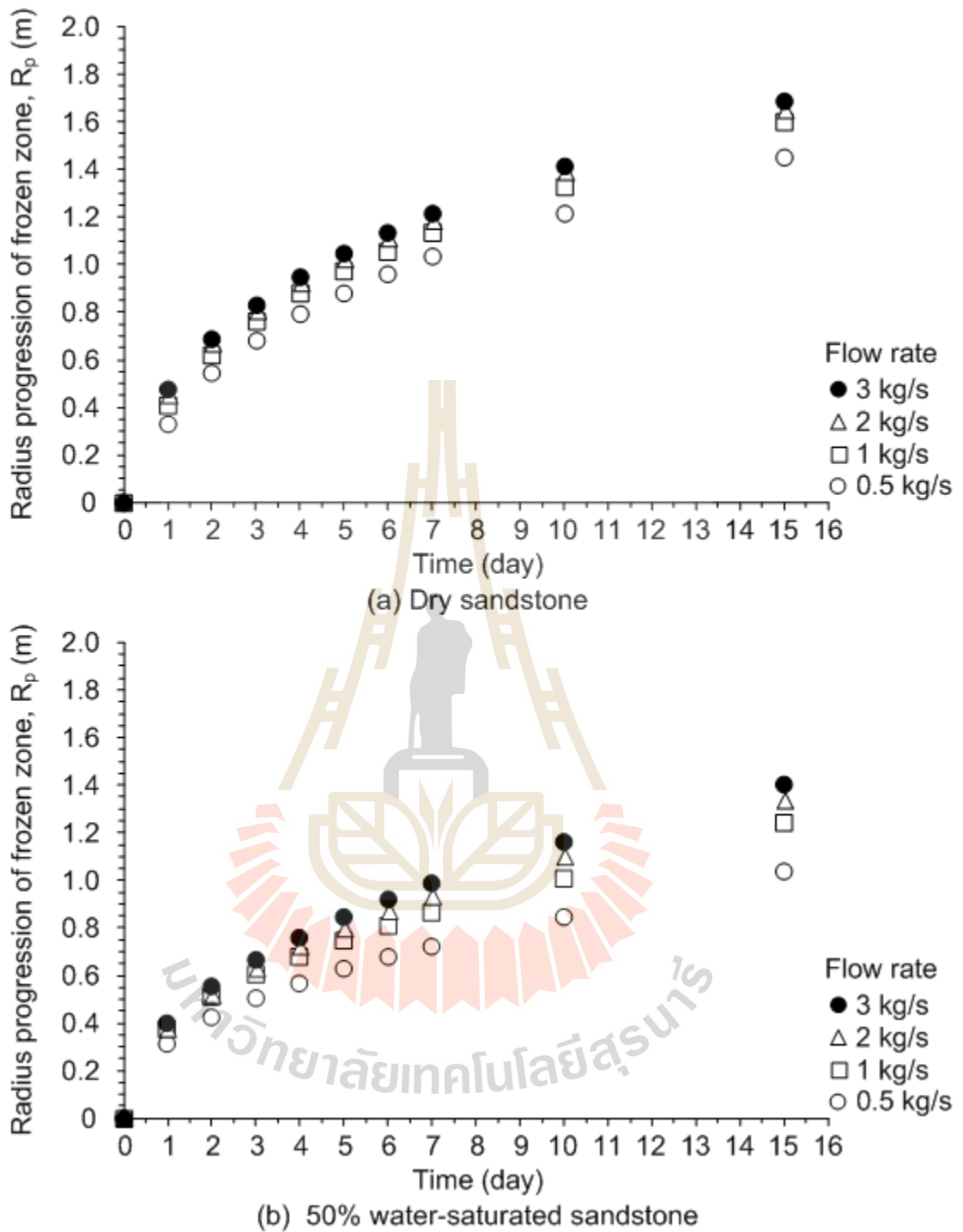


Figure 6.6 The radius distance progression of the frozen zone as a function of time in difference flow rates.

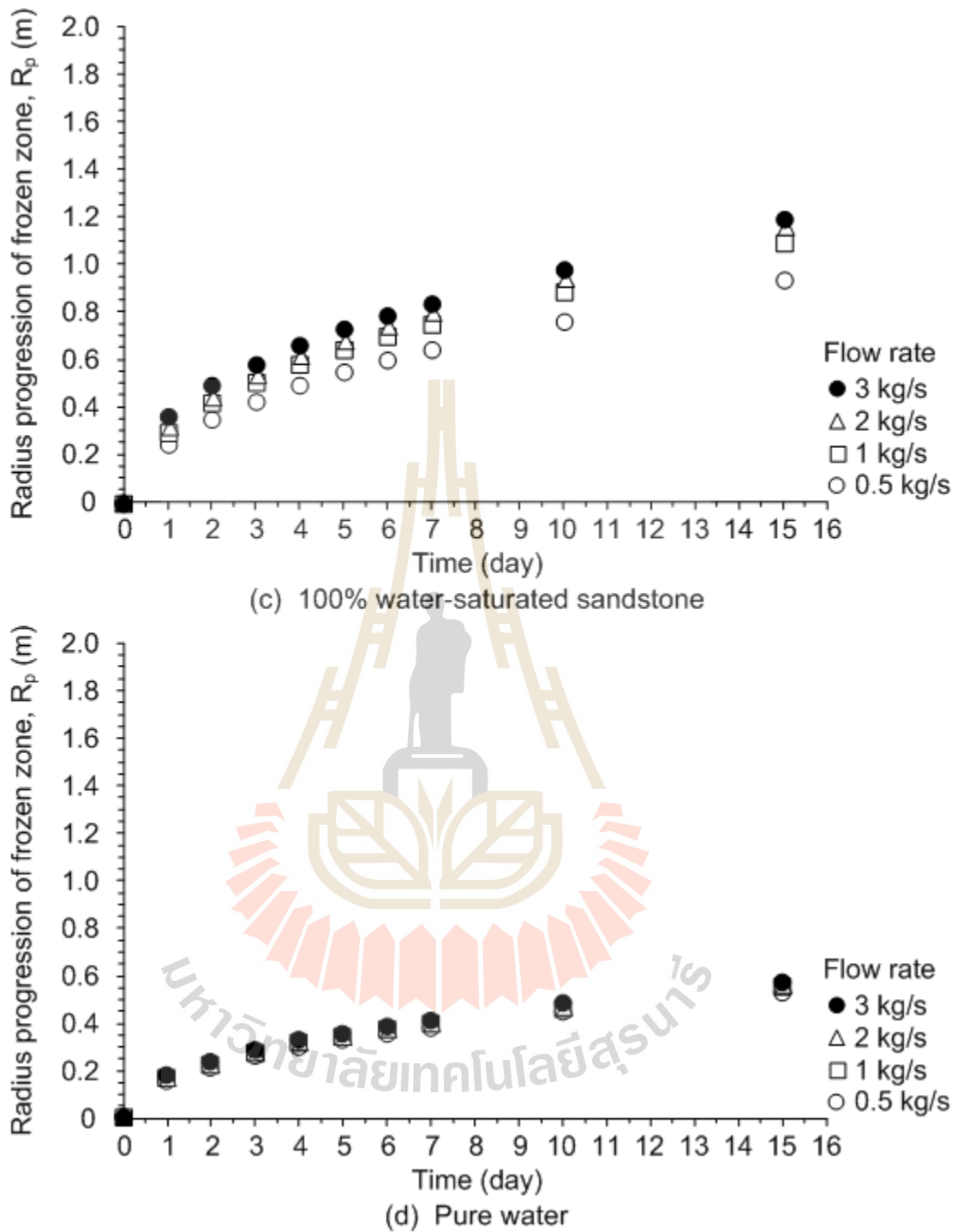


Figure 6.6 The radius distance progression of the frozen zone as a function of time in difference flow rates (cont.)

6.6 Mathematical relationship for prediction progression of frozen zone

The ground freezing process requires to design the freezing pipe system, circulates coolant through the pipe and time for freezing. In order to know the design information, it is necessary to analyze by computer simulation to recognize the distance progressive of frozen zone. However, the analyze by the computer simulation takes time to calculate for maximum accuracy. Therefore, the data from the computer simulation is created the mathematical relationship. The mathematical equation is developed to predict the location of the frozen zone. It is derived to link the thermal properties (c_p , λ), coolant flow rate and time for freeze. The equation as follow as:

$$R_p = A \left(\frac{\lambda}{c_p} \right)^B \text{rate}^C \text{time}^D \quad (6.1)$$

where R_p is the radius distance progressive of frozen zone (m), λ is thermal conductivity (W/m-K), c_p is heat capacity (J/kg-K), rate is coolant flow rate (kg/s), time is time of simulation (day) and A, B, C and D are empirical constants. The empirical constants are obtained from the regression analysis on the data using SPSS statistical software (Table 6.4). A good correlation ($R^2 = 0.910$) between the proposed equation and the data is obtained. Figure 6.7 compares the data with the prediction of the proposed equation. In this research, it does not consider the data of the ground that is pure water. Because of the fact that the groundwater flows into the excavation site is usually groundwater where is flowed through the rock strata.

Table 6.4 Parameters of mathematical relationship.

Constant parameters	Value	R^2
A	134.531	0.910
B	1.081	
C	0.118	
D	0.465	

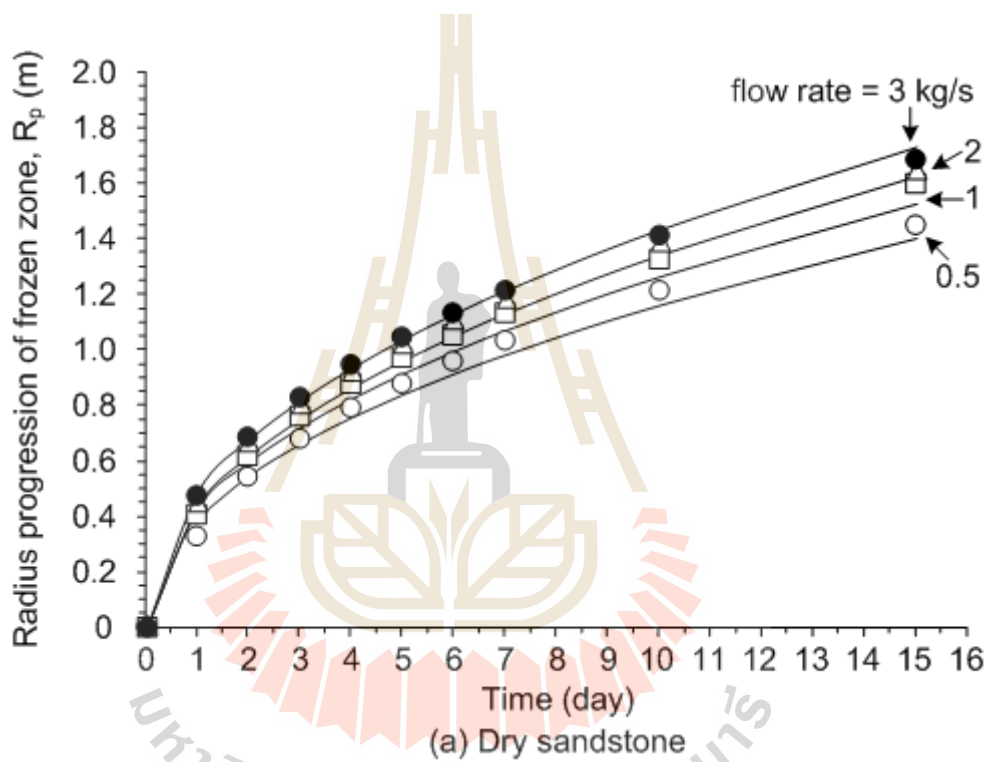


Figure 6.7 Comparison between data result (points) and proposed equation (lines) of the radius distance progression of the frozen zone

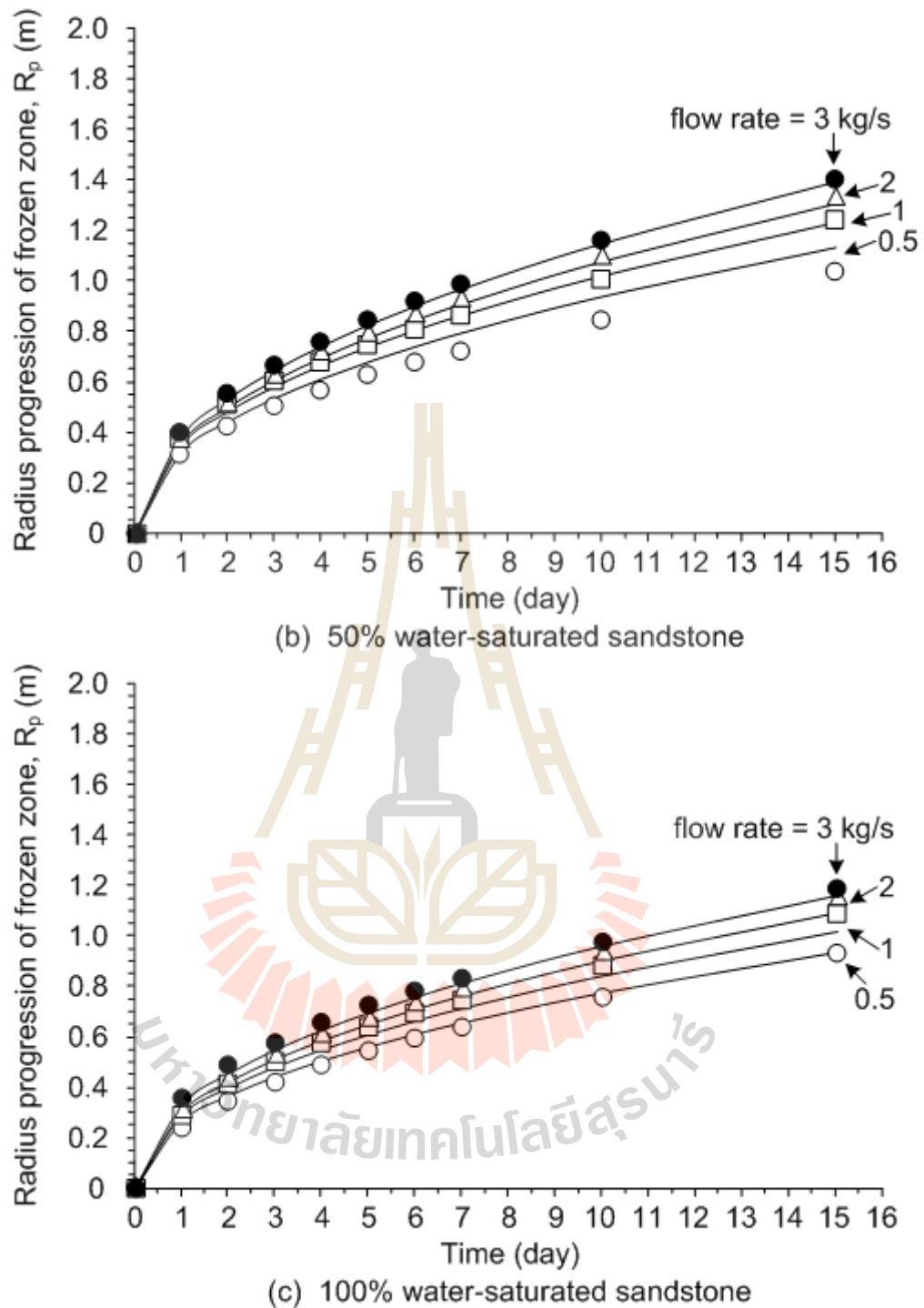


Figure 6.7 Comparison between data result (points) and proposed equation (lines) of the radius distance progression of the frozen zone (cont.)

Sager and Sayles (1979) provide the closed-form equation to predict the grow of a frozen zone around a freezing pipe follow as:

$$t = \left(\frac{R^2 L_1}{4v_s \lambda} \right) \left[2 \ln \left(\frac{R}{r_0} \right) - 1 + \left(\frac{c_p v_s}{L_1} \right) \right] \quad (6.2)$$

where

$$L_1 = L + \left(\frac{a_r^2 - 1}{2 \ln(a_r) \cdot (c_p v_0)} \right) \quad (6.3)$$

and t is time requirement of frozen zone (hr); R is radius of the frozen zone interface (m); L is latent heat of fusion of the pore water (J/m^3); v_0 is difference between the original ground temperature and the freezing point of water (Kelvin); a_r is factor which when multiplied by the frozen zone (the value a_r is typically taken to be 3 (Hofmann, 1997)); v_s is the difference (absolute value) between the temperature at the edge of the freeze pipe and the freezing point of water (Kelvin); and r_0 is radius of the freeze pipe (m).

Figure 6.8 shows the comparison between the mathematical equation in this study and the closed-form equation of Sager and Sayles (1979). It is observed that the closed-form equation is overpredicts the radius distance progression of the frozen zone that is predicted with the mathematical equation in this study. The possible explanation of the difference in the predicted frozen zone is the different temperature of coolant between in and out of a freeze pipe. The numerical simulation of this study defines the transient state of heat flow in freezing pipe, but the closed-form equation of Sager and Sayles defines the heat flow in the pipe is steady state. However, the radius progression of the frozen zone of the mathematical equation in this study tend to consistent with the

closed-form equation. The discrepancy of radius progression of the frozen zone between the mathematical equation in this study and the closed-form equation of Sager and Sayles is less than 10 percent. Hence, the mathematical equation in this study can be used to predict the radius progression of the frozen zone and design freeze pipe system for the ground freezing method.

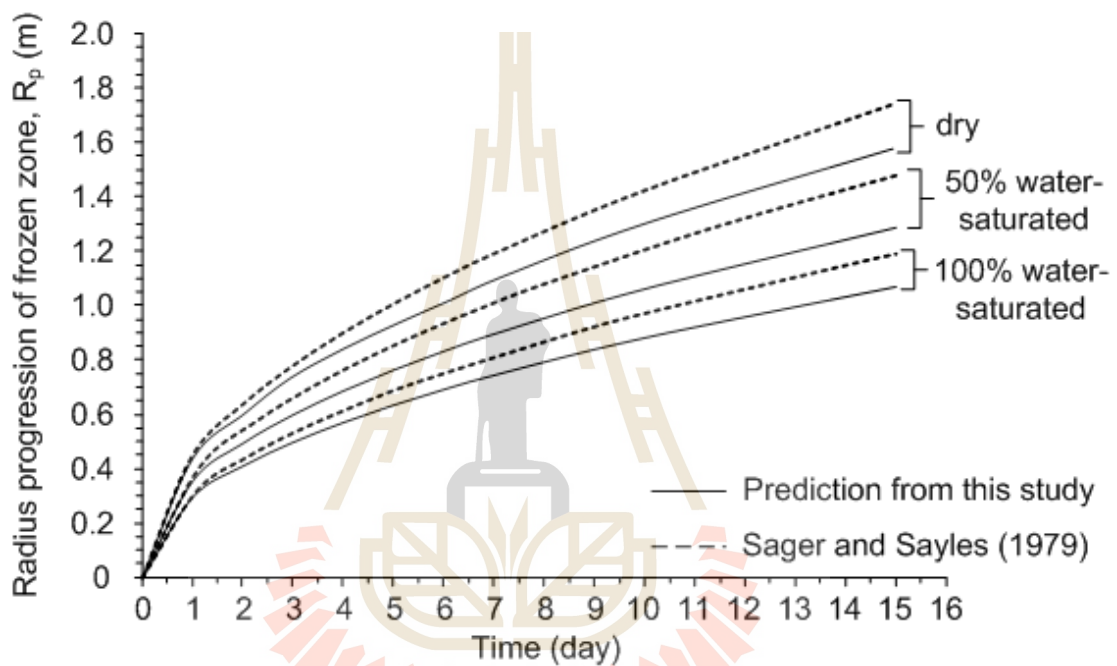


Figure 6.8 Prediction of the radius distance progression of the frozen zone from the mathematical equation in this study and the closed-form equation of Sager and Sayles (1979)

CHAPTER VII

DISCUSSIONS, CONCLUSIONS AND RECOMMENDATIONS FOR FUTURE STUDIES

7.1 Discussions

The section discusses the effects of subzero temperature on the mechanical properties of sandstone for use to predict and design of stability for excavations and simulation of heat transfer during ground freezing method.

The result of mechanical properties from laboratory testing determine the strength and deformability of Phar Wihan sandstone specimens using different confining pressures, range from 0 to 12 MPa and subzero temperatures freeze up to 233 Kelvin (-40 °C). The specimens are carried out under different three conditions (dry condition, water-saturated condition and brine-saturated condition). The testing is assumed to be under isothermal conditions (constant temperature with time during loading). It is found that the compressive strength increases with increasing confining pressure and inversely with temperatures in all of conditions. At room temperature (298 Kelvin), the strength of dry specimens is higher than the brine-saturated specimens and water-saturated specimens, respectively. This study corroborates the results of Shukla et al. (2013) and Khamrat et al. (2016). The water-saturated specimens have affected by the pore water pressure that can reduce the strength up to 1-27 percent in the ambient temperature. The strength of brine-saturated specimens is higher than those of the water-saturated specimens due to some particles of salt (NaCl) interrupts the seepage

of fluid. The strength of the specimens at 268 Kelvin is slightly higher than the specimens at 298 Kelvin in all of conditions. This is because mineral grains begin to shrink and the fluid in pore space being to freeze. When the temperature drops below 273 Kelvin (0°C), microcrack occur because of the shrinkage of mineral particles and the volume expansion when the water changes to ice. However, the findings of Walder and Hallet (1985), who report that the water in saturated rocks will be migrate toward free surfaces or large empty pores when freezing occurs in partially saturated rocks. Hence these extending cracking do not cause rock damage. At subzero temperatures (255 and 235 Kelvin), the strength of brine-saturated specimens and the water-saturated specimens are higher than dry specimens. These results are consistent with Inada and Kinoshita (2003) and Hara et al. (2014) and suggest that the strength of saturated samples is greater than that of the dry ones due to the conversion of the water in the pores to ice. The freeze point of brine is approximately about 253 Kelvin (-20°C) that is a eutectic mixture between ice and salts (NaCl). Therefore, the specimens of brine-saturated are highest strength at the subzero temperature.

The Brazilian tensile strength increased with decreasing temperature. At the temperature below 253 Kelvin, the tensile strength of brine-saturated specimens and the water-saturated specimens are greater than that of the dry one. The result is in agreement with Kodama et al. (2013) findings which showed the case of saturated rocks samples, the tensile strength is higher than dry rocks samples when the temperature freeze down to 258 Kelvin (-15°C). The dry specimens there is little increase in tensile strength at the subzero temperature. Therefore, it can be said that ice is also acted an adhesive material with contributed to increase the strength of sandstone.

The effect of subzero temperature on deformability of sandstone specimens is displayed as elastic modulus and Poisson's ratio. There is just a little bit change in the shape of the curves with temperature for the dry, brine-saturated and water-saturated conditions. The elastic modulus of brine-saturated condition is a similar value of water-saturated condition. This indicate that brine has effects on the deformation of sandstone specimen as well as water. The elastic modulus is increased with decreasing the temperature under dry, brine-saturated and water-saturated conditions. At 268 Kelvin, the elastic modulus of both brine and water saturated specimens is lower than dry specimens suggest that in porous rock is ice filled that has thin films of unfrozen water forming between ice and grain of rock. This process is occurring at temperatures in range 277 to 258 Kelvin (Vlahou and Worster, 2015). Therefore, the pore pressure is affected on deformability of rocks is reflected as a reduction of elastic modulus. This study confirms that result is accorded with Dasir et al. (2013). Poisson's ratio obtained from this study ranged from 0.27 to 0.30 for the sandstone specimens under all of conditions. This indicates that Poisson's ratio is slightly sensitive of temperatures.

On the basis of corresponding test results on rock specimens developed strength and deformability formulations as affected by the subzero temperature along with confining stresses. The empirical relation is proposed in term of principal stresses that is represented in equation 5.1. The maximum principal stresses tend to increase with decreasing temperature which is managed a non-linear. Based on the results of principal stresses and confining stresses can be calculated octahedral shear stress at failure as a function of mean stress which using the relations given by Jaeger et al. (2007). Equation 5.4 is proposed the octahedral shear stress that correlate with mean stress and temperature by determining the empirical constants in different condition. The results

of deformability are determined as elastic modulus and Poisson's ratio that can be calculated shear modulus and bulk modulus follow the relations equation from Jaeger et al. (2007). The four parameters of elastic respect to temperatures can be represented in equation 5.5 to 5.16 under different condition.

Two strength criteria used here give a good estimation of the specimen compressive strength. The Coulomb criterion can describe the cohesion and internal friction angle from the strength results for each temperature. At the subzero temperature, the effect of temperature more evidently affects the cohesion than the internal friction angle for all of conditions. The brine-saturated specimens and water-saturated specimens have the cohesion greater than the dry specimen. It can be described from this study that the ice content is bonding together the particles of rock. The Hock-Brown criterion can sufficiently predict the strength of sandstone specimen as well. The Hoek and Brown criterion uses only two material constants (m and s), the parameter "s" for intact sandstone specimens is equal 1.00. The parameters m for specimens decrease with subzero temperature. The calculated uniaxial compressive strengths of the rock specimens (σ_c) increase with decreasing temperature.

A numerical simulation based on the heat transfer is simulated to predict the radius distance progression of the frozen zone at 273 Kelvin. ANSYS 14.0 is used to simulate the numerical model for ground freezing method. The numerical ground model is validated in homogenous formation under difference four conditions include dry, 50% water saturated, 100% water saturated and pure water. The simulation is based on the thermal properties of Phara Wihan sandstone. Running time of the simulation is set at 1 to 15 days. This simulation circulates the coolant (liquid nitrogen, LN_2) flow rate at 0.5, 1, 2 and 3 kg/s. The radius distance progression of freezing zone at the ground

increases with increase of times and flow rate of coolant. The radius distance progression of dry condition is biggest than 50% water saturated, 100% water saturated and pure water, respectively. Due to the dry condition has low heat capacity value and high thermal conductivity value that lead to low energy to remove the heat and high the transmission of heat energy than other conditions. Therefore, the heat capacity (c_p) and thermal conductivity (λ) of the ground are an important factor for design freeze pipe system and the period for forming the freezing zone. The influence of the coolant flow rate on the radius distance progression can be observed from the difference temperature between the coolant in the outer pipe and outer pipe wall. The high flow rates are the expansion of frozen zone faster than low flow rates. However, the discrepancy of the radius distance progression between flow rates at 1 to 3 kg/s is less than 0.1 m. Under conditions of this study, the coolant flow rate of 1 kg/s seems to be the optimum.

The mathematical equation is proposed in equation 6.1 what uses to predict the location of the frozen zone by deriving the thermal properties of ground, coolant flow rate and time for freeze zone grow up. The result observed that the radius distance progression of frozen zone from the mathematical equation agree well with the measurement from the numerical simulation. The mathematical equation in this study is compared with the closed-form equation (Sager and Sayles, 1979). It is found that the closed-form equation is overpredict of the location of the frozen zone than the mathematical equation in this study less than 10 percent. The radius progression of the frozen zone of both equations are consistent pattern. Therefore, the mathematical equation in this study can be applied to predict the location of the frozen zone and design freeze pipe system for the ground freezing method.

7.2 Conclusions

The objectives of the research are to investigate the strength and deformability of sandstone under subzero temperature and predict the location of frozen zone during ground freezing by numerical simulation. From the obtained results, the following conclusion can be drawn:

The effect of subzero temperature on the mechanical properties of sandstone is concluded that the strength and elastic modulus increases with decreasing temperature. The mechanical properties of sandstone at 268 Kelvin (-5°C) exhibit behavior as same as the mechanical properties of sandstone at room temperature. However, at about 253 Kelvin (-20°C), the strength of brine-saturated and water-saturated is higher than dry one. The effect of subzero temperature is much more remarkable when the rock is in saturated conditions more than in dry condition. It is attributed to the freezing of the water in pore space to ice. In brine-saturated condition under subzero temperature (less 253 Kelvin) is higher strength than other condition due to ice and salt (NaCl) raise strengthen.

For the results of deformability of rock specimens is displayed elastic modulus and Poisson's ratios. This indicated that the elastic modulus of brine-saturated and water-saturated specimen are higher than dry specimens at subzero temperature. But, the Poisson's ratios of all conditions show no significant difference. From the observed in this study brine-saturated condition do not affect of the elastic modulus and Poisson's ratios of rock.

In this research proposes the empirical relation that is useful for predicting the strength and deformation characteristics of in-situ rocks subject to subzero temperature and different conditions. The empirical relations are defined in terms of principal

stresses and octahedral shear stress under subzero temperature. The maximum principal stresses increase with decreasing temperature in all condition which lead to more mechanical energy requires to apply the failure occuration. The cohesion and friction angle are calculated of the Coulomb criterion. The effect of temperature more evidently affects the cohesion than the internal friction angle. The parameters are calculated from based on Hoek and Brown criterion indicated that the parameter “m” constant decreases with decreasing temperature

The numerical simulation is capable of predicting the location of frozen zone during the ground freezing method. The distance of frozen zone increases with increasing time and flow rate. The thermal properties include thermal conductivity and heat capacity are the important factor for design the ground freezing method. The numerical results are developed the mathematical equation for predict the location of frozen zone that is proposes in Chapter 6. The mathematical equation from the numerical simulation in this study is reliable and suitable for predict the location of frozen zone.

7.3 Recommendation for future studies

The study in this research can be counted as a preliminary guideline and process of study for the ground freezing method. The research is studied in two parts include the laboratory testing under subzero temperature condition and analysis the heat transfer by the numerical simulation for ground freezing method. Thus, the requirement for future research related to this research is suggested below.

The suggestion of laboratory studies follows as:

(1) The mechanical properties test in this study carry out only Phra Wihan sandstone. Testing on a variety of rocks and soil would provide more the mechanical properties for disconformity of the ground under subzero temperature.

(2) The frozen rock mass should be should be investigated to understand of failure mechanisms for design the stability in weak zone.

(3) The effect of degree of saturation should be examined under subzero temperature and should be studies the behavior of microcrack that form by ice expansion in pore space.

(4) It is recommended that the creep test under subzero temperature condition for assess the behavior of the ground material in the long term of ground freezing method.

(5) More testing is required on the thermal properties of the ground material in difference saturated conditions for estimate fundamental thermal behavior.

(6) It is proposed that the laboratory testing confirms changes in rock properties due to freezing, numerical modeling approaches can be applied to assess the stability of mining excavations under varied conditions.

In part of numerical simulation of heat transfer recommended include the following:

(1) The numerical results of this study are simulated in a homogeneous ground without disconformity and hydraulic conductivity. but in fact, the ground freezing method must be done in a variety disconformity and encounter of hydraulic conductivity. It is suggested that the influence of these factor is investigated in future studies.

(2) It is known that the cooling system of ground freezing method divided up two main type which use the different type of coolant. It would be interesting to compare the location of frozen zone from simulation of the heat transfer in different type of coolant.

(3) The research performed here concentrated on the numerical simulation. It should be performed the physical model of ground freezing for comparison the location of frozen zone progression.

The above suggestion of future study may be costly and time consuming, however it will be reasonable in term of knowledge if this ground freezing method can be applied in Thailand.

REFERENCES

- Abdul-Rahman, H., Berawi, M.A., Berawi, A.R., Mohamed, O., Othman, M. and Yahya, I.A. (2006). Delay mitigation in the Malaysian construction industry. **Journal of Construction Engineering and Management**. 132(2): 125-133.
- Andersland, O.B. and Ladanyi, B. (2004). **Frozen ground engineering** (2nd ed). New Jersey: John Wiley and Sons Inc.
- ASTM C830. Standard Test Methods for Apparent Porosity, Liquid Absorption, Apparent Specific Gravity, and Bulk Density of Refractory Shapes by Vacuum Pressure. In **Annual Book of ASTM Standards** (Vol.15.01). West Conshohocken: American Society for Testing and Materials.
- ASTM D2216. Standard Test Methods for Laboratory Determination of Water (Moisture) Content of Soil and Rock by Mass. In **Annual Book of ASTM Standards** (Vol.04.08). West Conshohocken: American Society for Testing and Materials.
- ASTM D2664. Standard test method for triaxial compressive strength of undrained rock core specimens without pore pressure measurements. In **Annual Book of ASTM Standards** (Vol.04.08). Philadelphia: American Society for Testing and Materials.
- ASTM D3967. Standard test method for splitting tensile strength of intact rock core Specimens. In **Annual Book of ASTM Standards** (Vol.04.08). West Conshohocken: American Society for Testing and Materials.

- ASTM D7012. Standard Test Method for Compressive Strength and Elastic Moduli of Intact Rock Core Specimens under Varying States of Stress and Temperatures. In **Annual Book of ASTM Standards** (Vol.04.09). West Conshohocken: American Society for Testing and Materials.
- Beck, A. E. (1976). An improved method of computing the thermal conductivity of fluid-filled sedimentary rocks. **GEOPHYSICS**. 41(1): 133-144.
- Bergeron, F. and Pasquier, P. (2013). Simulation of ground heat exchanger for cryogenic applications. In Proceedings of the **2013 COMSOL Conference**. Boston, United States of America.
- Berggren, A.L. (2000). **Introduction to artificial ground freezing (AFG)** [On-line]. Available: <http://www.docplayer.net/42370291-Introduction-to-artificial-ground-freezing-afg.html>
- Buntebarth, G. (1991). Thermal properties of the KTB-Oberpfalz VB core samples at elevated temperature and pressure. **Scientific Drilling**. 2: 73-80.
- Cashman, P.M. and Preene, M. (2001). **Groundwater lowering in construction: A practical guide**. London and New York: Spon Press of the Taylor and Francis Group.
- Cermak, V. and Rybach, L. (1982). Thermal conductivity and specific heat of minerals and rocks, in Handbook **Physical properties of rocks (vol. 1-a)**. **Landolt-Bornstein**. edited by Angenheister G. (pp. 305-403). New York: Springer-Verlag.
- Chen, T. C., Yeung, M. R. and Mori, N. (2004). Effect of water saturation on deterioration of welded tuff due to freeze thaw action. **Cold Regions Science and Technology**. 38: 127-136.

- Clauser, C. and Huenges, E. (1995). Thermal conductivity of rocks and minerals. In T. J. Ahrens (ed.). **Rock physics & Phase relations: A handbook of Physical constants** (pp. 105-126). Washington, DC: American Geophysical Union.
- Currier, J.H. and Schulson, M. (1982). The tensile strength of ice as a function of grain size. **Acta Metallurgica**. 30(8): 1511-1514.
- Dasri, R., Phueakphum D. and Fuenkajorn, K. (2013). Indirect assessment of pore pressure effects on compressive strengths and elasticity of three Thai sandstones. In the Proceedings of **Fourth Thailand Symposium on Rock Mechanics** (ThaiRock 2013). Nakhon Ratchasima, Thailand.
- Dorst, R.V. (2013). Artificial ground freezing as a construction method for underground spaces in densely built up areas. **Master's Thesis**. Department of Geo-Engineering. Delft University of Technology. Delft, Netherlands.
- Dwivedi, R. D., Goel, R. K., Prasad, V. V. R. and Sinha, A. (2008). Thermomechanical properties of Indian and other granites. **International Journal of Rock Mechanics and Mining Sciences**. 45(3): 303-315.
- Dwivedi, R.D., Singh, P.K., Singh T.N. and Singh D.P. (1998). Compressive strength and tensile strength of rocks at sub-zero temperature. **Indian Journal of Engineering and Material Sciences**. 5: 43-48.
- Erguler, Z.A. and Ulusay, R. (2009). Water-induced variations in mechanical properties of clay-bearing rocks. **International Journal of Rock Mechanics and Mining Sciences**. 46(2): 355–370.
- Gold, L. W. (1988). On the elastic of the ice plates. **Canadian Journal of Civil Engineering**. 15: 1080-1084.

- Hara, S., Kodamab, J., Fujiib, Y., Fukudab, D., Mitsuib, Y. and Sugiuraa, T. (2014). Uniaxial compressive strength of Shikotsu Welded Tuff and Bibai Sandstone at sub-zero temperature. In Proceedings of the **Eighth Asian Rock Mechanics Symposium**. Sapporo, Japan.
- Harris, J.S. (1995). **Ground freezing in practice**. London: Thomas Telford Services Ltd.
- Hashin, Z. and Shtrikman, H. (1962). A variational approach to the theory of the effective magnetic permeability of multiphase materials. **Journal of Applied Physics**. 33: 3125-3131.
- Haß, H. and Schäfers, S. (2006) **Application of ground freezing for underground construction in soft ground**. London: Taylor and Francis Group.
- Hoek, E. and Brown, E. T. (1990). **Underground excavations in rock** (pp. 102-106). London: Institution of Mining and Metallurgy.
- Hooke, R.L.B., Mellor, M. Budd, W.F., Glen, J.W., Higashi, A. and Jacka, T.H. (1980). Mechanical properties of polycrystalline ice: An assessment of current knowledge and priorities for research: Report prepared for the International Commission on Snow and Ice, with support from the U.S. National Science Foundation. **Cold Regions Science and Technology**. 3(4): 263-275.
- Hurst, J.E. and Harrison, B.K. (1992). Estimation of liquid and solid heat capacities using a modified Kopp's rule. **Chemical Engineering Communications**. 122: 21-30.
- Inada, Y. and Kinoshita, N. (2003). A few remarks on storage of low temperature materials in rock caverns. In Proceedings of the **International Society for Rock**

- Mechanics. (Technology roadmap for rock mechanics).** South African Institute of Mining and Metallurgy.
- Inada, Y. and Yokota, K. (1984). Some studies of low temperature rock strength. **International Journal of Rock Mechanics and Mining Sciences & Geomechanics Abstracts.** 21(3): 145-153.
- Inada, Y., Kinoshita, N., Ebisawa, A. and Gomi, S. (1997). Strength and deformation characteristics of rocks after undergoing thermal hysteresis of high and low temperatures. **International journal of rock mechanics and mining sciences & geomechanics abstracts.** 34:3-4.
- Jaeger, J. C., Cook, N. G. W., Zimmerman, R. W. (2007). **Fundamentals of Rock Mechanics Fourth Edition** (pp. 17-73). Oxford: Blackwell Publishing.
- Jessberger, H. and Vyalov, S. (1978) General Report. In Proceedings of the **First International Symposium on Ground Freezing** (vol.2 pp. 15-20). Bochum, Germany.
- Johansson, T. (2009). Artificial ground freezing in clayey soils. Laboratory and field studies of deformations during thawing at the Bothnia line. **Doctor's Thesis.** Department of Civil and Architectural Engineering. Royal Institute of Technology. Stockholm, Sweden.
- Jones, S.J. (1982). The confine compressive strength of polycrystalline ice. **Journal of Glaciology.** 28(98):171-177.
- Jumikis, A. R. (1996). **Thermal soil mechanics.** New Jersey: Rutgers University Press.
- Jumikis, A.R. (1977). **Thermal geotechnics.** New Jersey: Rutgers University Press.
- Khamrat, S., Archeeploha, S. and Fuenkajorn, K. (2016). Pore pressure effects on strength and elasticity of ornamental stones. **Science Asia.** 42: 121-135.

- Kim, Y.S., Kang J.M., Lee, J. Hong, S.S. and Kim K.J. (2012). Finite element modeling and analysis for artificial ground freezing in egress shafts. **KSCE Journal of Civil Engineering**. 16(6): 925-932
- Kodama J., Goto T., Fujii Y. and Hagan, P. (2013). The effects of water content, temperature and loading rate on strength and failure process of frozen rocks. **International Journal of Rock Mechanics and Mining Sciences**. 62: 1-13.
- Kutas, R. I. and Gordiyenko, V. V. (1970). Thermal fields of the Eastern Carpathians. In Proceedings of the **United Nations Symposium on the Development and Utilization of Geothermal Resources** (Vol. 2, pp.1063-1066). Pisa, Italy.
- Liang, W., Yang, X. Gao, H. Zhang, C., Zhao, Y. and Dusseault, M. B. (2012). Experimental study of mechanical properties of gypsum soaked in brine. **International Journal of Rock Mechanics and Mining Sciences**. 53: 142-150.
- Liu, H., Yang, G. S., Shen, Y. J., Ye, W. J. and Zhang, H. M. (2015). Analysis of water and ice content during rock freezing based on the three-valued segmentation of frozen rock CT images. In Proceedings of the **Third ISRM Young Scholars Symposium on Rock Mechanics**. Xi'an, China.
- Liu, Q. S., Xu, G. M., Hu, Y. H. and Chang, X. (2006). Study on basic mechanical behaviors of rocks at low temperatures. **Key Engineering Materials**. 306-308: 1479-1484.
- Long, C. and Sayma, N. (2009). **Heat transfer** [On-line]. Available: <http://www.bookboon.com/en/heat-transfer-ebook>.

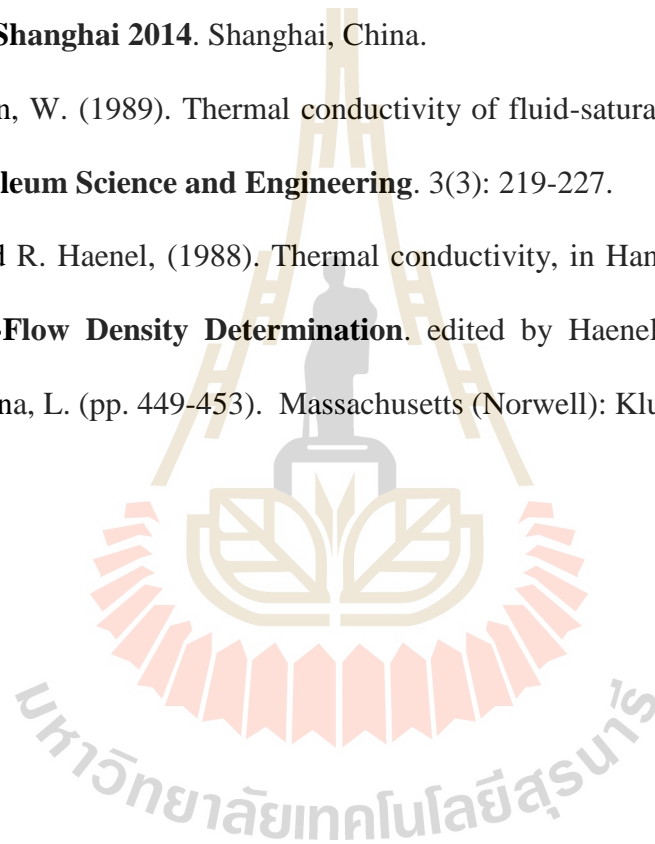
- Ma, L., Qi, J., Yu1, F. and Yao, X. (2016). Experimental study on variability in mechanical properties of a frozen sand as determined in triaxial compression tests. **Acta Geotechnica**. 11: 61-70
- Madenci, E. and Guven, I. (2006). **The finite element method and application in Engineering using ANSYS** (Chapter II). New York: Springer Science and Business Media, Inc.
- Matsuoka, N. (1990). Mechanisms of rock breakdown by frost action: an experimental approach. **Cold Regions Science and Technology**. 17: 253-270
- Mellor, M. (1971). Strength and deformability of rocks at low temperatures: Research Report 294. **U.S. Army Cold Regions Research and Engineering Laboratory**.
- Mellor, M. (1973). Normalization of specific energy values. **International Journal of Rock Mechanics and Mining Sciences**. 9: 661-663.
- Moore Trenching Machine excavator (2014). **New ground freezing brochure** [Online]. Available: <http://www.moretrench.com/wp-content/uploads/2014/11/New-Ground-Freezing-Brochure.pdf>
- Nater, P., Arenson, L.U. and Springman, S.M. (2008). Choosing geotechnical parameters for slope stability assessments in alpine permafrost soils. In Proceeding of the **Ninth International conference on permafrost**. Fairbanks, Alaska.
- Nemati, K. M. (2007). **Temporary structures: Construction dewatering and ground freezing**. Department of construction management. University of Washington. Seattle, Washington, United States.

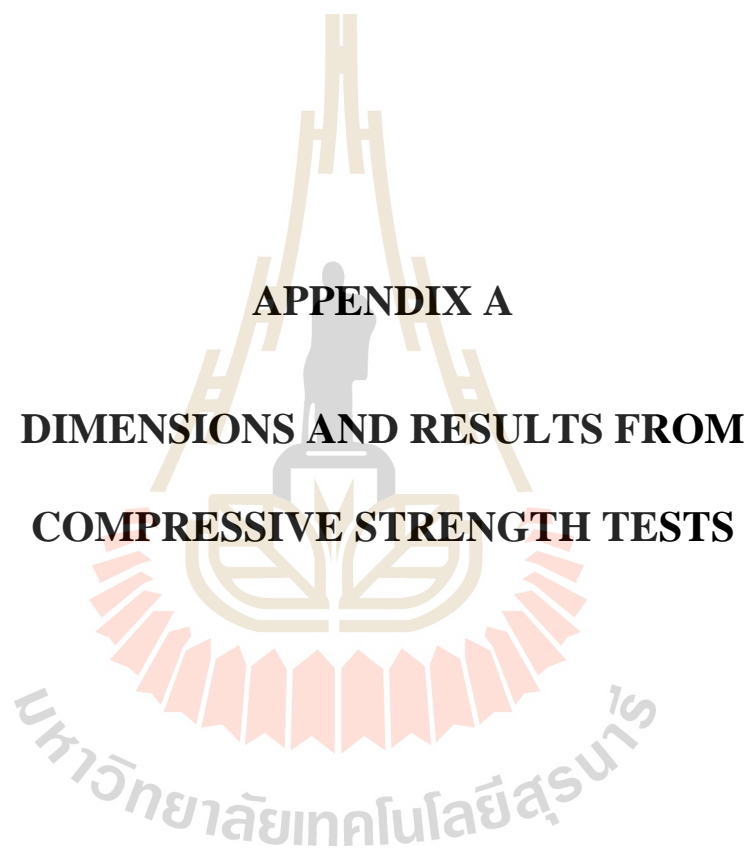
- Ou, C.Y., Kao, C.C. and Chen, C.I. (2009). Performance and analysis of artificial ground freezing in the shield tunneling. **Journal of GeoEngineering**. 4(1): 29-40.
- Parameswaran V. R. (1980). Deformation behaviour and strength of frozen sand. **Canadian Geotechnical Journal**. 17(1): 74-88
- Peaker, S. (2003). Minimizing geo-exposure through comprehensive investigation. **Journal of Professional Issues in Engineering Education and Practice**. 129(2): 77-79.
- Petrovic, J. J. (2003). Review mechanical properties of ice and snow. **Journal of materials science**. 38: 1-6.
- Phueakphum, D. (2008). Experimental assessment of solar thermal energy storage in basaltic rock fill. **Doctor's Thesis**. Engineering of Geotechnology. Suranaree University of Technology. Nakhon Ratchasima, Thailand.
- Rathnaweera, T.D., Ranjith, P.G. and Perera, M.S.A. (2014). Salinity-dependent strength and stress-strain characteristics of reservoir rocks in deep saline aquifers: An experimental study. **Fuel**. 122: 1-11.
- Sadeghpour, A. H. Ghanbari, A. and Fadaee, M. (2008). Groundwater lowering in deep excavation (case study: foundation excavation of shahid madani dam). In Proceedings of the **Sixth International Conference on Case Histories in Geotechnical Engineering**. Arlington, Virginia.
- Sanger, F.J. and Sayles. F.H. (1979). Thermal and rheological computations for artificially frozen ground construction. **Engineering Geology**. 13: 311-337

- Sass, J. H., Lachenbruch, A. H., Moses, T. and Morgan, P. (1992). Heat flow from a scientific research well at Cajon Pass, California. **Journal of Applied Physics**. 97: 5017-5030.
- Sayles, F. (1973). Triaxial and Creep Tests on Frozen Ottawa Sand. In Proceedings of the **North American Contribution to the Second International Conference on Permafrost** (pp. 384-391). Washington D.C., USA.
- Schmall, P.C. and Maishman, D. (2007). **Ground freezing a proven technology in mine shaft sinking**. [On-line]. Available: http://www.moretrench.com/wpcontent/uploads/2014/11/Ground_Freezing_a_proven.pdf
- Schulson, E.M. (1999). The structure and mechanical behavior of ice. **Journal of Minerals: Metals and Materials Society**. 51(2): 21-27
- Shster, J. (1980). Engineering quality assurance for construction ground freezing. In Proceedings of the **Second International Symposium on Ground Freezing**. Trondheim, Norway.
- Shukla, R., Ranjith, P. G., Choi, S. K., Haque, A., Yellishetty, M. and Hong, L. (2013). Mechanical behaviour of reservoir rock under brine saturation. **Rock Mechanics and Rock Engineering**. 46: 83-93.
- Sinnott, R. K. (1993). **Chemical Engineering Design** (2nd ed). Oxford: Pergamon Press Ltd.
- Somerton, W.H. (1992). Thermal properties and temperature-related behavior of rock/fluid systems (Chapter II). **Developments in Petroleum Science**. 37: 8-21.
- Sopoko, J. and Aluce, G. (2005). **Artificial Ground Freezing for Environmental Remediation**. [On-line]. Available: <https://www.groundfreezing.com>.

- Stoss, K. and Valk, J. (1979). Uses and limitations of ground freezing with liquid nitrogen. **Engineering Geology**. 13(1-4):485-494.
- Sundberg, J. (1998). **Thermal properties of soils and rocks**. Department of Geology. Chalmers University of Technology, University of Goteborg. Goteborg, Sweden.
- Suwanich, P. (2010). Geology and Geological structure of potash and rock salt deposits in Chalerm Phrakiat district, Nakhon Ratchasima province in northeastern Thailand. **Kasetsart Journal (Natural Science)**. 44: 1058-1068.
- Vitel, M., Rouabhi, A., Tijani, M. and Guérin, F. (2015). Modeling heat transfer between a freeze pipe and the surrounding ground during artificial ground freezing activities. **Computers and Geotechnics**. 63: 99-111.
- Vlahou, I. and Worster, M. G. (2015). Freeze fracturing of elastic porous media: a mathematical model. **Proceedings. Mathematical, Physical, and Engineering Sciences**. 471: 20140741.
- Wang, D.Y., Ma, W., Chang, X.X. and Wang, A.G. (2005). Study on the resistance to deformation of artificially frozen soil in deep alluvium. **Cold Regions Science and Technology**. 42(3): 194-200.
- Waples, A. W. and Waples, J. S. (2004). A review and evaluation of specific heat capacities of rock, minerals, and subsurface fluids, Part 1: Minerals and nonporous rocks. *Natural Resources Research* 13(2): 97-122.
- Weinberg, B. (1938). **Mechanical properties of ice** [On-line]. Available: <http://www.hydrologie.org/redbooks/a023/023045.pdf>
- Woodside, W. and Messmer, J.H. (1961). Thermal conductivity of porous media. II. consolidated rocks. **Journal of Applied Physics**. 32: 1669-1706.

- Yamabe, T. and Neupane, K. (2001). Determination of some thermo-mechanical properties of Shirahama sandstone under subzero temperature condition. **International Journal of Rock Mechanic and Mining Sciences**. 38: 1029-1034.
- Zhou¹, M.M. and Meschke, G. (2014). Numerical modeling of artificial ground freezing: multiphase modeling and strength upscaling. In Proceedings of the **Geo-Shanghai 2014**. Shanghai, China.
- Zimmwerman, W. (1989). Thermal conductivity of fluid-saturated rocks. **Journal of Petroleum Science and Engineering**. 3(3): 219-227.
- Zoth, G., and R. Haenel, (1988). Thermal conductivity, in Handbook of **Terrestrial Heat-Flow Density Determination**. edited by Haenel, R. Rybach, L. and Stegena, L. (pp. 449-453). Massachusetts (Norwell): Kluwer Academic.





APPENDIX A

**DIMENSIONS AND RESULTS FROM
COMPRESSIVE STRENGTH TESTS**

Table A.1 Dry sandstone specimens prepared for compression tests

Samples No.	Dimeter (mm)	Length (mm)	Weight (g)	L/D	Dry density (g/cm ³)
1	55.30	111.60	597.10	2.02	2.23
2	55.70	111.60	595.40	2.00	2.19
3	55.50	111.10	613.50	2.00	2.28
4	55.60	111.30	613.80	2.00	2.27
5	55.20	110.40	590.20	2.00	2.24
6	55.60	111.90	620.50	2.01	2.29
7	55.40	111.40	597.90	2.01	2.23
8	55.70	111.50	596.80	2.00	2.20
9	55.70	111.40	598.20	2.00	2.20
10	55.20	110.40	594.50	2.00	2.25
11	55.30	110.70	591.70	2.00	2.23
12	55.40	111.00	623.60	2.00	2.33
13	55.60	111.30	596.60	2.00	2.21
14	55.40	110.90	601.90	2.00	2.25
15	55.50	111.60	598.10	2.01	2.22
16	55.60	111.60	597.90	2.01	2.21
17	55.60	111.50	618.90	2.01	2.29
18	55.20	110.80	614.90	2.01	2.32
19	55.50	111.30	617.90	2.01	2.30
20	55.40	111.10	600.80	2.01	2.24
21	55.60	111.70	622.00	2.01	2.29
22	55.50	111.00	624.80	2.00	2.33
23	55.50	111.20	592.40	2.00	2.20
24	55.50	111.10	597.00	2.00	2.22
25	55.70	111.50	594.50	2.00	2.19
26	55.50	111.00	627.50	2.00	2.34
27	55.20	110.50	596.70	2.00	2.26
28	55.50	111.20	602.40	2.00	2.24
29	55.20	110.50	610.50	2.00	2.31
30	55.40	111.70	616.70	2.02	2.29
31	55.50	110.90	590.70	2.00	2.20
32	55.60	112.00	605.60	2.01	2.23
33	55.60	111.30	596.60	2.00	2.21
34	55.50	111.10	602.70	2.00	2.24
35	55.30	110.70	617.50	2.00	2.32
36	55.00	110.30	590.00	2.01	2.25

Table A.1 Dry sandstone specimens prepared for compression tests (cont.)

Samples No.	Dimeter (mm)	Length (mm)	Weight (g)	L/D	Dry density (g/cm ³)
37	55.60	111.20	617.20	2.00	2.29
38	55.50	111.30	600.20	2.01	2.23
39	55.30	110.70	590.80	2.00	2.22
40	55.50	111.00	592.80	2.00	2.21
41	54.00	111.00	570.50	2.06	2.25
42	54.00	111.80	571.00	2.07	2.23
43	54.00	111.60	564.50	2.07	2.21
44	54.40	110.40	572.50	2.03	2.23
45	54.10	110.40	571.50	2.04	2.25
46	54.00	111.40	573.00	2.06	2.25
47	54.00	110.30	569.50	2.04	2.26
48	54.00	112.00	573.00	2.07	2.24
49	54.40	110.60	583.00	2.03	2.27
50	54.20	111.90	571.50	2.06	2.21
51	54.00	112.00	573.00	2.07	2.24
52	54.40	110.80	569.50	2.04	2.21
53	54.20	110.00	561.00	2.03	2.21
54	54.20	109.10	574.50	2.01	2.28
55	54.20	109.70	568.00	2.02	2.25
56	54.00	110.40	574.00	2.04	2.27
57	54.00	111.70	569.50	2.07	2.23
58	54.00	111.00	570.50	2.06	2.25
59	54.50	110.80	591.50	2.03	2.29
60	54.30	111.80	596.00	2.06	2.30
61	54.00	109.50	562.00	2.03	2.24
62	54.00	110.00	561.50	2.04	2.23
63	54.00	110.30	581.50	2.04	2.30
64	54.10	109.30	573.00	2.02	2.28
65	54.00	111.00	569.00	2.06	2.24
66	54.00	109.60	563.50	2.03	2.25
67	54.20	109.00	572.00	2.01	2.28
68	54.00	109.70	570.00	2.03	2.27
69	54.00	110.40	580.00	2.04	2.30
70	54.00	108.50	560.50	2.01	2.26
71	54.00	108.00	563.00	2.00	2.28
72	54.00	110.00	566.50	2.04	2.25

Table A.1 Dry sandstone specimens prepared for compression tests (cont.)

Samples No.	Dimeter (mm)	Length (mm)	Weight (g)	L/D	Dry density (g/cm ³)
73	54.00	109.30	573.50	2.02	2.29
74	54.10	108.80	567.50	2.01	2.27
75	54.10	109.30	573.00	2.02	2.28
76	54.00	109.20	563.00	2.02	2.25
77	54.00	109.10	572.00	2.02	2.29
78	54.10	108.50	557.00	2.01	2.23
79	54.20	109.60	572.50	2.02	2.27
80	54.00	110.40	580.00	2.04	2.30



Table A.2 Water-saturated sandstone specimens prepared for compression tests

Samples No.	Dimeter (mm)	Length (mm)	Weight (g)	L/D	Dry density (g/cm ³)	Water content (%)	Water saturated density (g/cm ³)
1	54.20	108.30	574.50	2.00	2.30	4.35	2.40
2	54.40	111.50	587.50	2.05	2.27	4.77	2.38
3	54.40	110.25	581.50	2.03	2.27	4.99	2.38
4	54.40	109.75	589.00	2.02	2.31	3.99	2.40
5	54.40	111.10	593.00	2.04	2.30	4.47	2.40
6	54.20	108.40	576.00	2.00	2.30	5.12	2.42
7	54.30	110.95	583.00	2.04	2.27	4.72	2.38
8	54.50	110.85	591.50	2.03	2.29	4.90	2.40
9	54.60	108.95	571.00	2.00	2.24	4.38	2.34
10	54.40	109.30	583.00	2.01	2.30	4.97	2.41
11	54.40	110.60	583.00	2.03	2.27	5.06	2.38
12	54.30	110.40	587.00	2.03	2.30	4.60	2.40
13	54.30	108.60	569.00	2.00	2.26	5.18	2.38
14	54.35	110.00	590.50	2.02	2.32	3.98	2.41
15	54.35	110.40	577.50	2.03	2.26	5.89	2.39
16	54.20	109.60	577.50	2.02	2.28	5.37	2.41
17	54.25	108.85	570.50	2.01	2.27	4.56	2.37
18	54.30	109.00	583.00	2.01	2.31	4.03	2.40
19	54.20	111.00	585.00	2.05	2.29	4.10	2.38
20	54.40	110.00	591.00	2.02	2.31	4.65	2.42
21	54.20	109.15	575.00	2.01	2.28	6.00	2.42
22	54.35	111.80	596.00	2.06	2.30	4.45	2.40
23	54.40	110.95	576.00	2.04	2.23	4.95	2.35
24	54.20	111.45	596.00	2.06	2.32	4.28	2.42
25	54.50	111.50	594.00	2.05	2.28	4.12	2.38
26	54.30	110.70	574.50	2.04	2.24	4.87	2.35
27	54.00	111.82	573.50	2.07	2.24	5.06	2.35
28	54.10	111.40	582.50	2.06	2.28	4.81	2.39
29	54.00	111.30	576.00	2.06	2.26	5.21	2.38
30	54.15	110.65	567.00	2.04	2.23	5.56	2.35
31	54.20	109.60	575.00	2.02	2.28	4.78	2.38
32	54.40	110.00	587.00	2.02	2.30	4.94	2.41
33	54.10	109.60	571.00	2.03	2.27	4.64	2.37

Table A.2 Water-saturated sandstone specimens prepared for compression tests

(cont.)

Samples No.	Dimeter (mm)	Length (mm)	Weight (g)	L/D	Dry density (g/cm ³)	Water content (%)	Water saturated density (g/cm ³)
34	54.45	109.00	579.50	2.00	2.28	5.00	2.40
35	54.40	109.70	584.00	2.02	2.29	4.54	2.40
36	54.10	110.60	567.00	2.04	2.23	5.47	2.35
37	54.10	110.70	571.50	2.05	2.25	5.77	2.38
38	54.00	110.90	570.00	2.05	2.25	4.91	2.36
39	54.15	112.50	575.50	2.08	2.22	4.69	2.33
40	54.10	109.60	564.00	2.03	2.24	5.59	2.36
41	54.30	111.80	574.50	2.06	2.22	5.66	2.35
42	55.80	111.90	594.00	2.01	2.17	6.48	2.31
43	54.20	111.90	571.50	2.06	2.21	5.86	2.34
44	54.50	111.30	574.00	2.04	2.21	5.05	2.32
45	54.40	111.20	582.00	2.04	2.25	5.33	2.37
46	54.00	111.20	568.50	2.06	2.23	5.89	2.37
47	54.00	110.00	577.00	2.04	2.29	5.46	2.42
48	54.10	112.00	566.00	2.07	2.20	5.83	2.33
49	54.60	110.90	584.00	2.03	2.25	5.57	2.38
50	54.50	111.80	578.50	2.05	2.22	5.10	2.33
51	54.00	109.20	560.00	2.02	2.24	5.71	2.37
52	54.10	109.90	561.50	2.03	2.22	5.97	2.36
53	54.00	112.20	577.50	2.08	2.25	5.54	2.37
54	54.00	111.90	570.00	2.07	2.23	5.35	2.34
55	54.10	111.30	567.00	2.06	2.22	5.47	2.34
56	54.00	110.60	565.50	2.05	2.23	5.84	2.36
57	54.00	111.30	571.00	2.06	2.24	5.87	2.37
58	54.30	110.80	567.00	2.04	2.21	5.91	2.34
59	54.00	111.40	574.00	2.06	2.25	5.05	2.36
60	54.30	111.20	576.00	2.05	2.24	5.56	2.36
61	54.10	111.40	582.50	2.06	2.28	5.06	2.39
62	54.30	110.70	574.50	2.04	2.24	5.22	2.36
63	54.35	110.40	577.50	2.03	2.26	4.94	2.37
64	54.00	108.10	556.50	2.00	2.25	5.93	2.38
65	54.40	110.00	570.50	2.02	2.23	5.78	2.36
66	54.00	111.30	576.00	2.06	2.26	5.90	2.39

Table A.2 Water-saturated sandstone specimens prepared for compression tests

(cont.)

Samples No.	Dimeter (mm)	Length (mm)	Weight (g)	L/D	Dry density (g/cm ³)	Water content (%)	Water saturated density (g/cm ³)
67	54.00	111.82	573.50	2.07	2.24	6.19	2.38
68	54.15	110.65	567.00	2.04	2.23	5.47	2.35
69	54.00	109.50	571.00	2.03	2.28	5.25	2.40
70	54.00	110.00	574.00	2.04	2.28	5.05	2.39
71	54.00	110.90	570.00	2.05	2.25	5.88	2.38
72	54.15	112.50	575.50	2.08	2.22	5.65	2.35
73	54.00	109.00	565.00	2.02	2.26	5.22	2.38
74	54.20	108.50	561.50	2.00	2.24	5.43	2.37
75	54.20	109.60	572.50	2.02	2.27	5.33	2.39
76	54.10	109.60	564.00	2.03	2.24	5.14	2.35
77	54.00	110.80	571.50	2.05	2.25	5.16	2.37
78	54.00	110.00	574.00	2.04	2.28	5.14	2.40
79	54.00	110.40	580.00	2.04	2.30	5.00	2.41
80	54.00	108.50	560.50	2.01	2.26	5.44	2.38



Table A.3 Brine-saturated sandstone specimens prepared for compression tests

Samples No.	Dimeter (mm)	Length (mm)	Weight (g)	L/D	Dry density (g/cm ³)	brine content (%)	Brine saturated density (g/cm ³)
1	54.30	109.60	582.50	2.02	2.30	5.84	2.43
2	54.40	110.10	588.00	2.02	2.30	5.53	2.43
3	54.50	109.65	576.00	2.01	2.25	7.38	2.42
4	54.60	110.20	586.50	2.02	2.27	5.88	2.41
5	54.65	109.60	589.00	2.01	2.29	5.77	2.42
6	54.32	109.40	578.00	2.01	2.28	6.57	2.43
7	54.46	109.90	585.50	2.02	2.29	5.12	2.41
8	54.12	111.30	586.50	2.06	2.29	6.65	2.44
9	54.50	110.20	578.50	2.02	2.25	5.53	2.38
10	54.30	109.86	571.00	2.02	2.25	5.87	2.38
11	54.80	111.30	588.50	2.03	2.24	6.80	2.40
12	54.56	111.20	594.00	2.04	2.29	6.06	2.42
13	54.28	109.80	576.00	2.02	2.27	6.25	2.41
14	54.70	109.60	594.00	2.00	2.31	5.64	2.44
15	54.40	109.44	571.50	2.01	2.25	6.39	2.39
16	54.30	109.56	574.00	2.02	2.26	5.57	2.39
17	54.10	109.89	582.00	2.03	2.31	6.10	2.45
18	54.30	110.22	568.50	2.03	2.23	6.51	2.37
19	54.10	110.22	577.00	2.04	2.28	5.81	2.41
20	54.00	109.50	566.00	2.03	2.26	6.36	2.40
21	54.06	110.10	578.00	2.04	2.29	6.06	2.43
22	54.00	110.80	578.50	2.05	2.28	6.22	2.42
23	54.00	109.90	567.00	2.04	2.25	5.73	2.38
24	54.35	109.95	574.50	2.02	2.25	5.83	2.38
25	54.55	111.20	576.00	2.04	2.22	6.42	2.36
26	54.50	111.40	582.50	2.04	2.24	5.92	2.38
27	54.50	110.75	573.50	2.03	2.22	6.28	2.36
28	54.60	110.40	578.00	2.02	2.24	5.71	2.36
29	54.40	109.10	576.50	2.01	2.27	6.50	2.42
30	54.80	110.10	570.50	2.01	2.20	5.43	2.32
31	54.26	110.00	571.50	2.03	2.25	6.56	2.40
32	54.38	110.20	574.50	2.03	2.25	5.40	2.37
33	54.44	110.30	581.50	2.03	2.27	6.88	2.42

Table A.3 Brine-saturated sandstone specimens prepared for compression tests

(cont.)

Samples No.	Dimeter (mm)	Length (mm)	Weight (g)	L/D	Dry density (g/cm ³)	brine content (%)	Brine saturated density (g/cm ³)
34	54.90	110.30	581.50	2.01	2.23	5.93	2.36
35	54.15	110.40	573.00	2.04	2.25	6.54	2.40
36	54.60	110.20	571.50	2.02	2.22	6.56	2.36
37	54.30	109.60	570.50	2.02	2.25	6.75	2.40
38	54.40	109.50	572.50	2.01	2.25	6.29	2.39
39	54.40	109.30	572.00	2.01	2.25	5.77	2.38
40	54.50	109.40	581.00	2.01	2.28	6.11	2.42
41	54.60	110.30	584.00	2.02	2.26	6.34	2.41
42	54.60	109.60	575.00	2.01	2.24	6.61	2.39
43	54.60	110.30	573.00	2.02	2.22	6.63	2.37
44	54.30	111.00	583.50	2.04	2.27	6.00	2.41
45	54.50	110.30	567.50	2.02	2.21	6.26	2.34
46	54.50	110.10	573.50	2.02	2.23	5.67	2.36
47	54.30	110.60	576.00	2.04	2.25	5.90	2.38
48	54.52	110.63	585.00	2.03	2.27	6.15	2.41



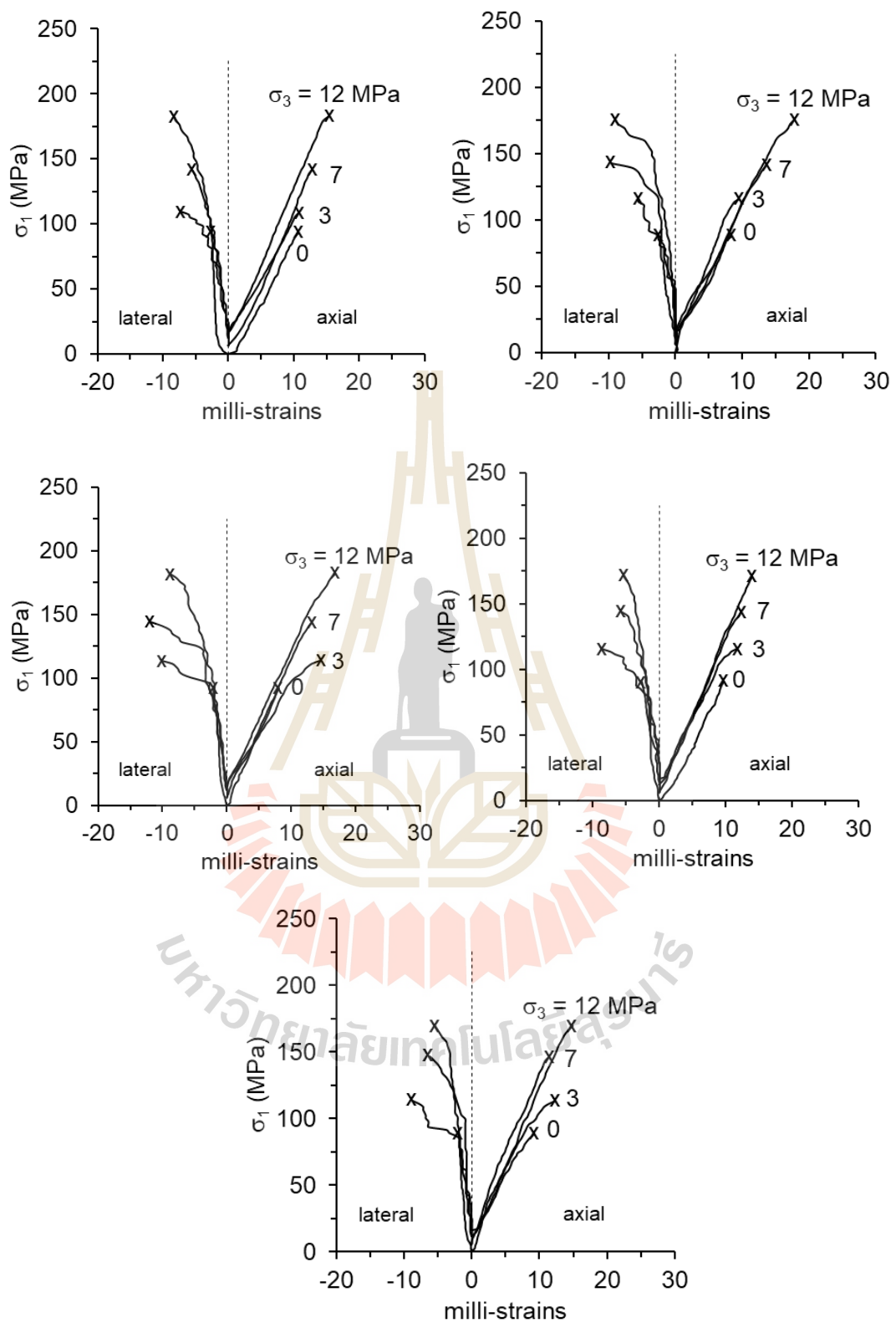


Figure A.1 Stress-strain curves obtained from dry sandstone specimens at 233

Kelvin

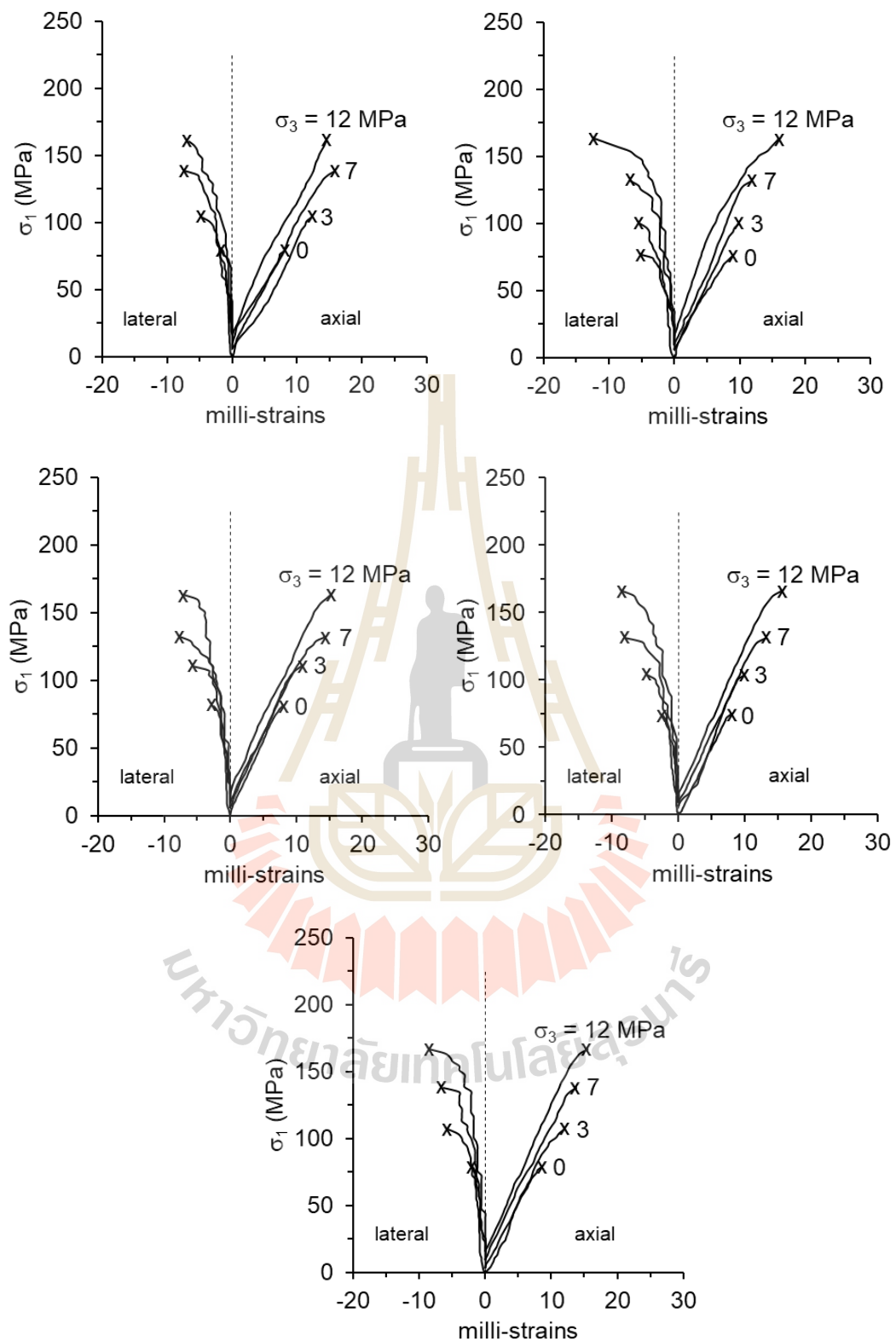


Figure A.2 Stress-strain curves obtained from dry sandstone specimens at 253

Kelvin

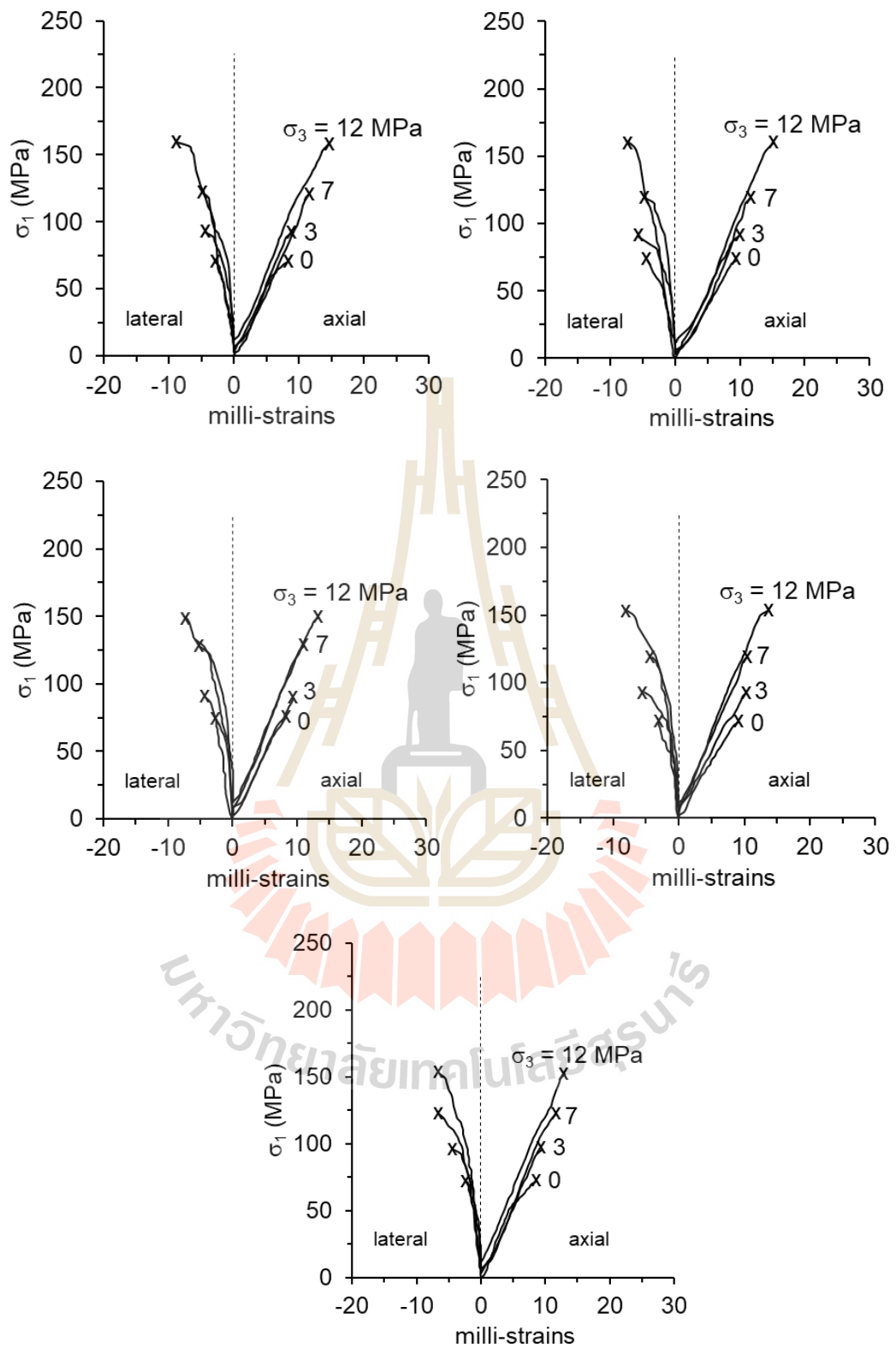


Figure A.3 Stress-strain curves obtained from dry sandstone specimens at 268

Kelvin

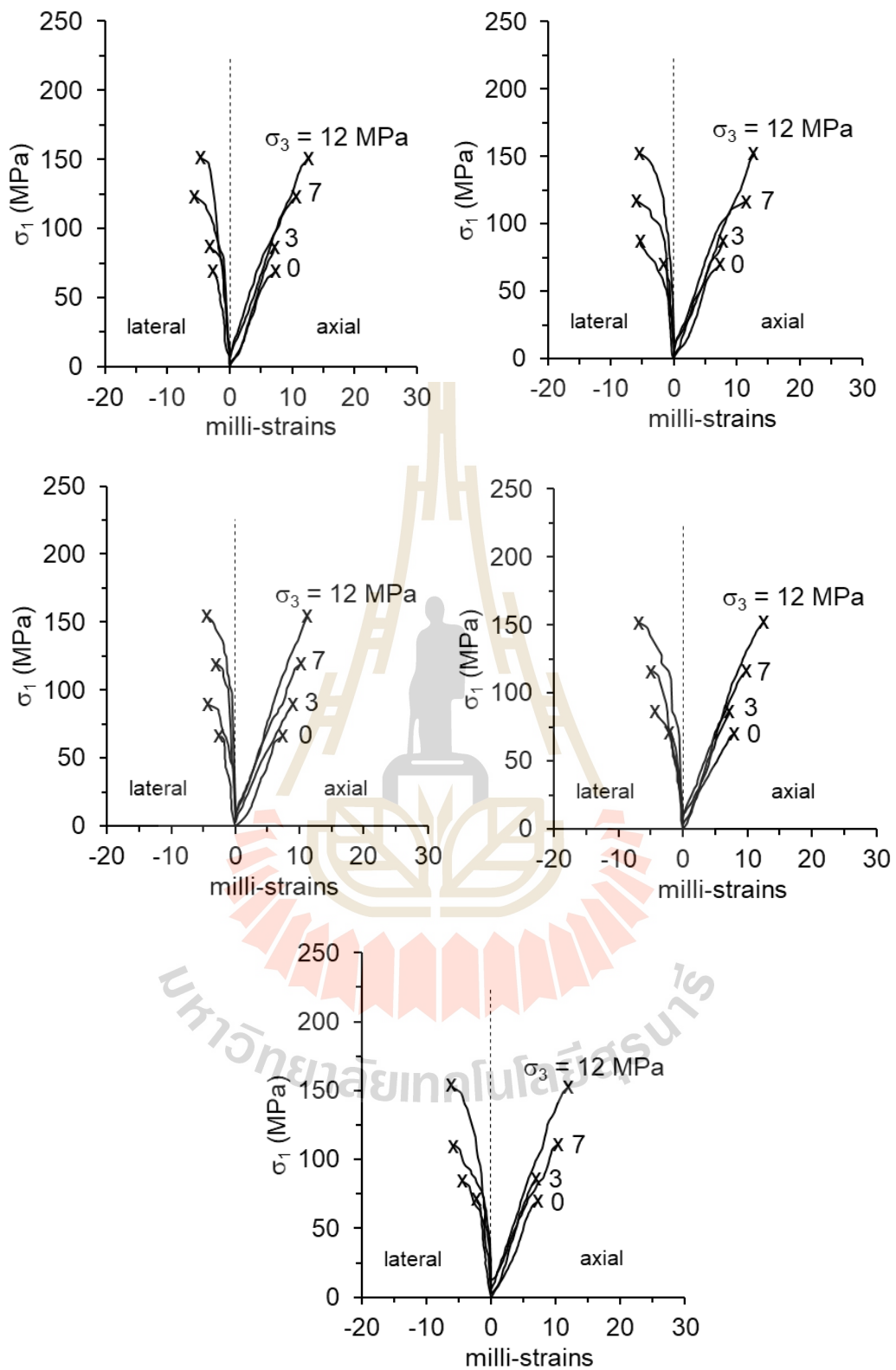


Figure A.4 Stress-strain curves obtained from dry sandstone specimens at 298

Kelvin

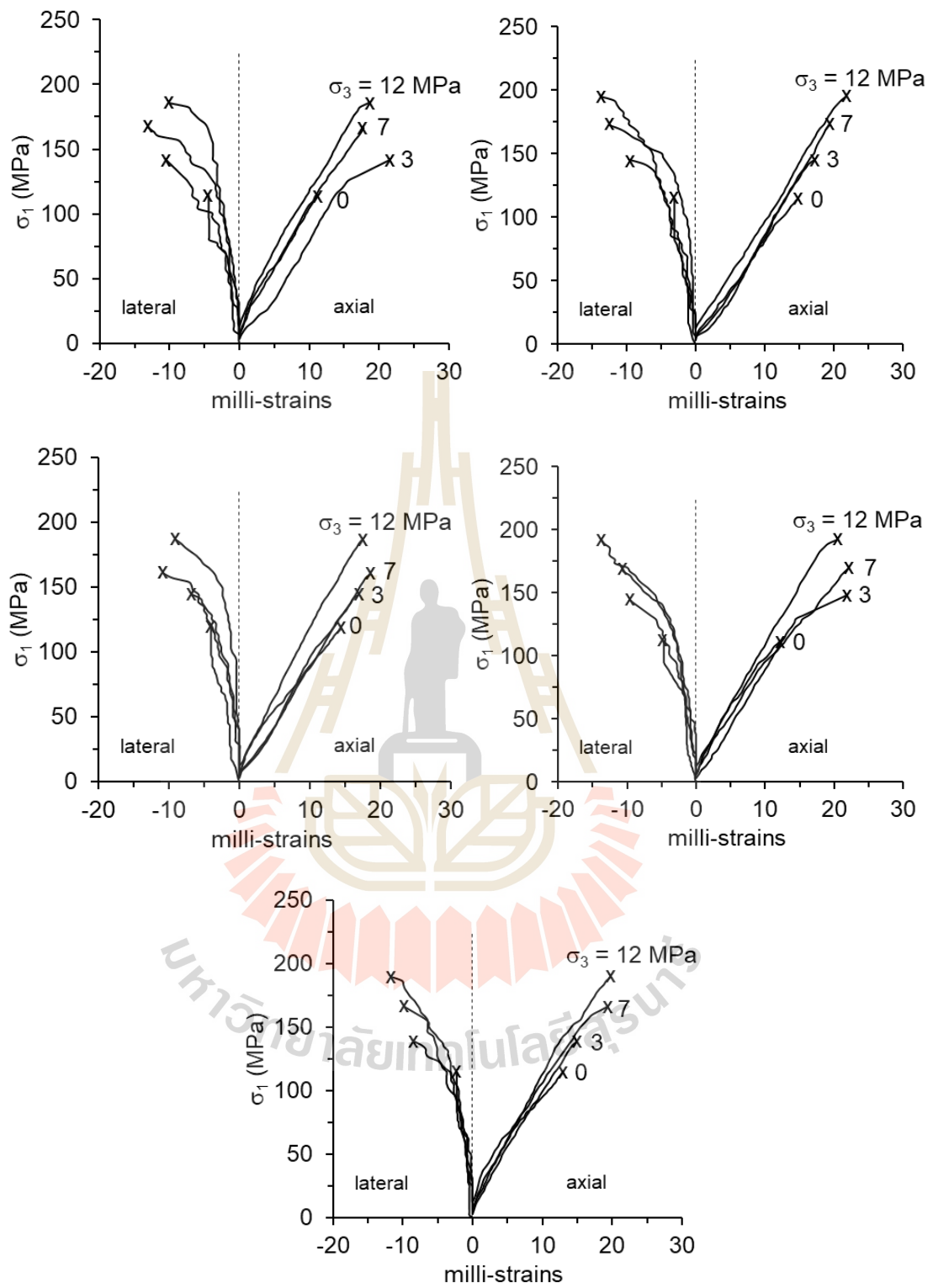


Figure A.5 Stress-strain curves obtained from water-saturated sandstone specimens at 233 Kelvin

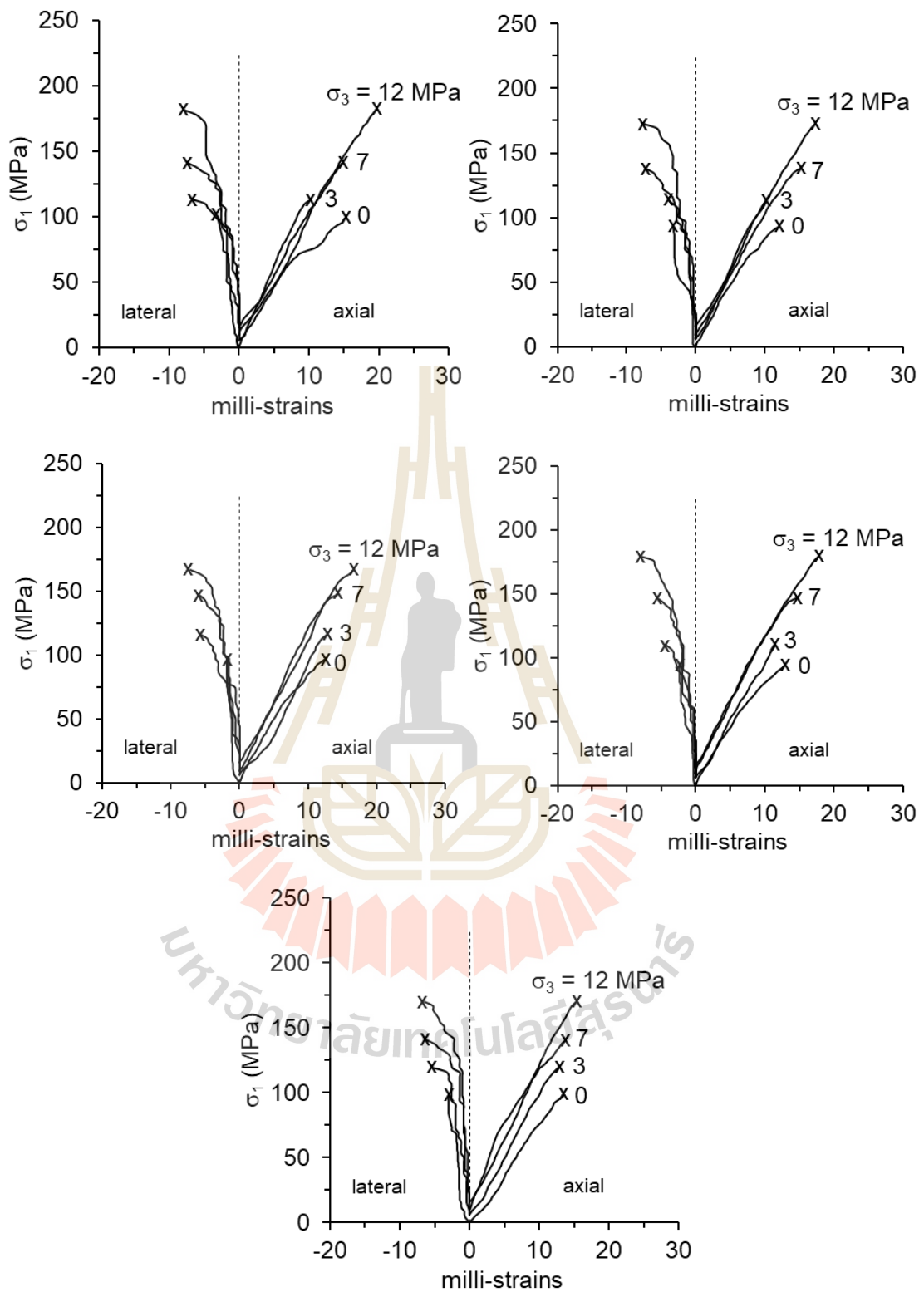


Figure A.6 Stress-strain curves obtained from water-saturated sandstone specimens

at 253 Kelvin

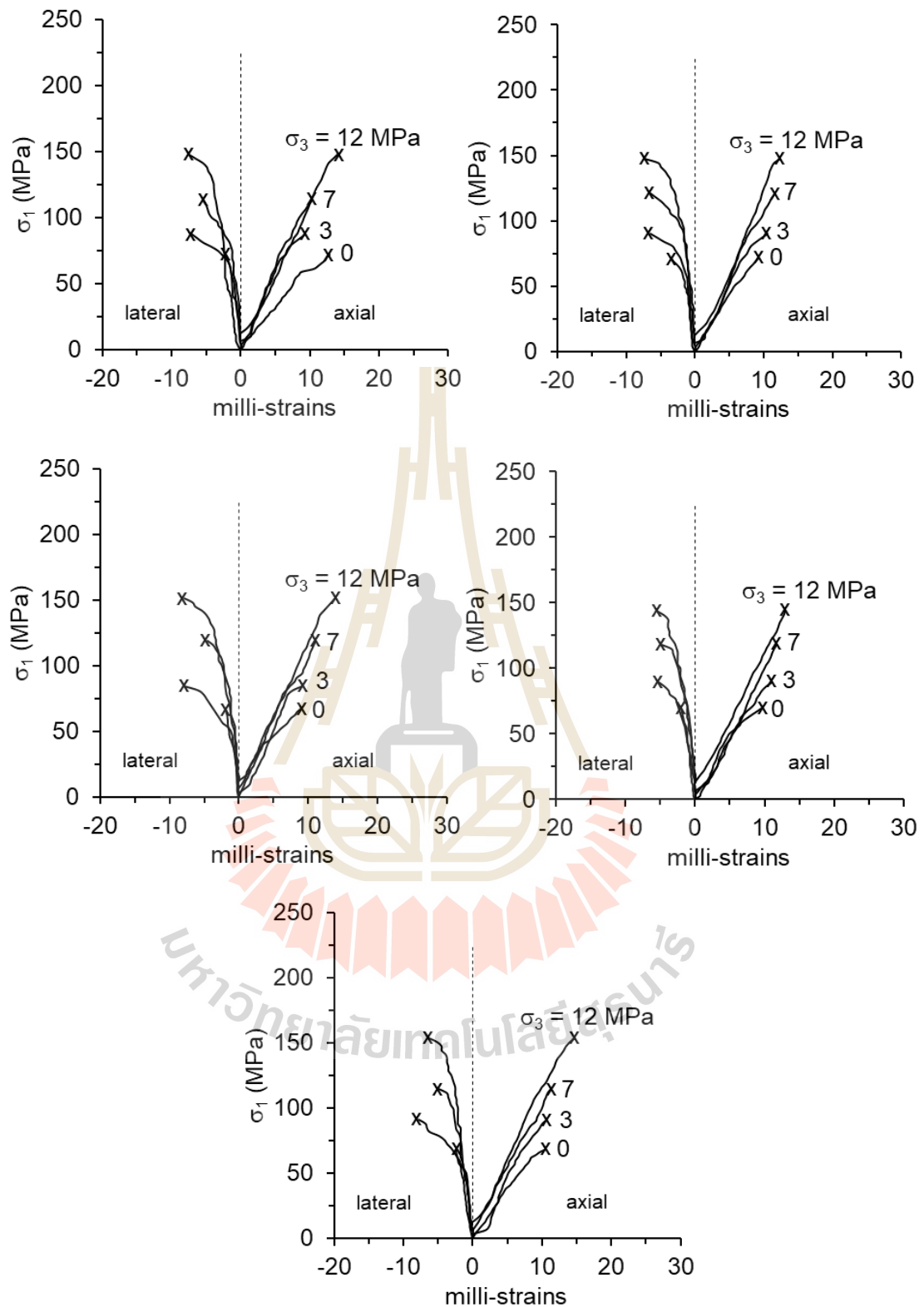


Figure A.7 Stress-strain curves obtained from water-saturated sandstone specimens at 268 Kelvin

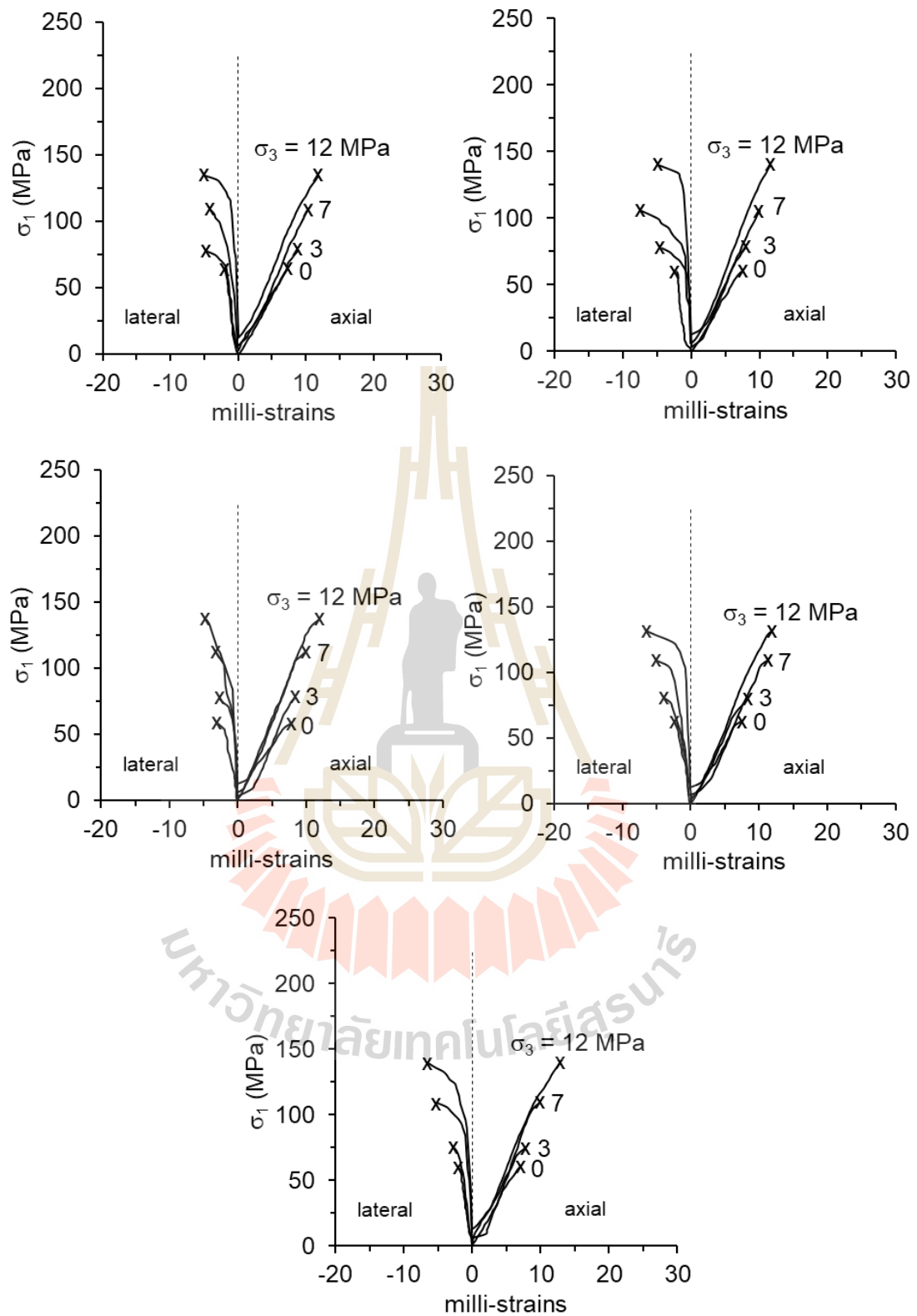


Figure A.8 Stress-strain curves obtained from water-saturated sandstone specimens at 298 Kelvin

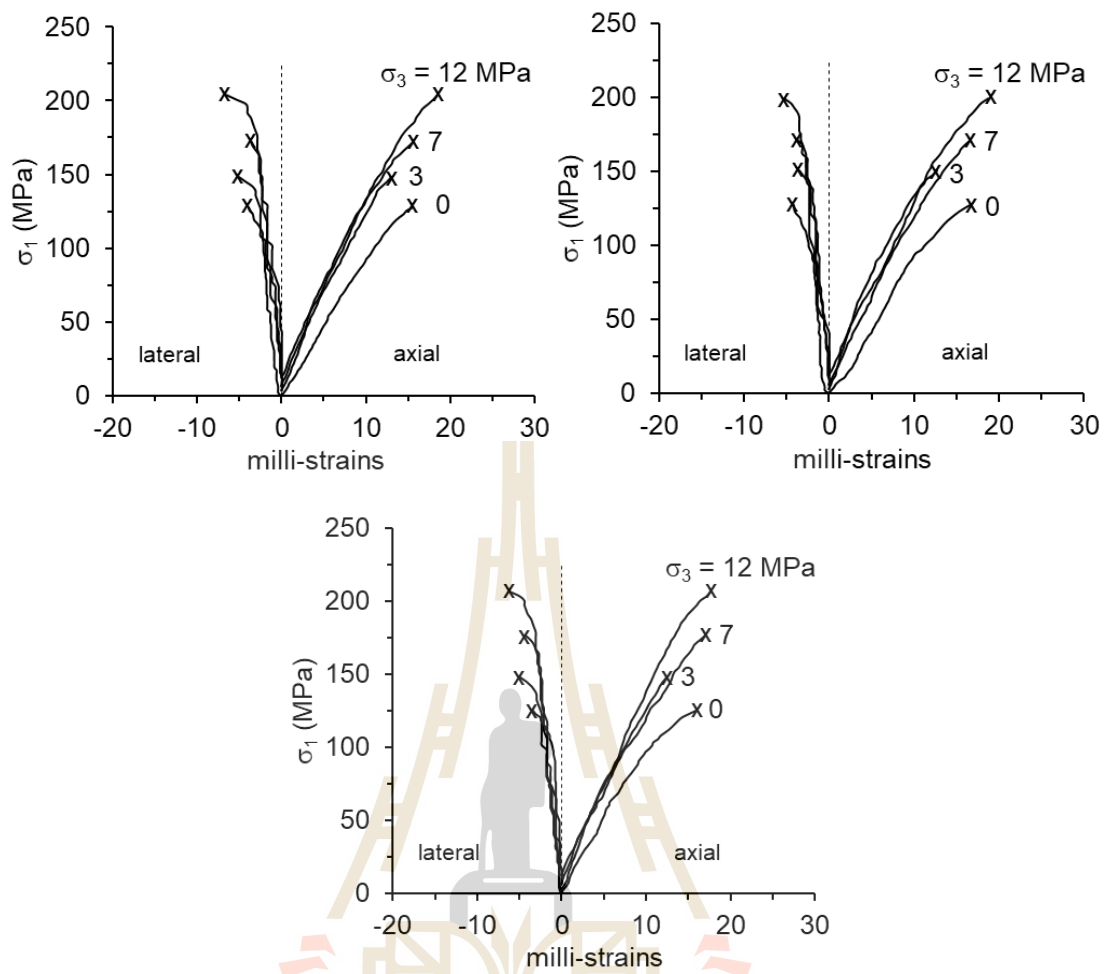


Figure A.9 Stress-strain curves obtained from brine-saturated sandstone specimens at 233 Kelvin

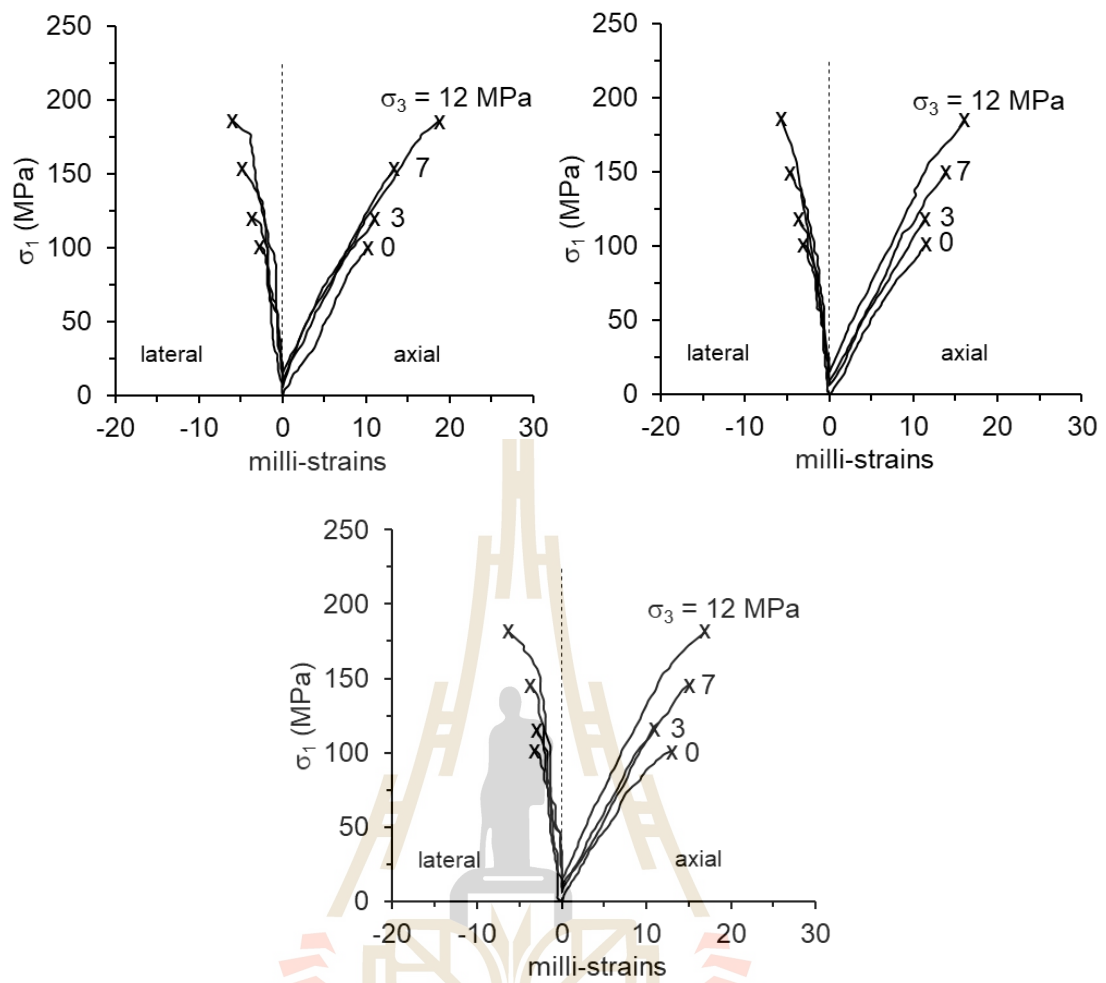


Figure A.10 Stress-strain curves obtained from brine-saturated sandstone specimens at 253 Kelvin

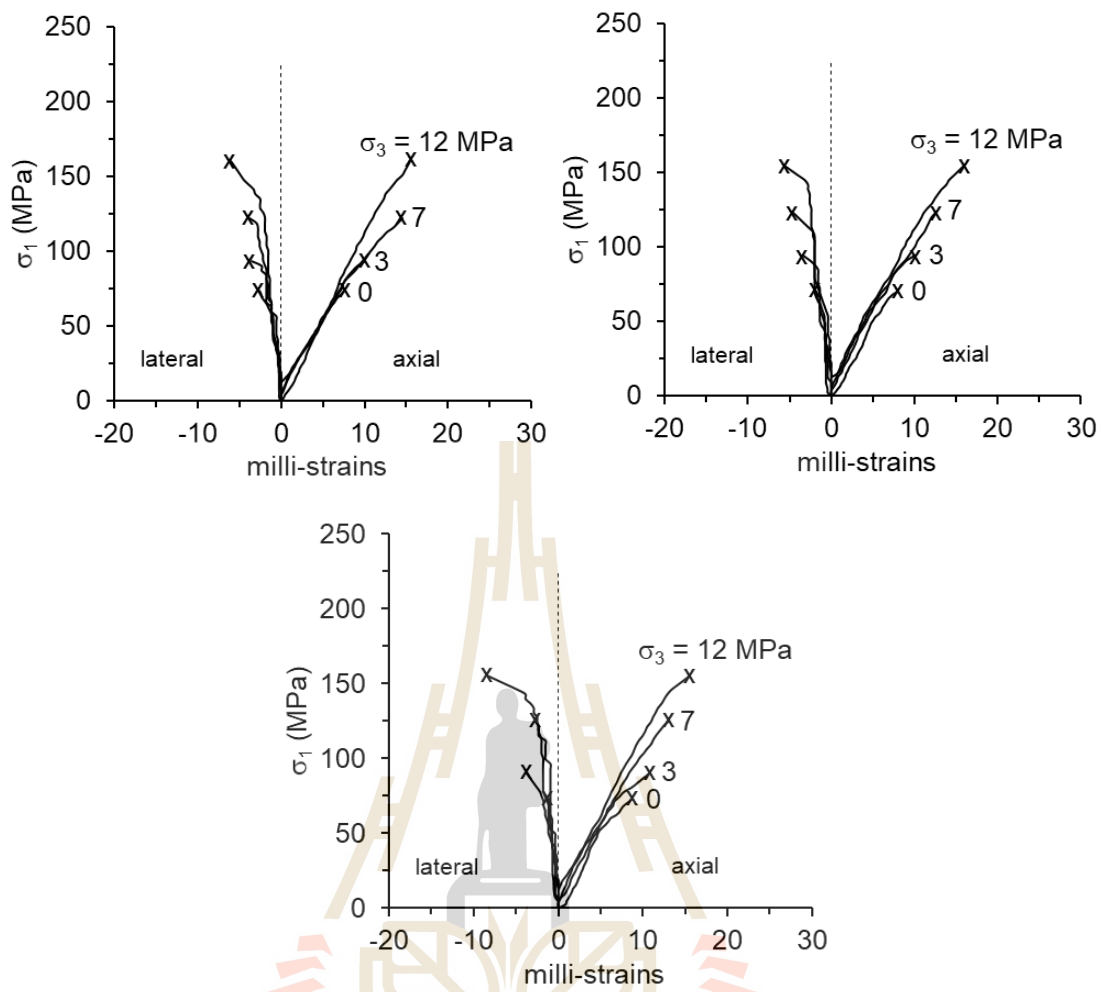


Figure A.11 Stress-strain curves obtained from brine-saturated sandstone specimens at 268 Kelvin

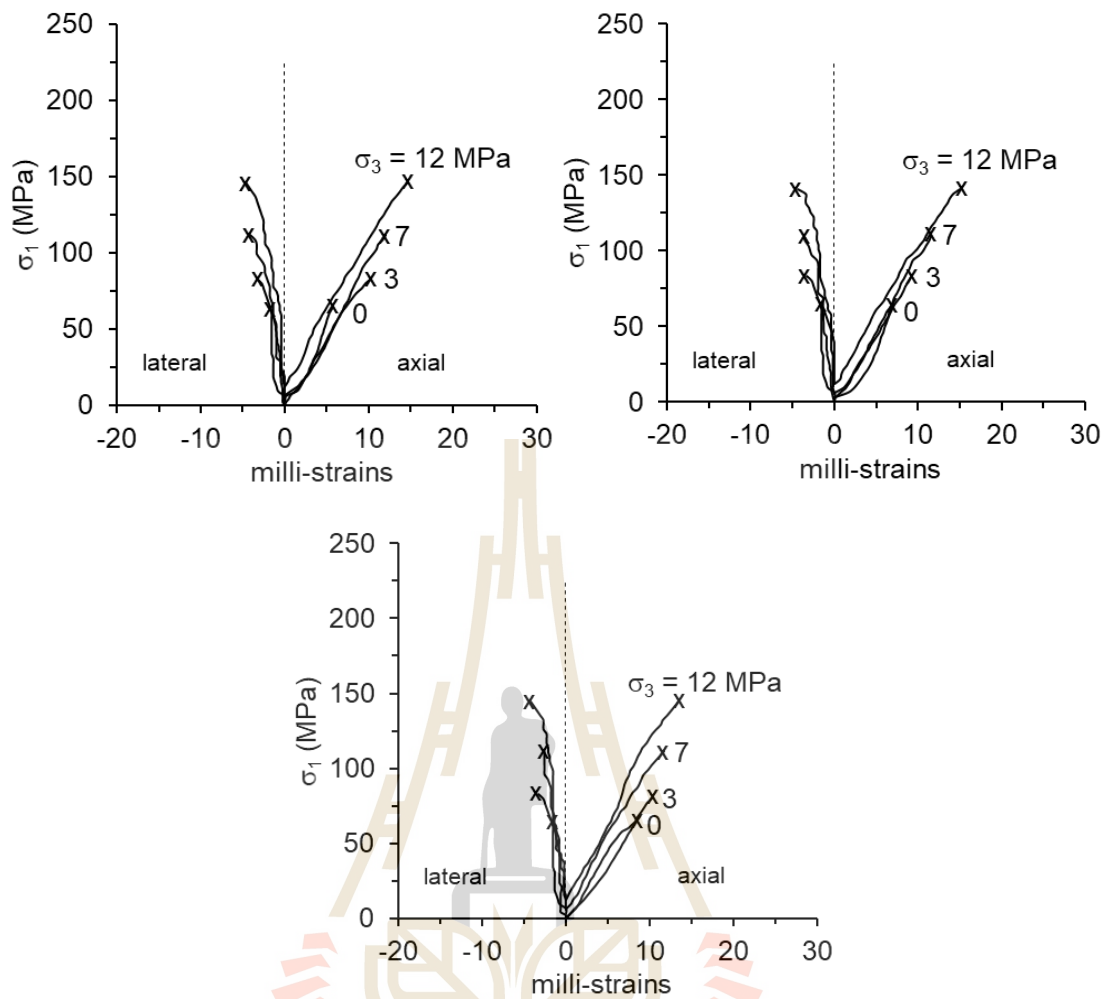


Figure A.12 Stress-strain curves obtained from brine-saturated sandstone specimens at 298 Kelvin

Table A.4 The result of compressive strength of dry specimens under difference temperatures

Confining pressure, σ_3 (MPa)	Compressive strength, σ_1 (MPa)				Elastic modulus, E (GPa)				Poisson's ratio, ν			
	233 K	253 K	268 K	298 K	233 K	253 K	268 K	298 K	233 K	253 K	268 K	298 K
0	93.93	78.63	70.05	68.73	8.65	11.04	10.27	10.40	0.29	0.29	0.29	0.28
	87.37	76.45	72.37	69.80	10.98	10.89	9.18	10.57	0.31	0.29	0.28	0.29
	91.74	80.82	74.98	66.17	11.63	11.03	11.50	10.21	0.26	0.27	0.29	0.28
	90.40	73.99	70.82	70.05	8.36	9.64	9.19	10.07	0.26	0.26	0.28	0.28
	89.23	78.63	71.86	68.98	12.01	9.92	13.73	10.65	0.27	0.27	0.28	0.28
Average	90.53	77.71	72.02	68.75	10.33	10.51	10.77	10.38	0.28	0.28	0.28	0.28
3	109.22	103.80	92.31	86.04	9.73	11.21	10.44	11.07	0.34	0.27	0.30	0.28
	115.77	99.91	90.30	86.66	12.05	11.00	9.83	8.32	0.28	0.33	0.29	0.28
	113.58	110.09	89.33	88.69	10.87	12.18	9.84	10.99	0.25	0.31	0.28	0.29
	115.77	103.80	92.64	85.73	8.05	10.39	10.05	10.98	0.31	0.30	0.31	0.27
	113.58	106.94	95.63	84.28	10.78	10.36	10.47	12.08	0.32	0.29	0.31	0.27
Average	113.58	104.91	92.04	86.28	10.30	11.03	10.13	10.69	0.30	0.30	0.30	0.28
7	141.54	138.40	121.21	122.97	10.32	9.96	10.93	10.06	0.28	0.29	0.26	0.31
	142.57	131.62	118.68	116.55	11.36	12.54	10.45	10.32	0.26	0.28	0.30	0.29
	143.62	132.11	127.58	118.68	10.85	11.64	12.49	11.01	0.29	0.30	0.27	0.27
	143.62	131.42	119.11	115.71	10.48	9.73	9.45	10.45	0.29	0.28	0.27	0.29
	146.74	137.63	122.08	110.17	11.42	8.55	10.99	10.22	0.31	0.28	0.28	0.30
Average	143.62	134.24	121.73	116.82	10.89	10.48	10.86	10.41	0.29	0.29	0.28	0.29
12	182.43	160.42	158.96	150.77	11.58	11.56	12.34	10.98	0.29	0.31	0.29	0.29
	175.05	163.56	160.22	151.86	11.00	11.44	9.97	8.31	0.29	0.27	0.30	0.27
	181.64	162.96	148.88	154.28	12.13	10.46	10.47	12.32	0.28	0.29	0.28	0.30
	170.96	165.48	152.96	151.32	12.48	11.41	11.07	10.18	0.32	0.29	0.29	0.32
	169.73	166.71	151.86	152.41	12.53	9.58	11.67	11.72	0.28	0.28	0.29	0.29
Average	175.96	163.82	154.58	152.13	11.94	10.89	11.10	10.70	0.29	0.29	0.29	0.29

Table A.5 The result of compressive strength of water-saturated specimens under difference temperatures

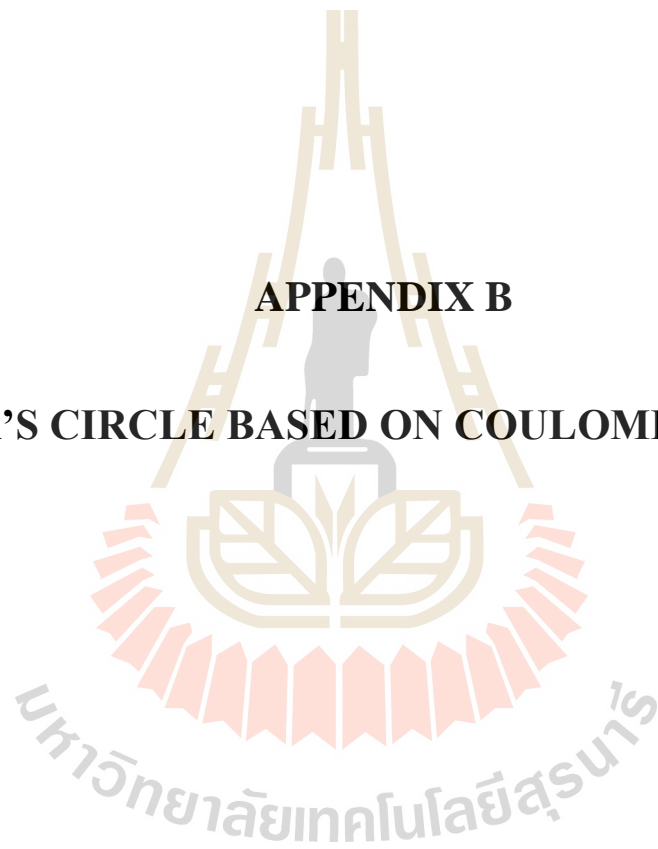
Confining pressure, σ_3 (MPa)	Compressive strength, σ_1 (MPa)				Elastic modulus, E (GPa)				Poisson's ratio, ν			
	233 K	253 K	268 K	298 K	233 K	253 K	268 K	298 K	233 K	253 K	268 K	298 K
0	114.49	100.11	71.55	64.10	11.94	9.70	8.16	8.73	0.28	0.30	0.28	0.30
	114.56	92.89	71.16	60.04	11.38	10.13	9.23	9.53	0.29	0.27	0.26	0.29
	119.25	97.03	66.72	58.11	11.18	10.16	11.40	8.98	0.30	0.28	0.26	0.29
	111.92	93.93	69.38	62.42	10.65	9.56	10.53	10.46	0.34	0.28	0.27	0.30
	115.80	99.01	68.62	59.97	11.28	10.52	8.62	9.69	0.29	0.29	0.29	0.29
Average	115.20	96.59	69.49	60.93	11.29	10.01	9.59	9.48	0.30	0.29	0.27	0.29
3	141.54	113.23	87.10	78.06	11.05	10.77	12.10	8.46	0.27	0.31	0.26	0.30
	144.69	113.23	90.21	77.77	10.65	12.06	13.56	9.41	0.27	0.29	0.29	0.27
	144.15	115.74	83.37	77.20	11.70	12.06	12.99	8.56	0.28	0.26	0.31	0.27
	147.68	110.09	89.55	79.99	12.41	10.46	9.61	10.13	0.27	0.29	0.29	0.30
	138.96	119.53	90.88	74.38	10.62	12.58	9.40	10.33	0.28	0.28	0.29	0.28
Average	143.40	114.36	88.22	77.48	11.28	11.59	11.53	9.38	0.27	0.29	0.29	0.28
7	166.71	141.54	112.40	108.48	12.57	10.34	9.78	10.18	0.29	0.28	0.34	0.27
	172.36	137.63	120.87	105.38	11.48	12.22	11.36	10.13	0.28	0.28	0.28	0.31
	160.42	147.83	119.08	111.99	11.76	11.60	9.37	11.45	0.29	0.29	0.28	0.31
	169.85	146.74	117.56	108.88	11.20	11.29	10.38	8.98	0.29	0.29	0.29	0.28
	166.09	140.50	114.67	108.68	12.37	10.27	11.23	10.10	0.27	0.27	0.27	0.30
Average	167.08	142.85	116.92	108.68	11.88	11.14	10.42	10.17	0.28	0.28	0.29	0.29
12	185.58	181.76	147.29	134.26	12.96	11.09	11.00	11.41	0.27	0.28	0.27	0.28
	195.01	172.36	147.29	140.24	11.02	11.49	11.56	11.31	0.29	0.27	0.29	0.28
	186.64	166.71	150.98	136.87	12.38	12.46	9.97	10.57	0.29	0.29	0.32	0.29
	191.87	179.29	143.89	131.13	11.26	10.43	8.80	11.55	0.29	0.30	0.31	0.32
	189.75	169.85	153.56	139.47	11.60	10.80	11.96	10.77	0.28	0.29	0.27	0.32
Average	189.77	173.99	148.60	136.39	11.84	11.25	10.66	11.12	0.29	0.29	0.29	0.30

Table A.6 The result of compressive strength of brine-saturated specimens under difference temperatures

Confining pressure, σ_3 (MPa)	Compressive strength, σ_1 (MPa)				Elastic modulus, E (GPa)				Poisson's ratio, ν			
	233 K	253 K	268 K	298 K	233 K	253 K	268 K	298 K	233 K	253 K	268 K	298 K
0	127.45	100.60	73.50	64.81	11.05	10.52	10.23	10.18	0.28	0.28	0.28	0.27
	126.99	102.93	70.25	64.57	11.78	11.94	10.16	10.16	0.28	0.27	0.28	0.27
	124.83	100.79	73.18	66.48	11.76	10.70	10.27	10.14	0.27	0.29	0.30	0.29
Average	126.42	101.44	72.31	65.28	11.53	11.06	10.22	10.16	0.28	0.28	0.28	0.28
3	148.22	119.99	93.32	83.07	11.26	11.32	10.49	10.17	0.27	0.29	0.28	0.28
	150.76	117.77	94.01	82.92	11.80	11.27	10.87	11.22	0.26	0.27	0.27	0.27
	147.68	119.11	90.21	80.82	11.24	10.29	10.83	9.72	0.29	0.27	0.27	0.28
Average	148.89	118.96	92.52	82.27	11.43	10.96	10.73	10.37	0.28	0.28	0.27	0.28
7	172.29	152.65	122.22	111.33	11.80	11.42	10.16	11.33	0.26	0.26	0.28	0.27
	171.09	148.88	122.67	109.60	11.51	10.94	10.92	10.25	0.30	0.27	0.28	0.28
	176.01	145.45	125.54	114.25	11.92	11.15	10.37	10.36	0.29	0.28	0.27	0.27
Average	173.13	148.99	123.47	111.73	11.74	11.17	10.48	10.65	0.29	0.27	0.27	0.27
12	203.80	185.63	160.42	146.20	11.72	11.60	11.62	10.94	0.30	0.27	0.25	0.28
	199.09	184.55	154.12	140.49	11.86	11.51	10.73	10.20	0.29	0.29	0.29	0.27
	206.74	181.52	155.25	144.81	11.77	10.57	11.38	10.45	0.29	0.27	0.27	0.28
Average	203.21	183.90	156.60	143.84	11.79	11.23	11.24	10.53	0.29	0.28	0.27	0.28

APPENDIX B

MOHR'S CIRCLE BASED ON COULOMB CRITERIA



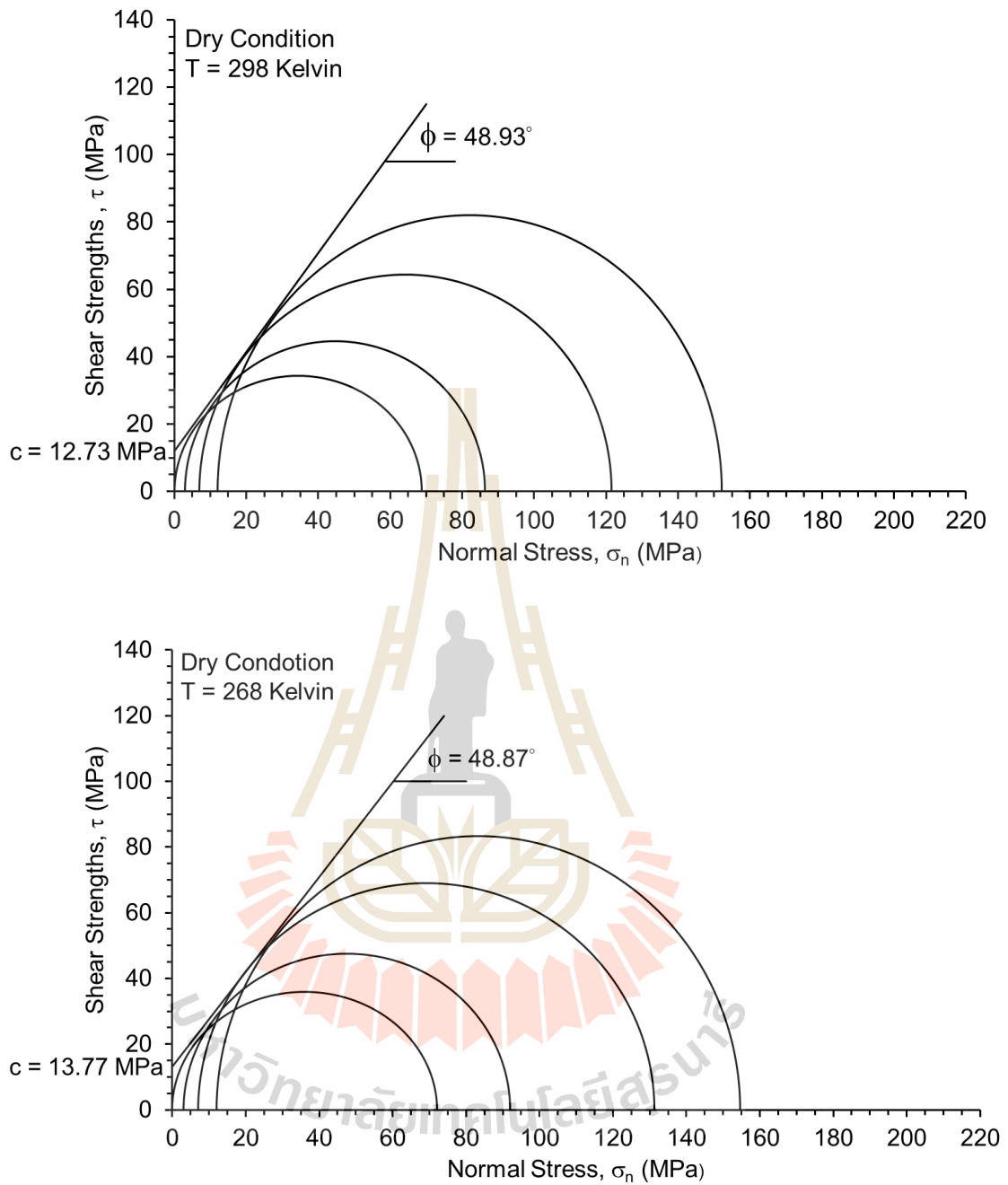


Figure B.1 Mohr's circles form Coulomb criterion of dry sandstone under difference temperatures

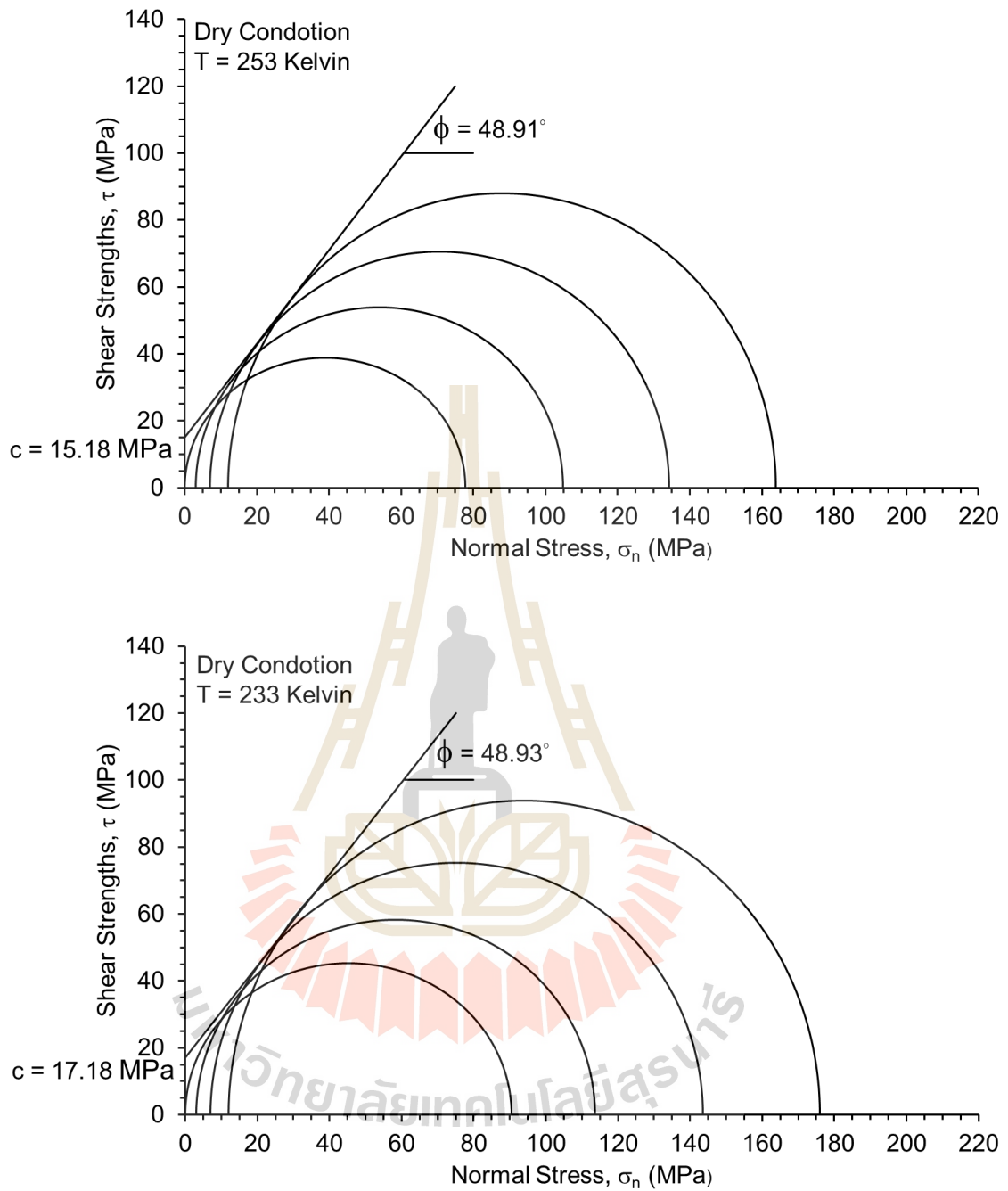


Figure B.1 Mohr's circles form Coulomb criterion of dry sandstone under difference temperatures (cont.)

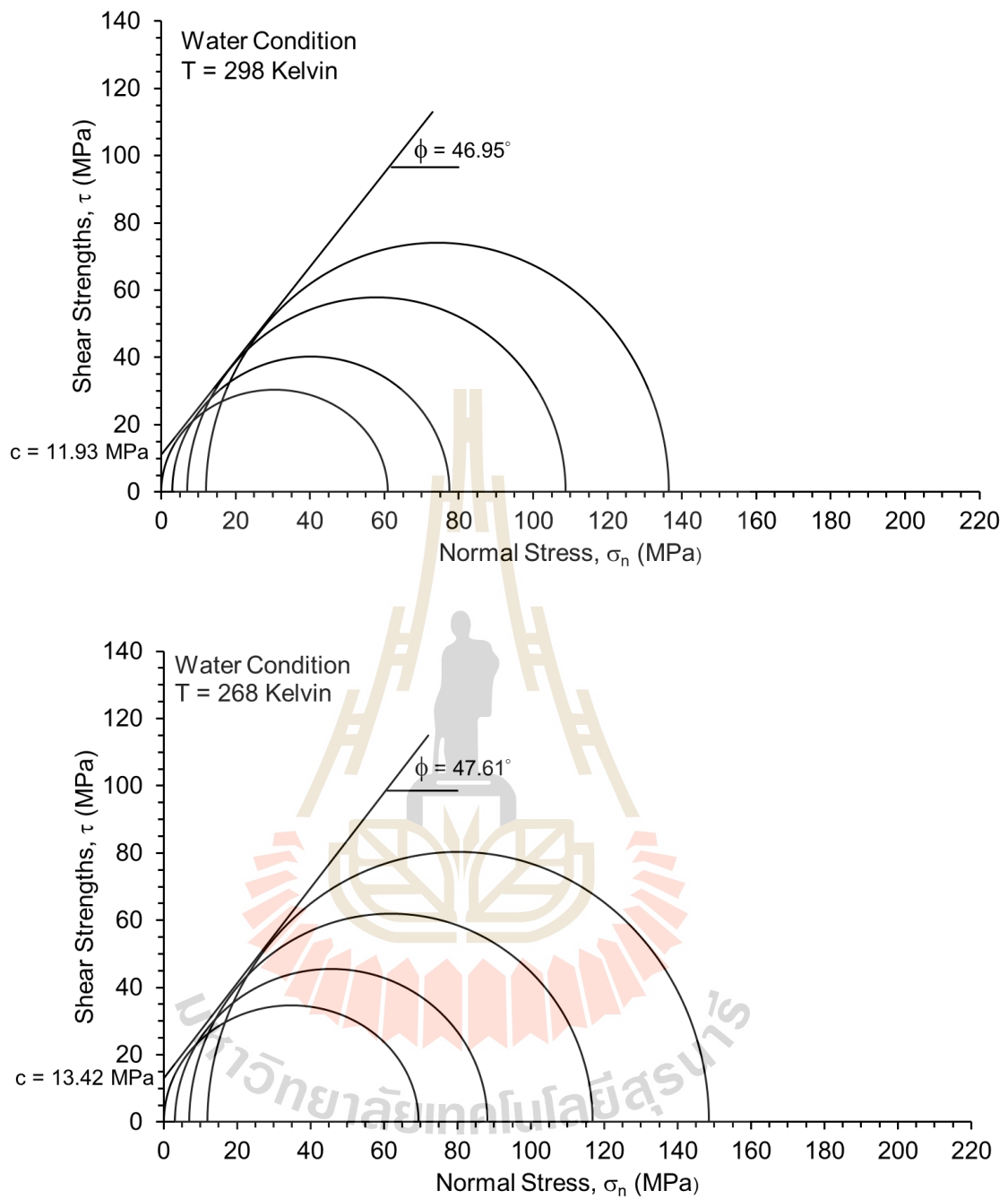


Figure B.2 Mohr's circles from Coulomb criterion of water-saturated sandstone under difference temperatures

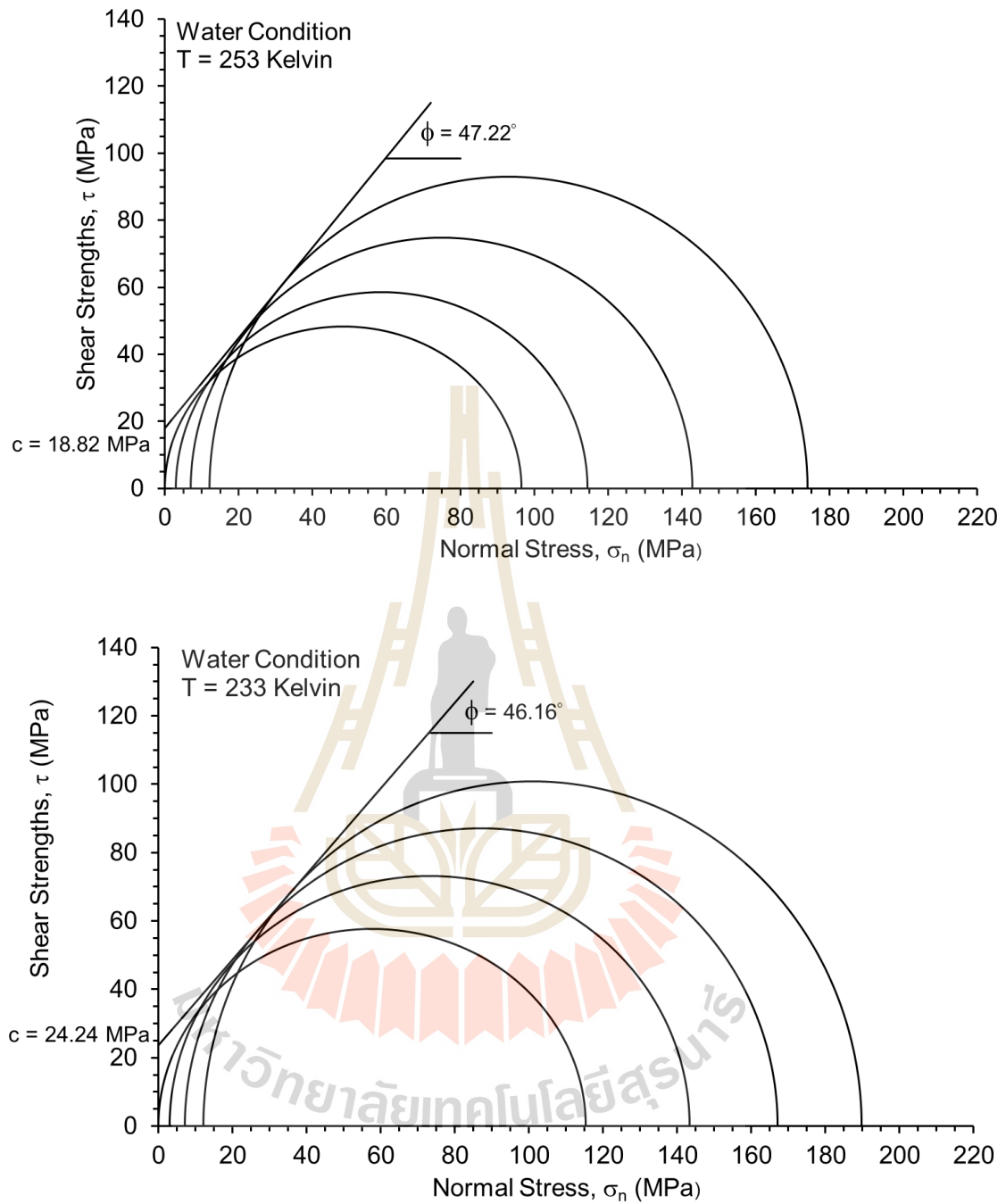


Figure B.2 Mohr's circles form Coulomb criterion of water-saturated sandstone under difference temperatures (cont.)

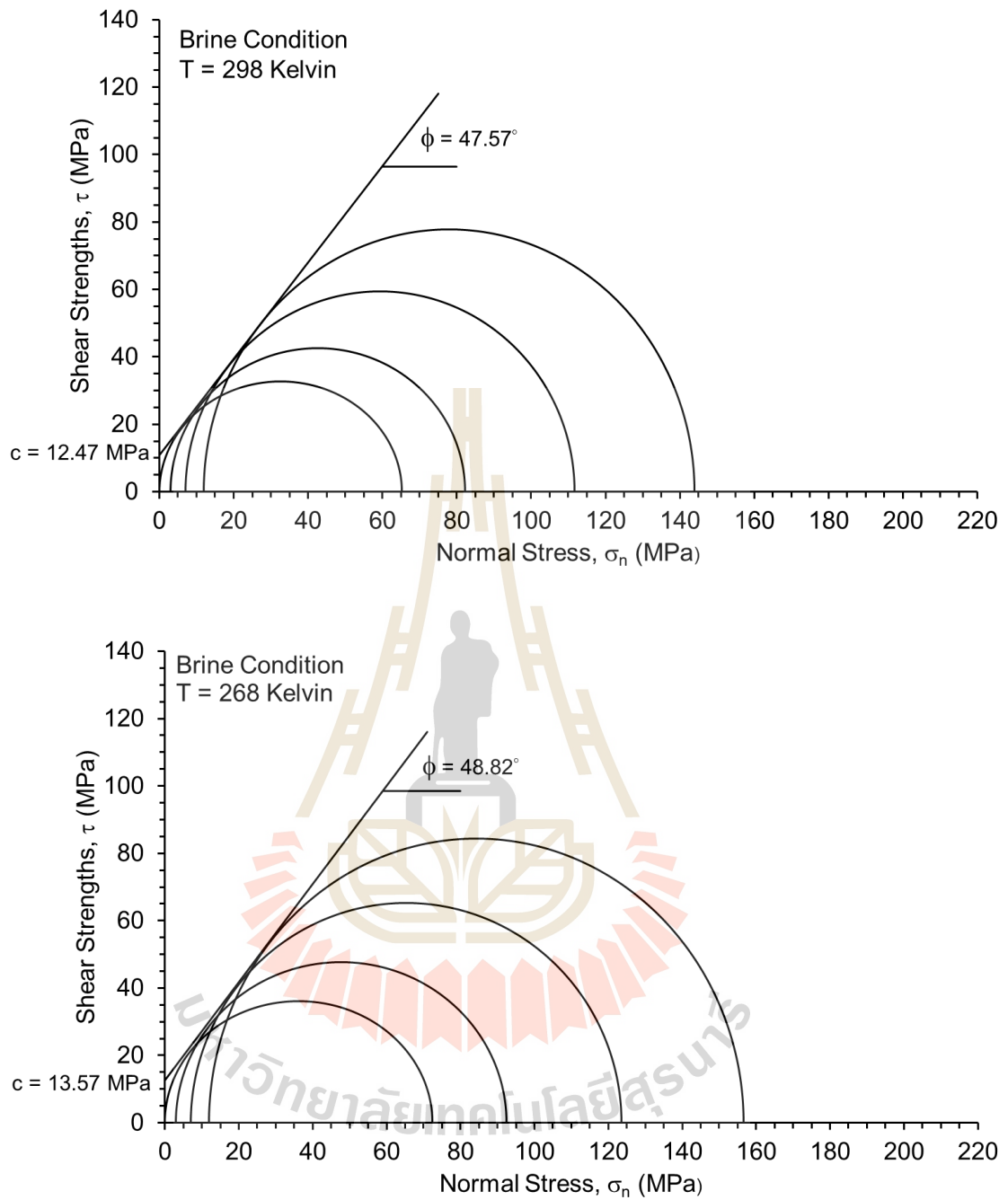


Figure B.3 Mohr's circles form Coulomb criterion of brine-saturated sandstone under difference temperatures

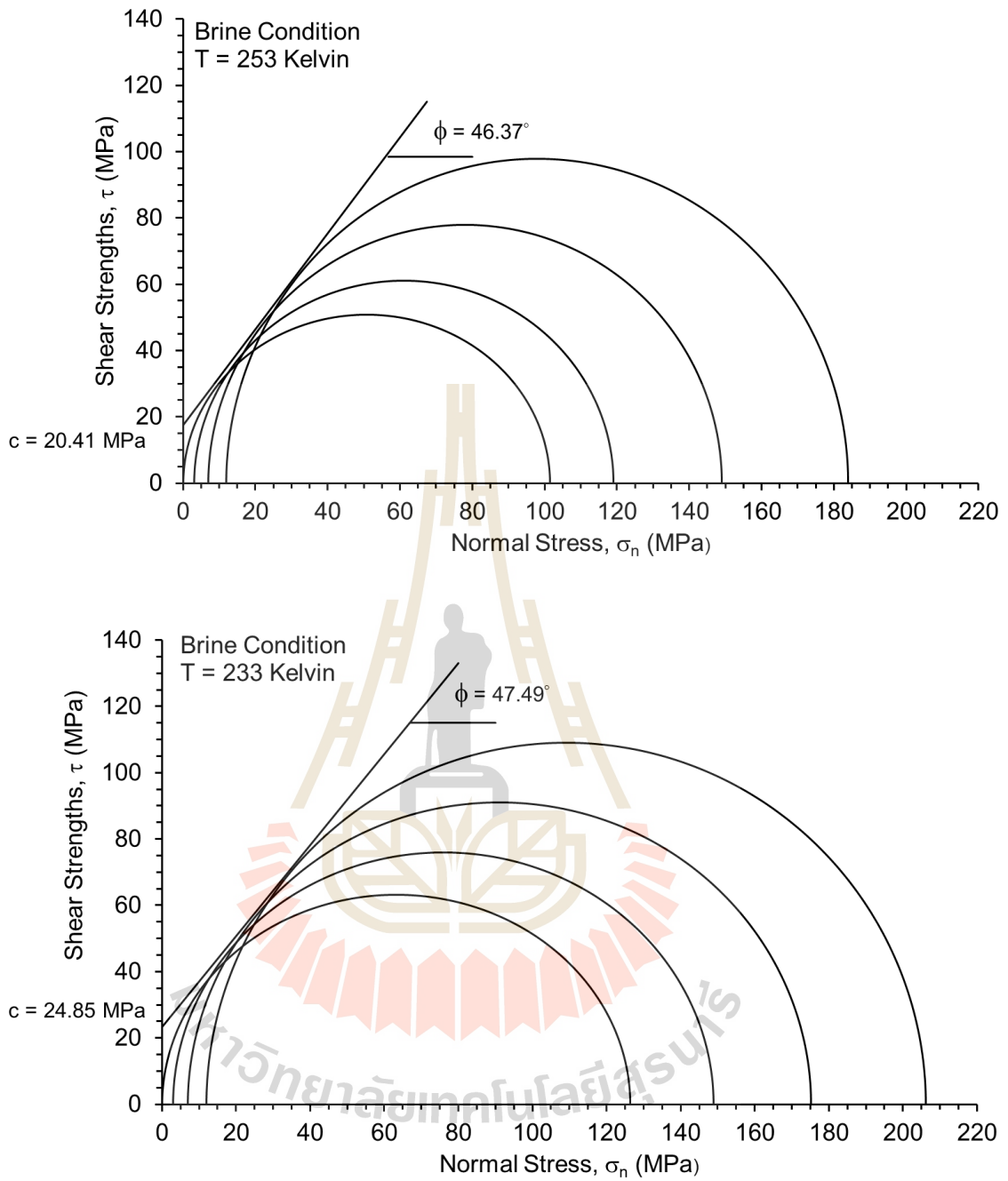
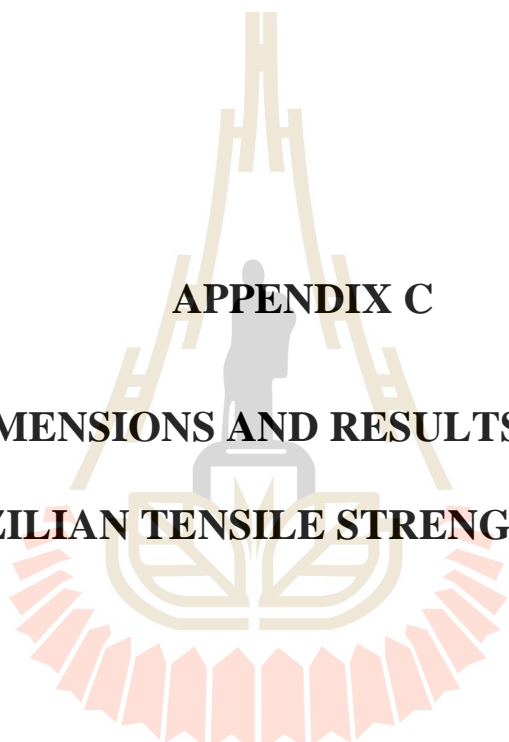


Figure B.3 Mohr's circles form Coulomb criterion of brine-saturated sandstone under difference temperatures (cont.)



APPENDIX C
DIMENSIONS AND RESULTS FROM
BRAZILIAN TENSILE STRENGTH TESTS

มหาวิทยาลัยเทคโนโลยีสุรนารี

Table C.1 The result of Brazilian tensile strength of dry specimens under difference temperatures

Sample No.	Temperature (Kelvin)	Diameter (mm)	Length (mm)	P (kN)	σ_B (MPa)
1	233	54.0	27.6	16.5	7.05
2		54.3	27.3	18.0	7.73
3		54.2	28.0	21.0	8.81
4		54.2	29.0	16.0	6.48
5		54.1	27.5	21.0	8.99
6		54.3	27.0	18.0	7.82
7		54.0	27.4	19.0	8.18
8		54.0	28.6	19.5	8.04
9		54.1	29.2	20.0	8.06
10		54.0	27.5	16.0	6.86
11	253	54.0	30.2	20.0	7.81
12		54.4	30.9	18.0	6.82
13		54.0	29.2	19.0	7.67
14		54.2	28.0	18.0	7.55
15		54.0	27.4	16.0	6.89
16		54.4	27.6	18.0	7.64
17		54.2	28.0	15.5	6.51
18		54.1	27.3	16.0	6.90
19		54.0	29.2	15.0	6.06
20		54.0	33.7	16.0	5.60
21	268	55.0	30.0	15.0	5.79
22		55.7	31.9	17.0	6.09
23		55.0	31.1	18.0	6.70
24		55.0	32.6	16.5	5.86
25		55.0	30.0	14.0	5.40
26		55.0	30.2	20.5	7.86
27		55.0	33.7	19.5	6.70
28		55.0	33.0	19.0	6.67
29		55.0	29.6	19.0	7.43
30		55.3	31.9	19.5	7.04
31	298	55.2	27.8	15.0	6.23
32		55.2	31.3	17.0	6.27
33		55.4	31.3	16.5	6.06
34		55.0	28.3	17.5	7.16
35		55.4	32.0	20.0	7.19
36		55.4	30.0	16.0	6.13
37		55.0	30.5	15.5	5.89
38		55.3	29.1	15.0	5.94
39		55.0	32.9	20.0	7.04
40		55.2	30.1	18.0	6.90

Table C.2 The result of Brazilian tensile strength of water-saturated specimens under difference temperatures

Sample No.	Temperature (Kelvin)	Diameter (mm)	Length (mm)	P (kN)	σ_B (MPa)
1	233	54.3	28.6	25.0	10.01
2		54.5	27.3	21.0	9.04
3		54.3	26.8	22.0	9.68
4		54.0	31.0	22.0	8.37
5		54.0	32.2	20.0	7.33
6		54.0	27.6	24.0	10.20
7		54.0	31.0	18.0	6.81
8		54.2	29.0	24.0	9.76
9		54.3	27.5	25.0	10.70
10		54.1	26.8	18.5	8.14
11	253	54.0	30.0	20.0	7.86
12		54.1	31.0	18.0	6.84
13		54.0	30.5	16.0	6.19
14		54.4	29.0	16.0	6.46
15		54.0	28.0	16.5	6.95
16		54.0	28.0	17.0	7.16
17		54.0	27.2	16.0	6.94
18		54.0	27.3	16.5	7.13
19		54.0	27.0	18.0	7.86
20		54.4	27.5	17.5	7.45
21	268	54.3	29.4	14.0	5.59
22		54.5	27.0	12.5	5.31
23		54.3	27.6	13.5	5.79
24		54.0	27.5	12.0	5.00
25		54.0	28.3	12.5	5.54
26		54.0	26.6	14.0	5.69
27		54.0	29.0	13.0	5.46
28		54.2	28.0	12.0	5.08
29		54.3	27.7	13.5	5.56
30		54.1	28.6	19.5	7.04
31	298	53.7	27.1	12.0	5.25
32		53.0	29.9	14.5	5.83
33		54.7	27.1	14.5	6.24
34		54.0	28.6	11.5	4.74
35		53.7	26.7	11.5	5.11
36		53.7	26.5	13.8	6.18
37		53.8	27.6	12.0	5.15
38		54.0	30.0	12.0	4.72
39		54.3	30.4	13.0	5.02
40		54.5	29.1	12.5	5.02

Table C.3 The result of Brazilian tensile strength of brine-saturated specimens under difference temperatures

Sample No.	Temperature (Kelvin)	Diameter (mm)	Length (mm)	P (kN)	σ_B (MPa)
1	233	54.0	29.0	25.0	10.17
2		54.7	29.3	23.5	9.34
3		54.6	29.5	21.0	8.30
4		54.3	30.0	25.0	9.78
5		54.0	33.0	27.0	9.65
6		54.0	29.0	23.0	9.35
7		54.2	28.1	23.0	9.62
8		54.1	29.2	23.0	9.27
9		54.3	30.1	26.0	10.13
10		54.0	30.0	26.0	10.22
11	253	54.3	28.6	19.0	7.79
12		54.3	29.0	18.0	7.28
13		54.0	29.6	20.0	7.97
14		54.1	30.0	18.0	7.06
15		54.0	31.0	21.5	8.18
16		54.0	30.5	17.0	6.57
17		54.7	32.0	21.5	7.82
18		54.0	33.1	19.5	6.95
19		54.2	28.0	19.0	7.97
20		54.0	29.6	20.0	7.97
21	268	54.5	30.0	16.0	6.23
22		54.5	28.0	15.0	6.26
23		54.6	29.6	16.0	6.31
24		54.2	31.1	16.5	6.23
25		54.2	32.0	16.5	6.06
26		54.0	28.0	13.0	5.48
27		54.0	29.1	14.0	5.67
28		54.1	29.1	14.5	5.87
29		54.7	28.3	16.5	6.79
30		54.7	29.3	14.0	5.56
31	298	54.4	28.2	12.5	5.19
32		54.2	30.1	16.5	6.44
33		54.0	32.6	15.0	5.43
34		54.3	29.6	15.5	6.14
35		54.6	29.0	12.0	4.83
36		54.0	28.0	15.5	6.53
37		54.3	28.4	16.0	6.61
38		54.2	28.6	12.0	4.93
39		54.0	29.1	13.0	5.27
40		54.7	30.3	15.0	5.76



APPENDIX D

RADIUS OF PROGRESSION OF FROZEN ZONE

SIMULATION BY ANSYS14.0

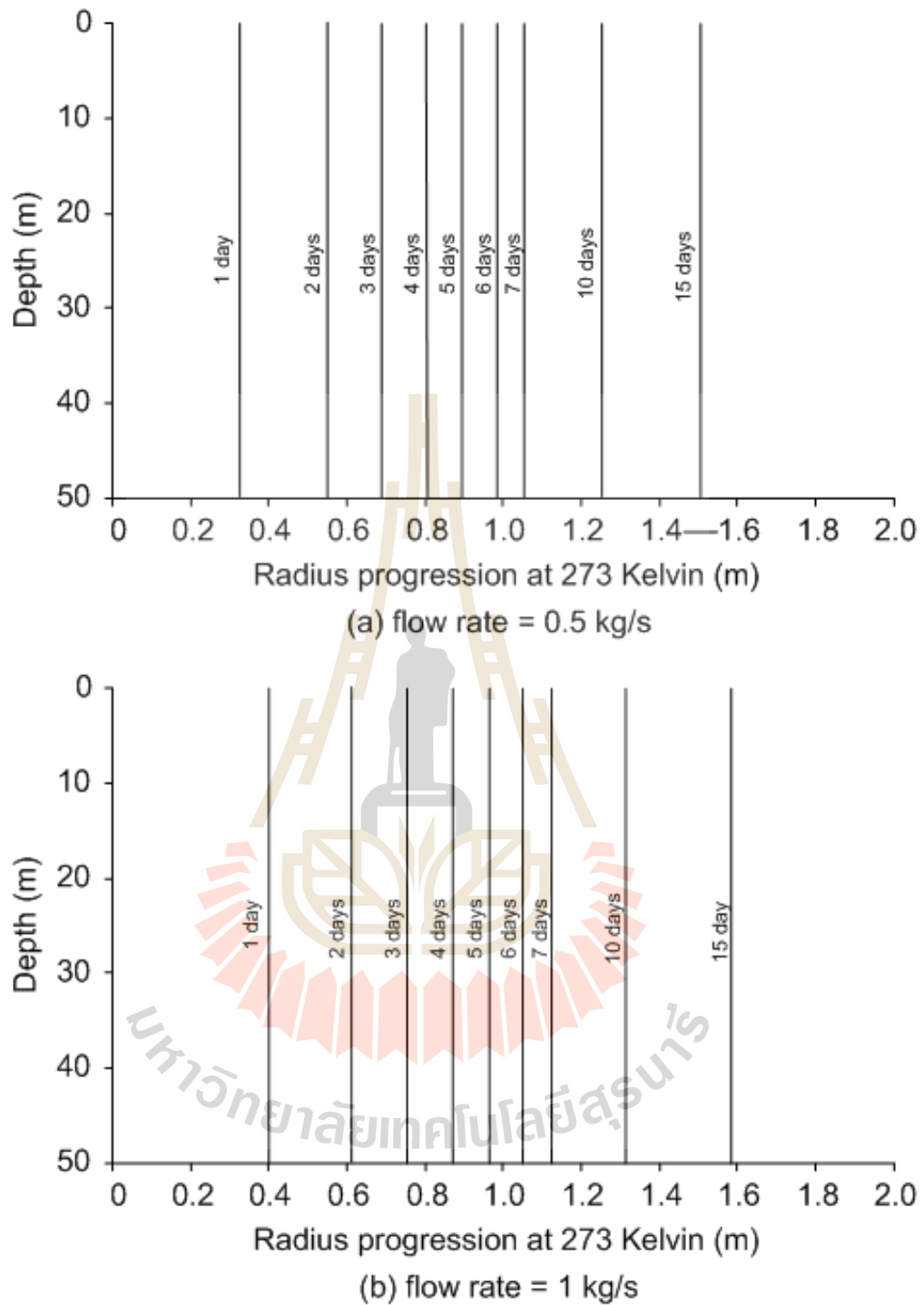


Figure D.1 Results of the radius progression of frozen zone at 273 Kelvin for dry ground surrounding condition in difference coolant flow rates

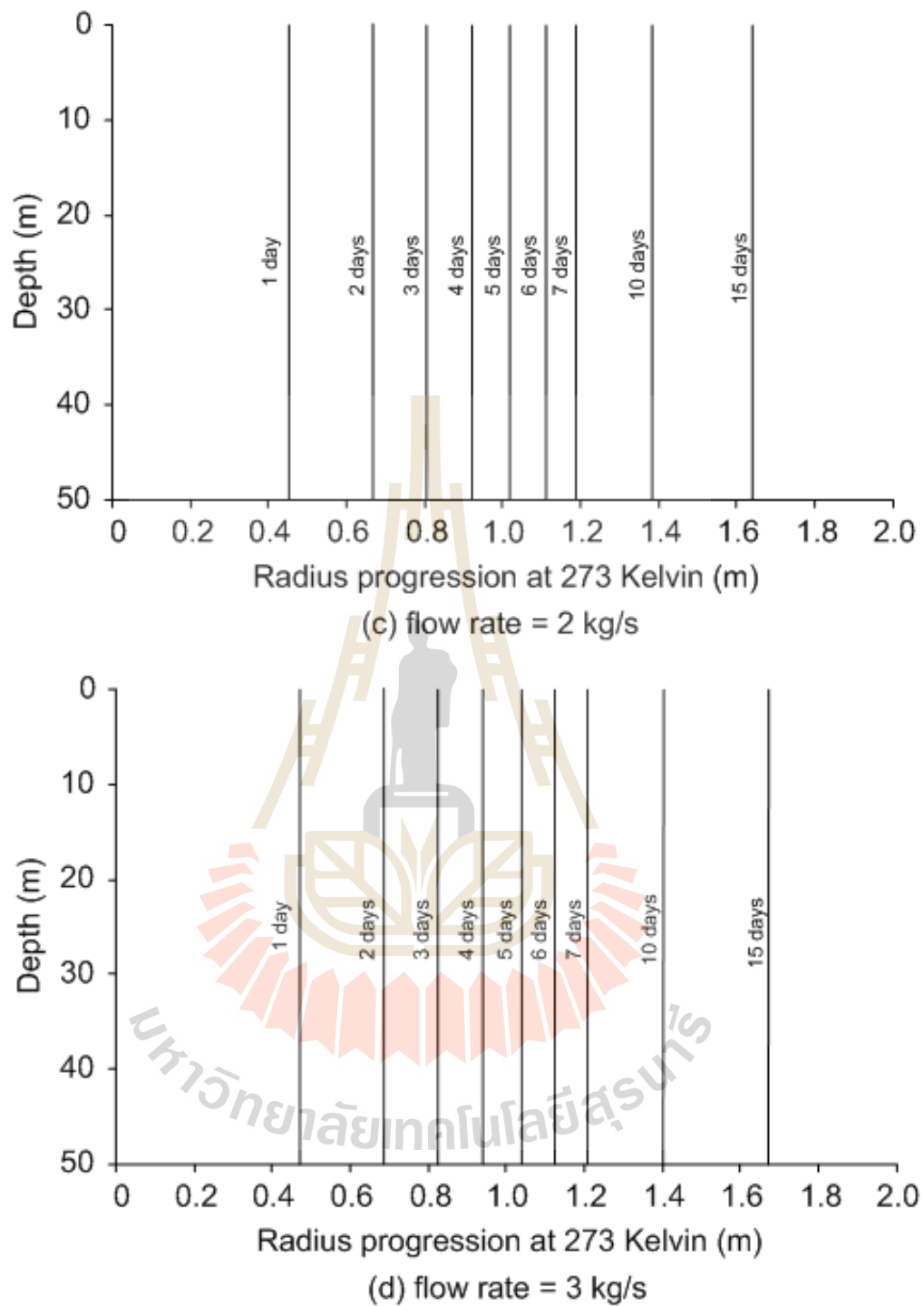
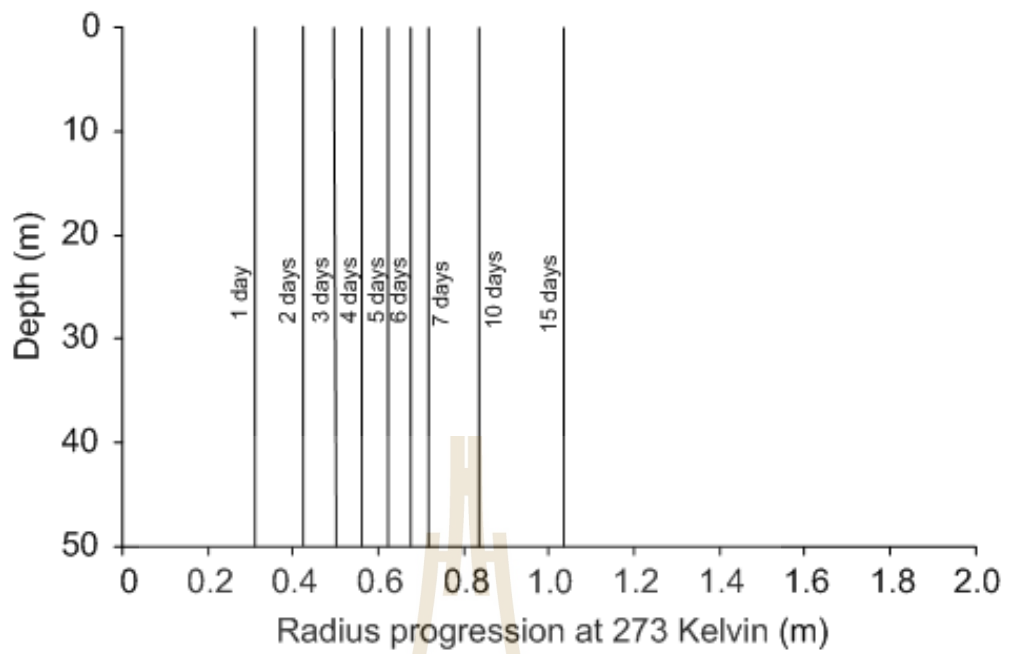
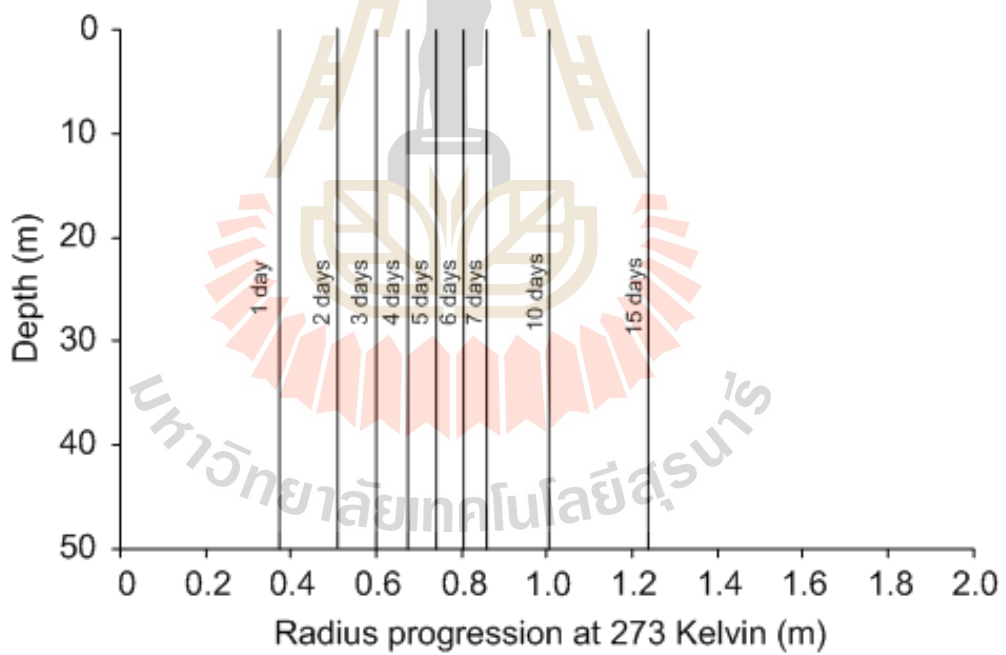


Figure D.1 Results of the radius progression of frozen zone at 273 Kelvin for dry ground surrounding condition in difference coolant flow rates (cont.)

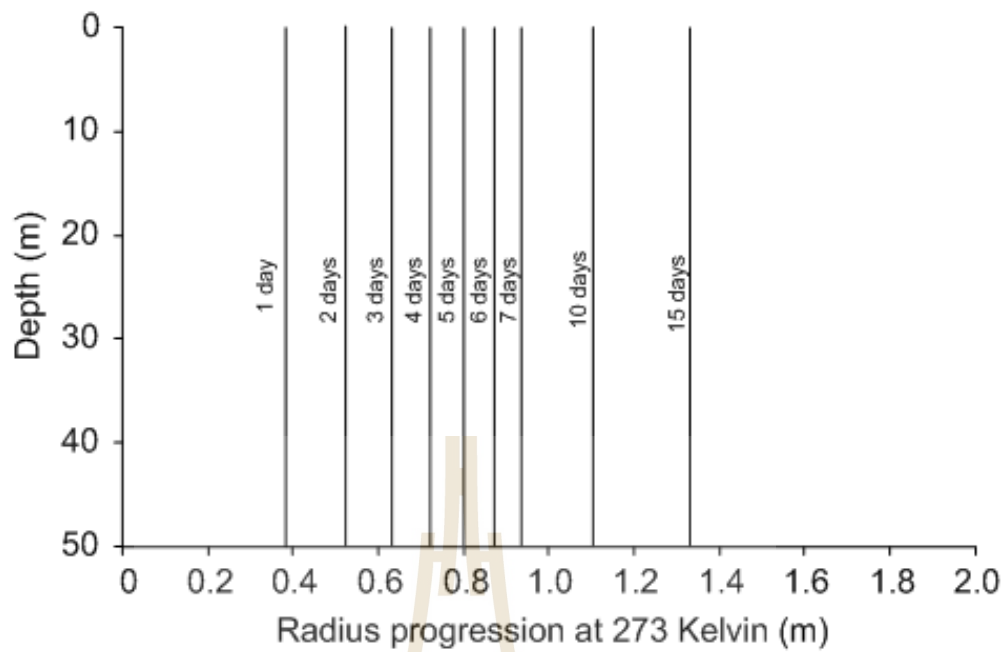


(a) flow rate = 0.5 kg/s

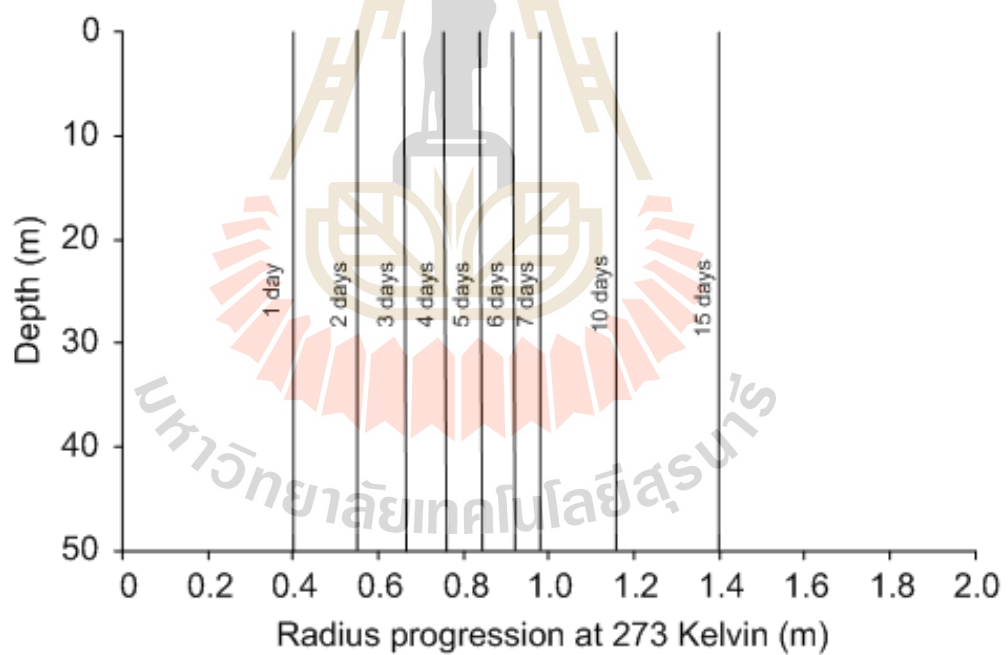


(b) flow rate = 1 kg/s

Figure D.2 Results of the radius progression of frozen zone at 273 Kelvin for 50% water-saturated ground surrounding condition in difference coolant flow rates



(c) flow rate = 2 kg/s



(d) flow rate = 3 kg/s

Figure D.2 Results of the radius progression of frozen zone at 273 Kelvin for 50% water-saturated ground surrounding condition in difference coolant flow rates (cont.)

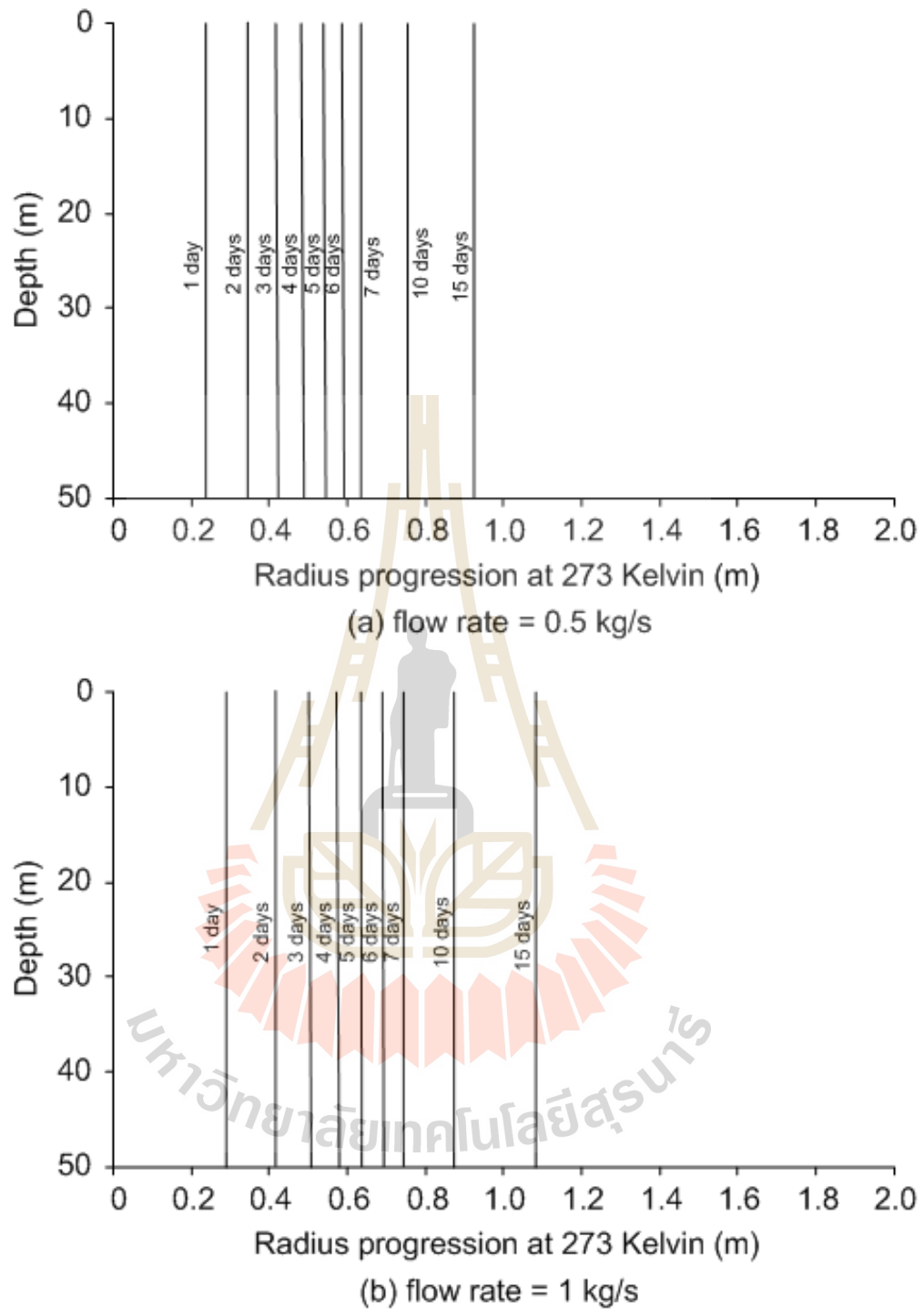
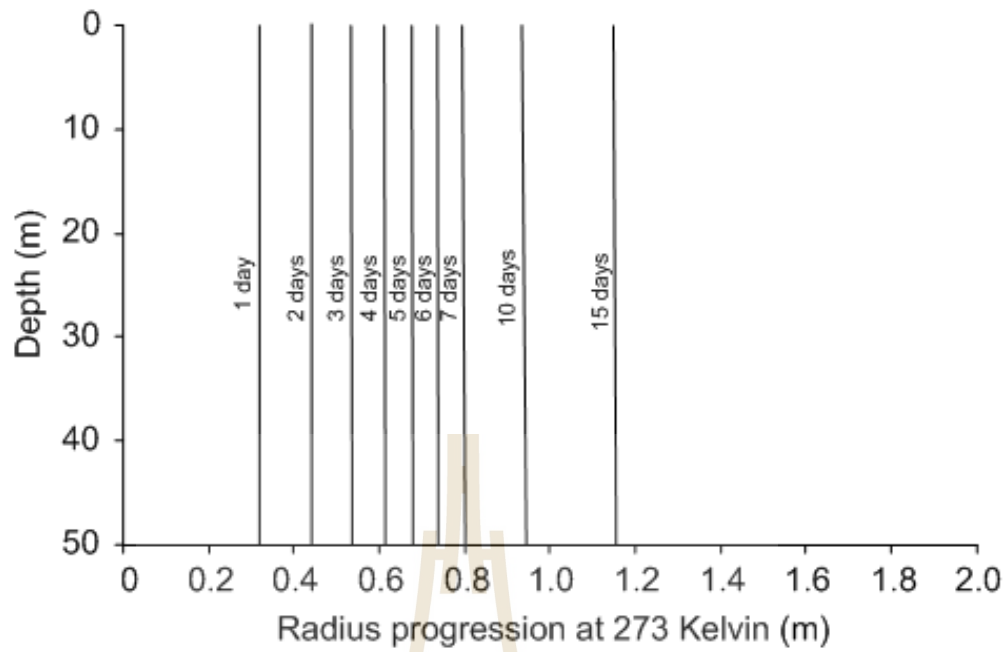
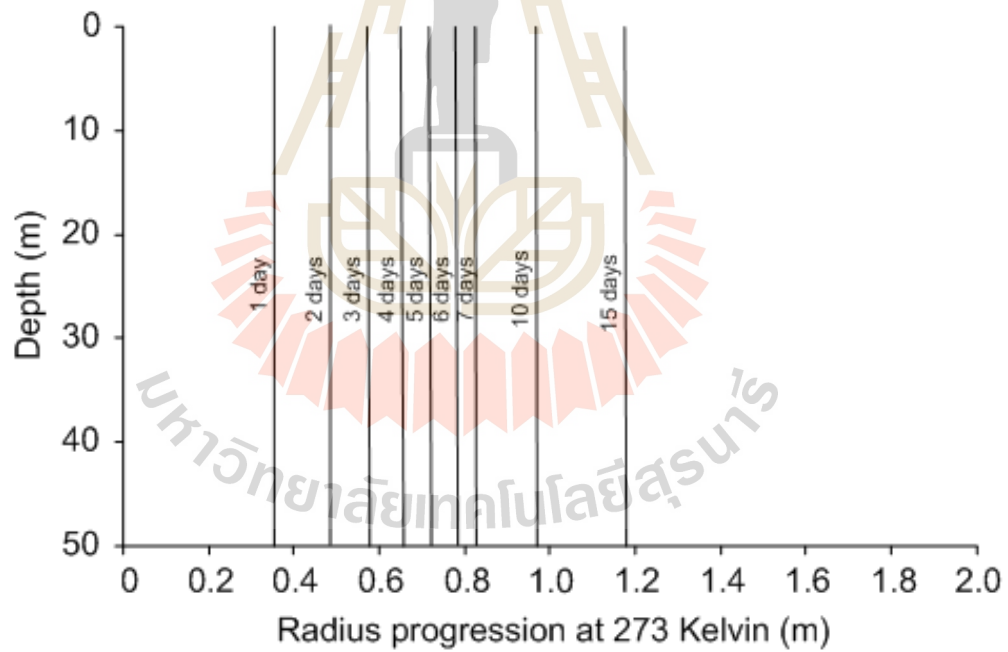


Figure D.3 Results of the radius progression of frozen zone at 273 Kelvin for 100% water-saturated ground surrounding condition in difference coolant flow rates



(c) flow rate = 2 kg/s



(d) flow rate = 3 kg/s

Figure D.3 Results of the radius progression of frozen zone at 273 Kelvin for 100% water-saturated ground surrounding condition in difference coolant flow rates (cont.)

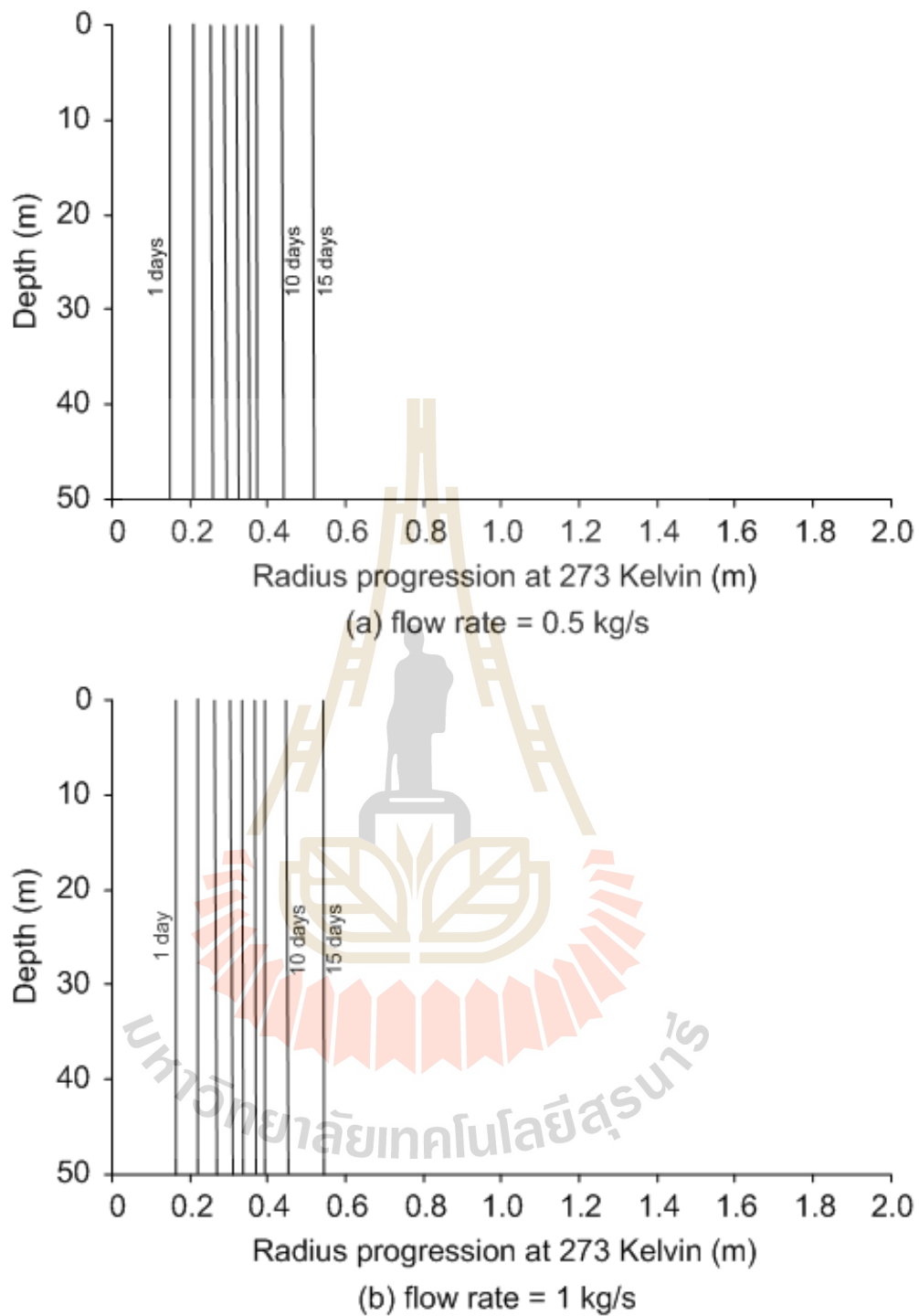
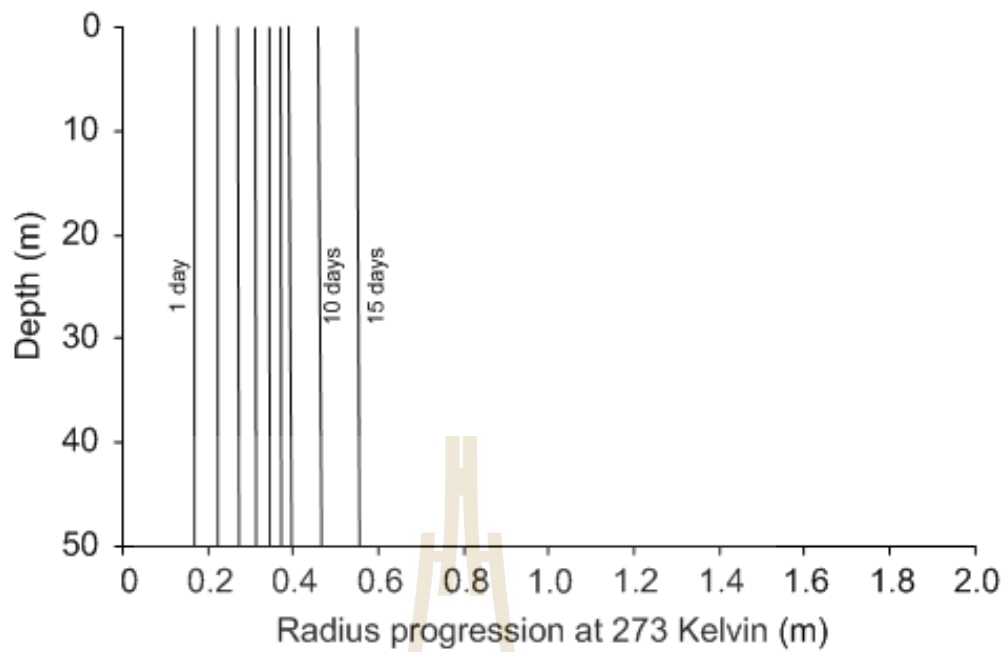
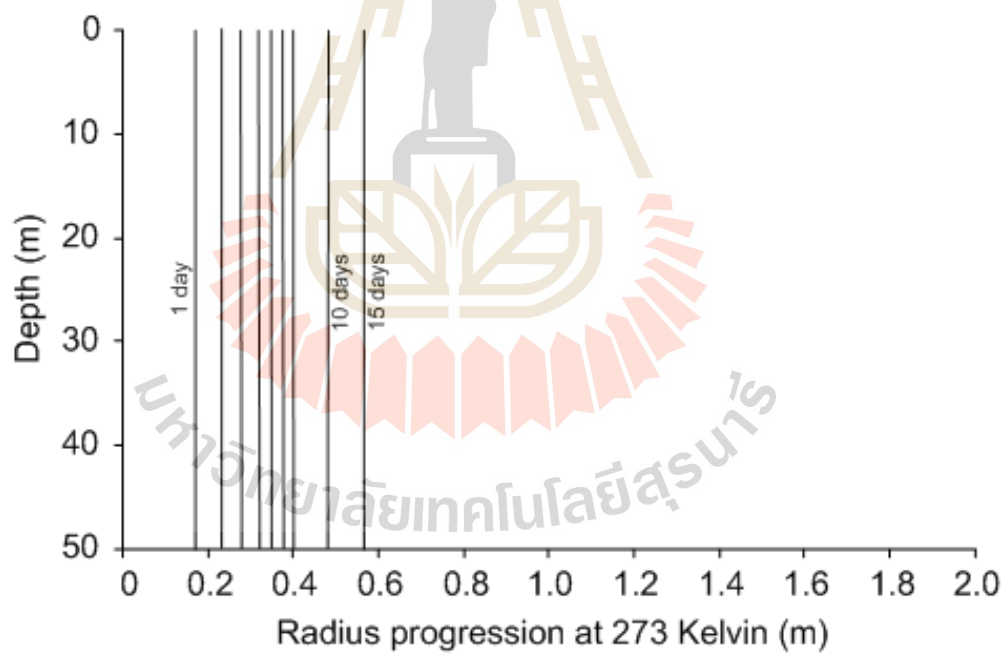


Figure D.4 Results of the radius progression of frozen zone at 273 Kelvin for pure water ground surrounding condition in difference coolant flow rates



(c) flow rate = 2 kg/s



(d) flow rate = 3 kg/s

Figure D.4 Results of the radius progression of frozen zone at 273 Kelvin for pure water ground surrounding condition in difference coolant flow rates (cont.)

BIOGRAPHY

Miss. Samerhkea Promma was born on March 16, 1990 in Chiang Rai province, Thailand. She received her Bachelor's Degree in Engineering (Geotechnology) from Suranaree University of Technology in 2012 and received her Master's Degree in Engineering (Geotechnology) from Suranaree University of Technology in 2015. For her post-graduate, she continued to study with a Doctor of Philosophy Program in the Civil, Transportation and Geo-resources Engineering Program, Institute of Engineering, Suranaree university of Technology. During graduation, 2013-2016, she was a part time worker in position of research assistant at the Geomechanics Research Unit, Institute of Engineering, Suranaree University of Technology.

